Blood Flow Dynamics through a Defective Mechanical Heart Valve

Othman Smadi

A Thesis

in

The Department

of

Mechanical and Industrial Engineering

Presented in Partial Fulfillment of the Requirements
for the Degree of Master of Applied Science (Mechanical Engineering) at
Concordia University
Montreal, Quebec, Canada

April 2008

Library and
Archives Canada

Published Heritage
Branch

395 Wellington Street
Ottawa ON K1A 0N4
Canada

Bibliothèque et
Archives Canada

Direction du
Patrimoine de l'édition

395, rue Wellington
Ottawa ON K1A 0N4
Canada

Your file Votre référence
ISBN: 978-0-494-40924-4
Our file Notre référence
ISBN: 978-0-494-40924-4

ABSTRACT

Blood Flow Dynamics through a Defective Mechanical Heart Valve

Othman Smadi

A model of asymmetrical 2-D defective bileaflet mechanical heart valve was used to simulate steady and pulsatile blood flow through a defective mechanical heart valve under several flow and malfunction severity conditions. The calculations used Reynolds-averaged Navier–Stokes equations with Newtonian blood properties. The results showed that the flow upstream and downstream of the defective valve is highly influenced by malfunction severity and this resulted in a misleading improvement in the correlation between simulated Doppler echocardiographic and catheter transvalvular pressure gradients. In this study, two potential non-invasive parameters were proposed using Doppler echocardiography and phase contrast magnetic resonance imaging, for an early detection of mechanical heart valve malfunction. Finally, the relation between the coherent structures downstream of the valve and the valve malfunction was shown and the significant impact of valve malfunction on platelet activation and as a consequence, on thrombus formation was also shown.

Acknowledgements

First of all, I would like to express my appreciation to my supervisors Dr. Lyes Kadem and Dr. Ibrahim Hassan for believing in me and for their continuous support during my research.

I am also grateful to our Cardiovascular Fluid Dynamics (LCFD) group for their technical support and also for the healthy and competitive environment that we work in.

I am also grateful to Dr. Vatistas and Dr. Ben Hamza for reviewing my work and attending my examination committee.

Table of Contents

List of Figures

List of Tables

Nomenclature

C	Speed of sound, $C = \sqrt{\gamma RT}$, $\left(\frac{m}{s}\right)$
F_d	Doppler shift, (Hz)
$f_\circ$	Transmitted frequency (Hz)
H	Enthalpy, $\left(\frac{J}{kg}\right)$
h	Tip clearance height, *(m)*
I	Turbulence intensity, $I = u'/U_\infty$
k	Turbulent kinetic energy, $\left(\frac{m^2}{s^2}\right)$
p	Pressure,
Δp	Pressure difference, *(Pa)*
Q	Volume flowrate, $\left(\frac{m^3}{s}\right)$
R	Gas constant, $\left(\frac{N \cdot m}{kg \cdot K}\right)$
r	Radial coordinate, *(m)*
SV	Stroke volume, $\left(m^3\right)$
S_{ij}	Strain rate tensor, $\left(\frac{1}{s}\right)$

t	Time, *(s)*
Δt	Time step, *(s)*
u_i	Time-averaged velocity component, $\left(\frac{m}{s}\right)$
u_i', v_i'	Fluctuation of velocity component from the time-averaged value, $\left(\frac{m}{s}\right)$
u_τ	Wall friction velocity, $\left(\frac{m}{s}\right)$
U, V	Velocity, $\left(\frac{m}{s}\right)$
$\vec{v}$	Velocity vector $\langle u, v, w \rangle$, $\left(\frac{m}{s}\right)$
VTI	Velocity time integral (m)
x	Axial coordinate, *(m)*
y	Circumferential coordinate, *(m)*
y^+	Non dimensional viscous sub layer height

Greek symbols

θ	Angular velocity, *(radians)*
ε	Turbulent dissipation rate, $\left(\frac{m^2}{s^3}\right)$
γ	Ratio of specific heats, $\gamma = c_p / c_v$

ν	Kinematic viscosity, $\left(\frac{m^2}{s}\right)$
μ	Dynamic viscosity, $\left(\frac{kg}{m \cdot s}\right)$
μ_{eff}	Effective viscosity, $\left(\frac{m^2}{s}\right)$
μ_t	Turbulent viscosity, $\left(\frac{m^2}{s}\right)$
ρ	Density, $\left(\frac{kg}{m^3}\right)$
$\bar{\bar{\tau}}, \tau_{ij}$	Stress tensor, *(Pa)*
τ	Shear stress, *(Pa)*
ω	Specific dissipation rate, $\left(\frac{1}{s}\right)$

Subscripts

LVOT	left ventricle outflow tract
rms	root mean square
Dop	Doppler
Cat	Catheterization
∞	freestream conditions
w	wall

Abbreviations

EOA	Effective orifice area
BPV	Bioprosthetic heart valve
MHV	Mechanical heart valve
CW	Continuous wave
PW	Pulsed wave
RPF	The repetition frequency
LDA	Laser Doppler anemometry
FSI	Fluid structure interaction
ALE	Arbitrary Lagrangian-Eulerian approach
DNS	Direct numerical simulation
DES	Detached eddy simulation approch
PIV	Particle image velocemetry
RES	The aortic valve resistance
MRI	Magnetic resonance imaging
WSS	Wall shear stress
AS	Aortic stenosis
TPG	Transvalvular pressure gradient
TSS	Turbulent shear stress

Chapter 1

Introduction

All body organs for all time need lifelong support of blood flow which is circulated by the heart. The human heart is an advanced pump that sends oxygenated blood and nutrients to the whole body and receives deoxygenated blood in a cycle. A human heart is composed of four chambers and four valves (Figure 1.1); the function of all of them is to circulate the blood around the body.

The heart can be divided into right and left sides; each side has two chambers (atrium and ventricle) and two valves (pulmonary and tricuspid valves for the right side and mitral and aortic valves for the left side). The left side is highly affected by diseases more than the right side due to the fact that, it carries higher pressure than the right one (i.e. pulmonic and tricuspid valves carry a pressure of about 30 mmHg, on the other hand, aortic valve carries a pressure of 100 mmHg, while the mitral valve carries a pressure of 150 mmHg (Yoganathan et al., 2004).

Even though the physiological (pulsatile) blood flow is not simple, the need for understanding it is essential to any one who wants to model the flow of the blood in the circulatory system. The cardiac cycle consists of two phases: *systole* (ejection phase) and *diastole* (filling phase). Each one of them has different acceleration-deceleration stages. In addition, during cardiac cycle flowrate and pressure distribution will be different from one valve to another. The left heart chambers, however, are more important than the right

one as mentioned before and flow and pressure distribution for the left side can be simply described as in Figure 1.2.

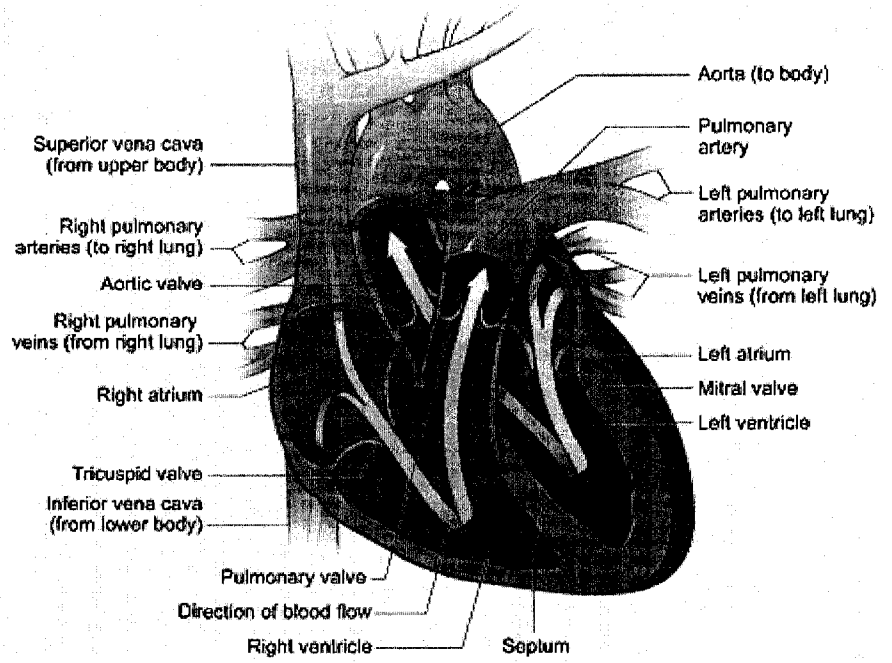

Figure 1.1 Illustration of cross-section of healthy human heart. (http://www.nhlbi.nih.gov/health/dci/Diseases/hhw/hhw_anatomy.html)

The complete cardiac cycle can be explained briefly as follows:

1- The left ventricle contracts and pumps blood to the aorta via the aortic valve and from aorta to the rest of the body. At the same time mitral valve will be closed to prevent back flow from left ventricle to left atrium (systole).

2- The left ventricle relaxes and is filled with blood again via the mitral valve. At the same time aortic valve will be closed to prevent reverse flow from aorta to left ventricle (diastole).

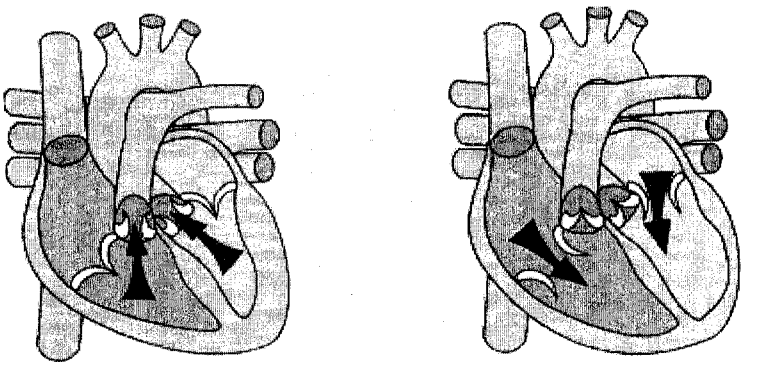

Ventricular Systole (step 1) Ventricular Diastole (step 2)

3- The same process will happen to the right side but with a smaller magnitude in velocity.

4- All the valves will be closed during isovolumic contraction and relaxation.

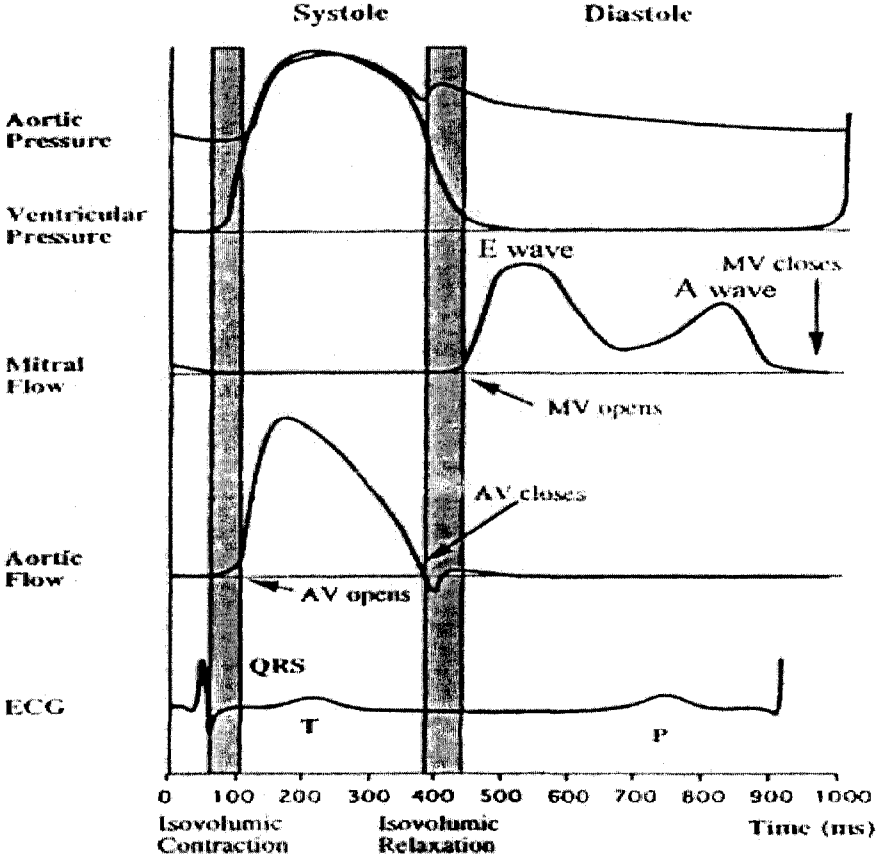

Figure 1.2 Pressure and flow curves for the aortic and mitral valves (Yoganathan et al., 2004).

The nature of blood flow through heart valves is very complex and this complexity comes out as a result of the pulsatile nature of flow combined with fluid-structure interaction. This leads to laminar unsteady flow with temporal transitional flow periods near the peak of systolic phase (Yoganathan et al., 2005).

1.1 Heart Valve Diseases

Among the four heart valves, the aortic and the mitral valves are exposed to heart valve disease more than others due to high load, as they are responsible to send the blood to the whole body. The major problem related to functioning of the valves is the failure; either in fully opening the valve to allow smoothly the blood to pass through the valve to the other side (stenosis) or in completely closing the valve to prevent regurgitation flow to the first side (incompetence) (Figure 1.3).

Figure 1.3 Degenerative aortic stenosis.

In case of stenosis, the stenotic valve will increase the load on the left ventricle in order to create enough pressure drops to push a sufficient amount of blood through the aortic valve. While, incompetence will let amount of blood that is pumped through the valve to leak back, which will force the chamber to enlarge more to compensate for this leakage. In sever cases the leakage amount could reach to 90 percent of the whole pumped blood. As a result of stenosis or incompetence, the heart muscle could thicken or congestive heart failure would occur if the patient did not have the proper treatment based on the severity or type of his problem.

Drugs, balloon valvuloplasty, surgical repair, and finally valve replacement in advance cases, could be used to treat these pathologies and help the patient to go back to their normal life, (Zaret et al., 1992). Recently, instead of valve replacement, a new technique is adapted to reduce the level of incision comparing with conventional heart replacement surgery. The method is called ***Percutaneous intervention*** where the balloon valvulopasty is used to insert a compressed tissue heart valve in the place of stenotic one without removing the native valve.

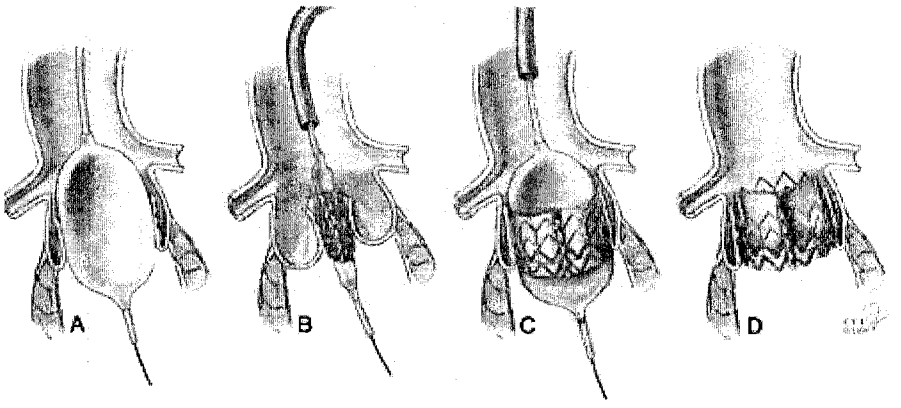

Figure 1.4 a) Balloon valvuloplasty, b) Balloon catheter with valve in the diseased valve, c) Balloon inflation to secure the valve, and d) Valve in place.

1.1.1 Aortic stenosis

Aortic stenosis is the most common indication in aortic valve replacement. Whether the cause is rheumatic, degenerative, or congenital the leaflets of the valve are usually covers with calcium deposits. Resistance to flow by the aortic valve imposes a pressure overload on the left ventricle. In order to compensate for the pressure overload, according to the law of Laplace, the thickness of the left myocardium increases (hypertrophy) so that the ratio of pressure to thickness remains constant, therefore minimizing wall stress and left ventricular work.

The law of Laplace states that:

$$Stress = \frac{pressure \times Radius}{2 \times Thickness} \tag{1.1}$$

In its turn, the thickening of the heart wall will lead to different problems like:

- Reduced left ventricular compliance,
- Increased myocardial oxygen demand,
- Decreased coronary blood flow, and
- Eventual left ventricular systolic dysfunction.

Eventually, the increased pressure load overwhelms left ventricular contractile reserve, leading to left ventricular systolic dysfunction and dilatation of the chamber (Crawford et al., 2004).

1.2 Diagnosis

1.2.1 Stethoscope

Stethoscope is the first method always used to evaluate any disorder in heart valves. Simply, the sound produced by heart valves will give an indication about the nature of blood flow. Rough, short and low-pitched murmur sound will be related to aortic stenosis; high-pitched, soft and long sound will be related to valve insufficiency. It is obvious that the clinician skills will influence the accuracy of the diagnosis.

1.2.2 Echocardiography

Echocardiography is a primary diagnostic technique in examining heart valve disease; the heart valve performance will be assessed invasively and painlessly by sending high-frequency sound waves, allowing physicians -when it is possible- to visualize the shape, size, opening space and motion of the valve. Moreover, the heart muscle thickness is another important part that is estimated by this method. In the meantime, ***Doppler echocardiography*** is one sort of this technique, detecting the direction and the magnitude of the velocity of moving blood within the heart.

Doppler echocardiography

Doppler echocardiography is being used widely to detect aortic stenosis and valve incompetence. Based on relative change between the returned ultra sound and the emitted one, and by using Doppler equation (1.2), the velocity of red blood cells (RBC) through the valve will be determined.

$$V = \frac{C}{2 f_o COS\theta} F_d \qquad (1.2)$$

Where V is RBC velocity, C is speed of sound in blood (1500 m/s), F_d is Doppler shift, and θ is the angle between the beam of the ultrasound transmitted from the transducer and the moving red blood cells. However, the clinician usually try to have the ultrasound beam parallel to the blood flow direction, therefore, the angle will be negligible.

Pulsed and Continuous Wave Doppler

There are two main types of Doppler echocardiography techniques, continuous wave (CW) and pulsed wave (PW). Both techniques have special advantages and drawbacks. In PW we can measure the velocity in a small range cell at a variable depth along the ultrasonic beam. The size of the range cell depends on the instrument and the frequency. In the PW mode, however, the maximum velocity that can be measures is limited. The **aliasing phenomenon** (Figure 1.5) will occur if the maximum velocity increased over the **Nyquist limit** (Eq.1.3). In turn, the Nyquist limit states that to have proper measurements for the velocity, the Repetition Frequency (RPF) should be twice of the maximum velocity magnitude. This limitation is a drawback of this technique.

$$\textbf{Nyquist limit} = \frac{Number\ of\ pulses / \sec ond}{2} \tag{1.3}$$

The CW technique has no range resolution, but at the same time it has no limit on the measurable maximum velocity. The two techniques, therefore, complete each other, and the instrument combines the two is a much more powerful tool for diagnosis than a single PW or CW instrument. Conventional using of CW is for measuring the highest velocity through the valve, while measuring the volume flow rate is considered by the PW.

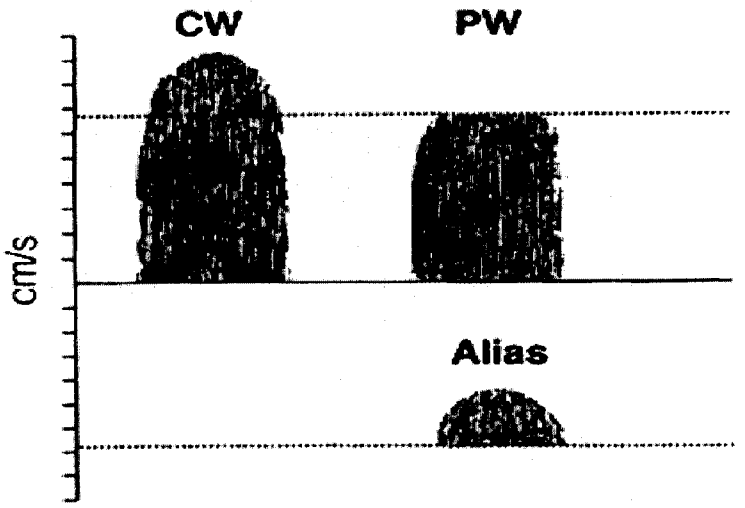

Figure 1.5 Schematic rendering of the full spectral display of a high velocity profile fully recorded by CW Doppler. The PW display is aliased, or cut off, and the top is placed at the bottom.

The information can be extracted from the CW are the valve jet velocity; transvalvular pressure difference (clinically called pressure gradient) and valve area. The pressure difference ΔP (clinically called pressure gradient) is calculated based on simplified Bernoulli equation

$$P_1 - P_2 = \frac{1}{2}\rho(V_2^2 - V_1^2) + \rho\int_1^2 \frac{d\vec{V}}{dt} d\vec{s} + R(\vec{V}) \qquad (1.4)$$

($\frac{1}{2}\rho(V_2^2 - V_1^2)$: =0; $\rho\int_1^2 \frac{d\vec{V}}{dt} d\vec{s}$: =0)

$$P_1 - P_2 = \frac{1}{2}\rho(V_2^2 - V_1^2) \qquad (1.5)$$

(V_1^2: =0)

$\rho_{Blood} = 1060\,Kg/m^3$ And 1Pa = 0.0075 mmHg then;

$$\Delta P(\text{mmHg}) = 4V^2 \qquad (1.6)$$

Where $R(\vec{V})$ is viscous friction term, $\rho\int_1^2 \frac{d\vec{V}}{dt} d\vec{s}$ is flow acceleration term, ΔP is transvavular pressure gradient (mmHg) and V is the velocity at the systolic peak

downstream of the valve (m/s). It is worth to point out that the final equation (Eq.1.6) is conventionally used by the clinicians. By using this equation, the clinicians consider that the friction and time dependant acceleration terms as negligible terms. In addition, the velocity V_1 in the Left Ventricle Outflow Tract (LVOT) is assumed to be very small when compared with the maximal velocity downstream of the valve. Furthermore, the velocity profile through the valve has been assumed flat, therefore, in the above equation, the maximum velocity equal the average one at every position through the valve (Hatle and Anglesen, 1985).

This assumption is reasonable and valid for the healthy valves. However, this assumption is questionable in the case of malfunction or obstruction in one or both leaflets in Bileaflet mechanical heart valves or in the case of normal valves but with low cardiac output (flowrate) (Kadem et al., 2005). The most common parameter that is used to evaluate both prosthetic and native heart valve is the Effective Orifice Area (EOA). EOA is area of the flow jet at the **vena contracta** and it is calculated based on continuity equation:

$$Q_{LVOT} = Q_{EOA} \tag{1.7}$$

$$SV_{LVOT} \times Heart\ rate = SV_{vena\ contracta} \times Heart\ rate \tag{1.8}$$

$$SV_{LVOT} = SV_{vena\ contracta} \tag{1.9}$$

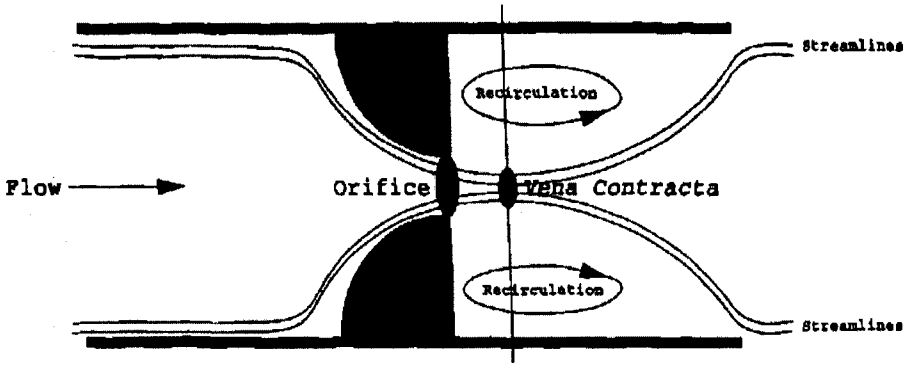

Figure 1.6 The vena contracta formation through an orifice (DeGroff et al., 1998).

$$SV_{LVOT} = EOA \times \int_0^T V_{venacontacta}\, dt \tag{1.10}$$

$$SV_{LVOT} = EOA \times VTI_{vena\ comtracta} \tag{1.11}$$

$$EOA = \frac{SV_{LVOT}}{VTI_{vena\ contracta}} \tag{1.12}$$

Where Q is volume flow rate (L/min), LVOT is left ventricle out tract, SV is stroke volume (m^3) (derived by direct flow measurement), and VTI is velocity time integral (m) (measured by CW Doppler) (Crawford et al., 2003).

If there is any constriction or stenosis exists in the way of flow, the opening area will be smaller and therefore the velocity will be higher at the stenosis area. In other words, if the EOA calculated is less than the normal value (4 cm^2) the existence of valve stenosis will be highly possible. The level of aortic stenosis severity can be classified as follows: mild at EOA > 1.5 cm^2; moderate at EOA = 1.0 -1.5 cm^2; and severe at EOA < 1.0 cm^2 (Garcia et al., 2003).

1.2.3 Cardiac catheterization

In cardiac catheterization, a small tube (catheter) is inserted from an artery or vein through the aorta into the heart. Several tasks could be done by the catheterization; pressure drop measurement through the valve, imaging a specific part by fluoroscopy (special type of x-ray) or collecting a sample of heart tissue c during the procedure to be examined later under the microscope for abnormalities. For the aortic stenosis, as mentioned above in Doppler echocardiography, the EOA orifice area will be measured invasively, but this time based on pressure drop instead of velocity and by using Gorlin formula (Baumgartner et al., 1992).

$$\text{EOA } (\text{cm}^2) = \frac{Qrms}{44.3\sqrt{\Delta p}} \tag{1.13}$$

Where $Qrms$ the root mean square systolic/diastolic flow rate (cm^3/s) and Δp is mean systolic/diastolic pressure drop (mmHg).

In the mean time, the fluoroscopy with EOA will be important specifically in MHV as the accuracy for detecting the malfunction of mechanical heart valves will be more difficult than in native or bioprosthetic valves (Montorsi et al., 2003). However, the limitations are that the catheterization is done invasively and also the process could free the deposited calcium from the surface of leaflet and exposes the arterial system to the risk of blocking one of its vessels (Fukumoto et al., 2003). Therefore, when it is possible this method should be avoided.

1.3 Prosthetic heart valves

Stenosis or incompetence at severe levels reduce the performance of the heart and place additional stress and strain upon it. Surgical replacement of the diseased valve with a prosthetic heart valve is necessary to restore valve function.

The first operation to replace defective native valve with prosthetic one has been done in 1952, the caged-ball valve was put to solve aortic stenosis in aortic valve. After that different designs have been proposed with using different materials to solve many problems that accompany using the prosthetic valves (i.e. thrombus formation, high pressure gradient and red blood cells and platelet damage).

Prosthetic heart valves could be categorized in two groups: bioprosthetic valve (BPV) and mechanical heart valves (MHV) (Figure 1.7). Each group has advantages and disadvantages. Generally, for prosthetic heart valves many features should be included to compensate original (native) heart valves. Durability, biocompatibility and falling in line with physiological flow are the main features. However, on one hand, for BPV the lack of durability (10-12 years) is the major problem. On the other hand, BPV do not need any anticoagulant as they are fabricated from biological tissues (Yoganathan et al., 2005). Conversely, MHV have a good durability, but in the meantime, they suffer from various clinical complications like thromboembolisms, cavitation and in some cases blood hemolysis (Yin et al., 2004).

Recently, polymeric heart valves have started to draw more attention due to their significant performance in terms of blood hemodynamic and mechanical properties. The valve design is similar to the natural valve and provides a large orifice in the ejection phase and reduces the disturbance in the aortic blood flow comparing with other MHV. However, the major obstacle to the success of the polymeric heart valves is the valve material degradation and calcification rate (Yin et al., 2005).

In spite of using widely BPV these days after a promising development in tissue engineering field and a noticeable success in BPV, MHV are still the most favourable choice in the market (Yoganathan et al., 2005). Therefore, the focus of the present study will be on MHV as they represent the most popular valves.

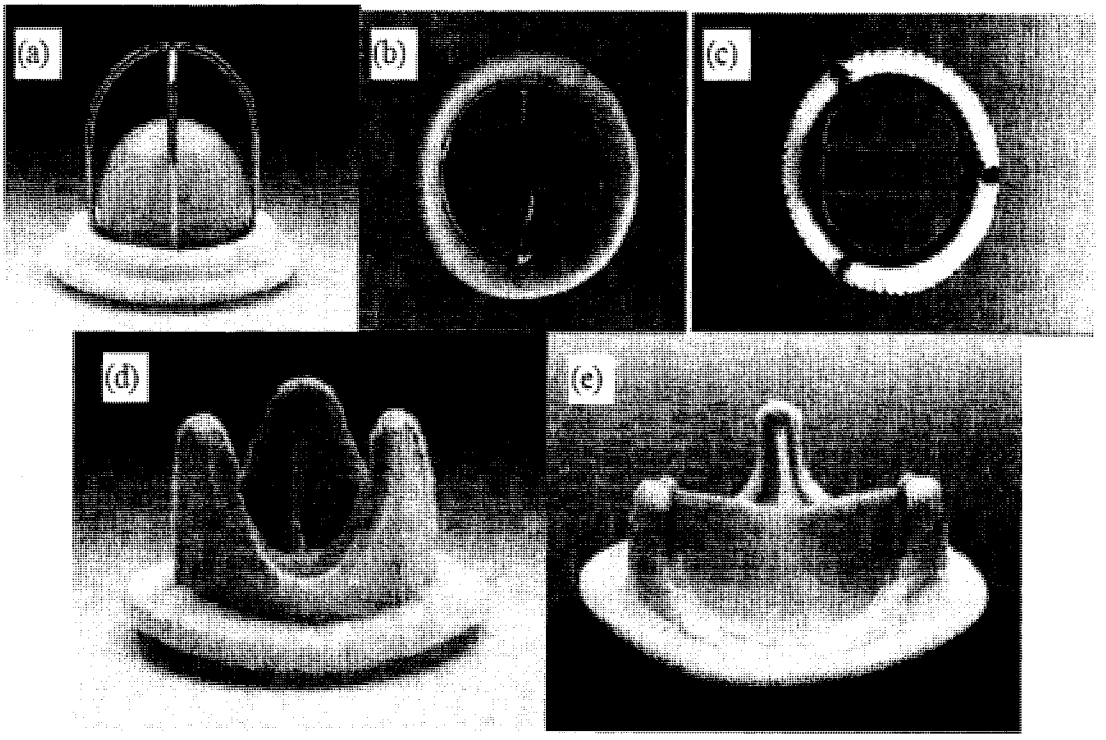

Figure 1.7 Different bioprosthetic and mechanical prosthetic heart valves:
a- caged-ball, b- tilting disc, c- bileaflet, d- porcine valve, and e- pericardial valve.

1.3.1 Mechanical heart valves (MHV)

Numerous MHV have been proposed since 1952 when a doctor in medicine used a caged-ball type to fix stenotic aortic valve. All these valves can be categorized into three types depending on their shape: caged-ball, tilting disc, and bileaflet (Figure 1.7). Caged-ball valve was the first model that has been used among other MHV. Unfortunately, the valve design creates high shear stress regions around the ball which obviously increases the possibility for thrombus formation. In addition the caged-ball valve creates high pressure drop through the valve which forces the heart to be over loaded to overcome the high pressure difference.

Tilting disc valve has been introduced as an alternative solution to solve caged ball problems and to increase the flow rate. Noticeable improvements have been achieved in terms of reducing the shear stress and pressure drop. However, the tilting disc valve suffers from weakness in the hinge area and rapid fatigue and damage comparatively (Gott et al., 2003).

The last generation of MHV was bileaflet valve. Bileaflet valves have two semicircular leaflets that create three orifices available for the forward flow (one central and two laterals). Gott-Daggett Bileaflet Valve was the first fabricated bileaflet. Different bileaflet valves have been proposed with modification in design and material. Noticeable reductions in pressure difference value across the valve and shear stress level (Table (1.1)) made the St. Jude Medical bileaflet valve the most common valve that is being used nowadays.

Table 1.1 A comparison between different mechanical hear valves.

	Caged-ball	**Tilting disc**	**Bileaflet**
Pressure drop	The highest	In the middle	The lowest
Material	silicone elastomer ball and stellite metal cage.	Pyrolyte-Titanium stellite-Derlin	Pyrolyte
Regurgitant flow	Closing volume (5ml/beat)	Closing + leakage volume (9ml/beat)	Closing + leakage volume(11ml/beat)
Shear stress (downstream of the valve)	185 Pa	120-150 Pa	115-150 Pa

1.3.2 Clinical Complications

Despite the remarkable improvement in valve design resulting in a decrease in prosthetic valve complications, thromboembolic events are highly possible with MHV Implantation. Surface characteristics of the prosthesis (material and design), blood flow (cardiac output, turbulence, and stagnation), and characteristics of the blood elements of the patient (hypercoagulability) are the major factors of thrombus formation (Cannegieter et al., 1994). Clinically, this may result in significant valve dysfunction and a life-threatening event. In some cases, the thrombus may travel away from the valve and stick in the small vessels in the brain or in any part of the circulatory system resulting in a spectrum of effects ranging from transient to sometimes fatal events.

Pannus formation is another clinical complication that results from MHV replacement. Pannus formation is defined as a tissue growth around the valve housing and represents one of the most severe complications of valve replacement. The reasons of pannus formation are still unknown and efficient protective methods have not been fully clarified (Sakamoto at al., 2006).

The purpose of the present study is to develop new non-invasive parameters allowing an accurate and an early detection of mechanical valve malfunction, and to study the blood hemodynamics and the clinical complications by conducting steady and pulsatile studies for blood flow through defective bileaflet heart valves under several flow conditions and for different malfunction severities. However, the dysfunction of only one leaflet will be taking it in to account, as one of possible scenarios of valve obstruction due to pannus or thrombus formation. The typical physiological conditions and properties will be considered.

The present work will be presented in the following manner. First, a sequential review of the studies focusing on numerical and experimental works will be presented in Chapter 2. Next, a steady flow analysis for the defective bileaflet valve with mesh validation will be presented in Chapter 3. In Chapter 4, the effect of pulsatile blood flow through defective bileaflet valve will be presented in order to show the blood hemodynamics and the related clinical complications. Finally, conclusions from the present study will be given in Chapter 5, as well as the challenges and future directions that are required to study the blood flow through mechanical heart valves in normal and pathological conditions.

Chapter 2

Literature Review

Numerous studies have been conducted on MHV after implantation to determine the nature of blood flow and the medical complications. Results were analyzed in terms of material, design, hemodynamics, medical complications and performance diagnosis.

The studies could be divided into two main categories: numerical studies and experimental studies.

2.1 Numerical Studies

Currently, computational fluid dynamics (CFD) are widely used in investigating blood flow through MHV. Due to the complex nature of the physiological flow, different assumptions have been considered. The laminar assumption has been used to simulate the pulsatile nature of the cardiac cycle due to the absence of a numerical method capable of covering the laminar, transitional and turbulent regimes. On the other hand, recently, the development of low Reynolds Wilcox $(k-\omega)$ model (Wilcox 1998) encouraged researchers to simulate the pulsatile flow under turbulent regime assumption. Adding to that, the fluid structure interaction (FSI) between the valve leaflets and the blood flow has been studied to include the effect of blood flow on the leaflet and vice versa. Moreover, different regions in the MHV were modeled and consequently different assumptions have been made (i.e., clearance region between the leaflet and the housing of bileaflet valve).

2.1.1 Laminar Blood Flow

A comparison between 3-D numerical simulation for a bileaflet valve and experimental results using Laser Doppler Anemometry (LDA) measurements was performed by King et al. (1997). The group considered only quarter of the geometry by applying two planes of symmetry. The nature of flow was unsteady and laminar. The aim of this study was to validate the CFD solution and to get the optimum opening angle for the leaflet. Significant differences between CFD and LDA were found and were explained by limitations in CFD itself. However, good agreement was found between the numerical and the experimental results in terms of the quality and behaviour of the flow like existence of vortex shedding downstream of the valve and slow moving fluid in the sinus area. Finally, the authors concluded that numerical simulations are able to predict the flow characteristics downstream of a MHV and to improve, therefore, the future MHV design.

Blood flow in the clearance area between the leaflet and the housing during the valve closure was investigated by Aluri et al. (2001). Three different cases were considered; static, gravity closure and normal closure. For the first case the leaflets remained in a fully closed position while the pressure difference between the inlet and outlet was kept as 100 mmHg. The negative pressure in the atrium was not able to induce cavitations. In addition, the shear stress in the clearance area and the leaflet tip was insufficient to activate platelets or damage the red blood cells (hemolysis). No great difference was found in the second case (gravity closure) with respect to shear stress and the negative pressure value when the leaflet remained closed but the pressure was changed from 0-100

mmHg by increasing rate 2000 mmHg/s. In the last case, the normal closure case was done under the same pressure changing conditions for the gravity closure case. In addition, the leaflet was moved by an independent governing equation and showed a great transient negative pressure and high shear stress in the clearance region that may lead to cavitation and platelets activation, respectively.

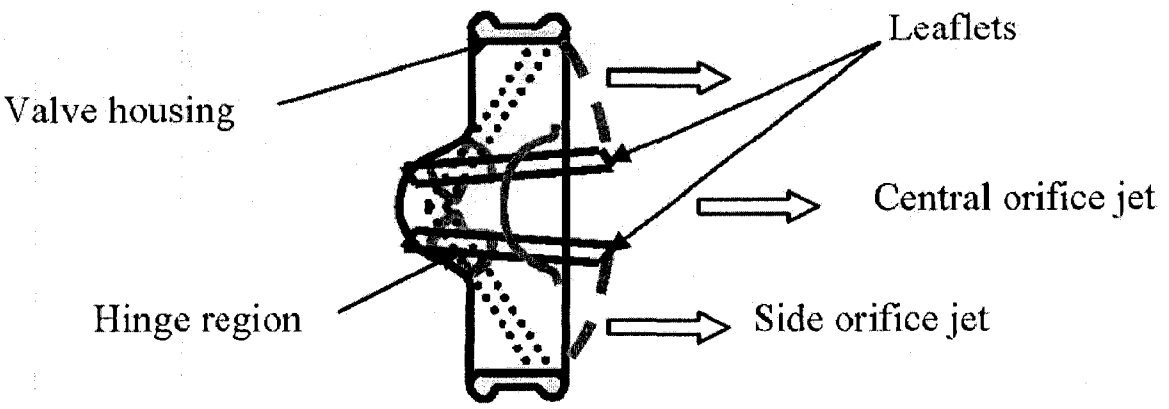

Figure 2.1 Schematic of the St. Jude Medical valve with leaflets show in open and closed (dotted line) positions.

Modeling a bileaflet valve in closing stage from fully open position to fully closed one was carried out by Lai et al. (2002). U^2RANS CFD code (The code is based on unstructured grid data structure using arbitrarily shaped elements) was used based on Arbitrary Lagrangian-Eulerian approach (ALE). The authors aimed to validate the ability of CFD to predict the fluid flow dynamics throughout the closing phase. Numerous geometries were applied by changing the clearance space and leaflet tip geometry. In fact, only two cases were presented on the article because of the same flow transition features in all cases. Numbers of observations were shown in this study. First of all, the maximum negative pressure was not on the tip of the leaflet and instead of that it was

found on the atrial side of leaflet and close to the housing. Consequently, the higher transient negative pressure was found a few steps before the complete closure. However, in terms of clearance geometry, the pressure gradient through the clearance space was decreased by increasing the gap and choosing inclined leaflet tip. Finally, an extra case was added to the study by decreasing the leaflet closing velocity. The authors concluded that a significant reduction in negative pressure and shear stress was observed when the leaflet velocity was decreased which will continue to minimize the risk of cavitation.

A new technique for moving mesh was proposed by using multi-zone unstructured moving grid scheme by Yubingshi et al. (2003). In few words, the mesh will be created for the entire geometry without considering the solid domain (the leaflet) and once the leaflet position is calculated the nodes which that are in contact with the solid phase will be considered as a moving boundary for the solid phase. The CFD results showed that the leaflet tip is the most sensitive region for hemolysis due to high velocity and velocity gradient near the tip.

Both 2-D and 3-D simulation for bileaflet valve closing behaviour were run by Cheng and co-authors (2003, 2004). ALE method was used to describe the mesh and U^2RANS method to describe the laminar flow. The FSI model describes effects of friction, pressure and gravity forces on the leaflet. Furthermore, a successful modeling for closing phase behaviour with closing and rebound processes was achieved. On the other hand, 2-D assumption was reliable to predict pressure and velocity values around the valve.

In contrast, the rebound magnitude was higher in 2-D and not consistent with 3-D results. 2-D simulations were recommended as a sufficient tool for MHV design.

3-D and laminar blood flow dynamics through bileaflet valve in mitral position were studied numerically by Cheng et al., (2004). In their study, symmetry was assumed. Therefore, only a quarter of geometry was considered due to computation difficulties and also to reduce the large number of elements (210000 elements to mesh the quarter). The real FSI was taken into account by considering the effect of the fluid on the leaflet and vice versa. The study was performed during valve closing and rebound phases, and the space between the housing and the leaflets was studied to show the flow behaviour and its relation to red blood cells damage and platelet activation.

During closing process, the most significant local negative and positive pressure occurred on the leaflet surfaces. In the meantime, high velocity and wall shear stress have been observed on the leaflet surfaces specially the clearance area. However, the negative pressure in the atrium side did not reach the vapour pressure of the blood. On the other hand, higher negative pressure and shear stress have been seen in rebound phase, and there is a possibility for cavitation to happen.

ALE method was used by Dumont et al. (2004). They used FLUENT (commercial software) and ALE method to implement FSI to MHV 2-D unsteady (pulsatile) laminar flow condition. They compared their results with CCD camera to record the valve positions at different instants. User defined function (UDF) was used to write an external

code to describe the leaflet motion and a dynamic mesh was used to redefine the mesh with each small movement of the solid boundaries. The authors concluded that the simulation gave a good agreement with the experimental results.

3-D pulsatile blood flow through a St. Jude bileaflet valve was simulated by Redaelli et al. (2004). Only a part of the systolic phase was considered to simulate the valve opening process. They used a user defined function and laminar model to implement FSI using FLUENT. In parallel, experimental work was performed to validate the numerical simulation by considering the same valve design and the same inlet condition. Further improvements to the current model were suggested like: considering normal flow rate and including the transitional and turbulent effects in the simulation by using an appropriate turbulence model.

Liang et al. (2003) investigated grid resolution and flow symmetry, focusing mainly on grid resolution and its effect on the accuracy of the results obtained using CFD. For this purpose, 3D, steady and fully developed flow through a bileaflet mechanical valve was simulated for different Re numbers. They concluded that the results are very sensitive to mesh independence under physiological conditions. Furthermore, they questioned the validity of a symmetrical model assumption, since they found that asymmetry in the flow can appear for Re as low as 120, even though the flow was assumed laminar and steady.

In 2005, Liang et al. extended their work mentioned above by increasing the flow rate to near-peak systole flow rates. The flow was fully turbulent with Re as high as 6000. Two

Re numbers were chosen to be modeled, Re = 750 and Re = 6000. For laminar flow the direct numerical simulation (DNS) was employed. For turbulent flow, two different models were used – the Reynolds-average Navier-Stokes approach (URANS) and the detached eddy simulation approach (DES). In few words, DES method is a hybrid technique proposed as a precise approach for predicting separated flows. It combines two concepts: URANS for the entire boundary layer and Large-Eddy Simulation (LES) for the separated regions.

To validate their numerical results, they performed experimental measurements using Particle Image Velocimetry (PIV) under the same conditions. For laminar flow, a good agreement between numerical and experimental results was observed and the unsteadiness of flow was remarked as early as for Re = 350. DES approach was recommended to catch the feature of the flow in the sinus region more than URANS approach. URANS showed steady, stable, ring-shaped vortices. On the other hand, DES showed a very complex flow with multiple eddies. The damaging of red blood cells has a direct relation with the number and the form of the eddies generated downstream of the valve. For DES results the red blood cell will stay for less duration inside the vorticity field therefore will cause a lower blood elements damage. In addition, DES results showed a good agreement with PIV results.

The flow-driven opening of a leaflet was studied by Pedrizzetti et al. (2006) by considering rectilinear rigid inertia-less leaflet in a 2-D channel. Even though the problem was simplified, the results were important to describe vortex shedding

formation. The valve opening was divided into three phases; the first phase was named no-shedding phase and the leaflet was controlled by mass conservation and Kutta condition was applied by neglecting the component of relative velocity around the edge. Subsequently, the second phase was called roll-up phase, and during this phase a significant deceleration in leaflet moment was observed. In the meantime, the vortex formed and finally left the leaflet edge to generate a multiple vortex wave. Finally, the third phase was described by vortex-sheet phase when the vortex sheet will be formed. New equations have been proposed to represent the flow in these three different phases.

The flow through a St. Jude bileaflet valve in aortic position with co-existing suboartic stenosis was investigated by Guivier et al. (2007). 2-D laminar and pulsatile flow simulations were performed by taking into account the fluid-structure interaction effect. Guivier et al. concluded that the major jet flow will be laterally more than central as a result of the present of suboartic stenosis. Furthermore, the leaflet in suboartic side will not work properly compared to a healthy case. Therefore, more awareness should be considered by clinicians to align the echo-Doppler beam in the right way to avoid an underestimation of the effective orifice area of the valve.

2.1.2 Turbulent Flow

Thalassoudis et al. (1987) conducted a numerical study to investigate blood flow through a caged-ball prosthetic heart valve. Turbulent, steady and axisymmetrical flow assumptions were considered using $k-\omega$ turbulence model to simulate the flow. The valve was fixed in fully open position. Various flow rates were tested as inlet conditions; starting from relatively low Re (600) to relatively high Re (6000). Additionally, a simple

power law expression was proposed to predict the value of turbulent shear stress for different regions in the aortic root.

Peacock et al. (1997) investigated the onset of turbulence under pulsatile flow condition in a straight tube. A new empirical equation stated that the critical peak Reynolds number is related to Womersley parameter (α) and Strouhal number (St) in the form of power law function. While the α parameter was related to the frequency, the St number was related to the stroke volume.

$$\mathrm{Re}_{peak(critical)} = 169\,\alpha^{.83} St^{-.27} \tag{2.1}$$

Comparing to the actual experimental values, the mean error was found -1.1% and the root mean square error (rms) was found 15.2%. Moreover, a validation for a previously suggested formula for the onset of turbulence by Nerem and Seed 1972 was done and the mean error was -3.5% and rms error was 53.5%. Nerem and Seed equation had only relation between α and $\mathrm{Re}_{peak(critical)}$ as follows:

$$\mathrm{Re}_{peak(critical)} = 250\,\alpha \tag{2.2}$$

Based on equation (2.1), in human aorta, the range of critical peak Reynolds number is 5500-9800.While the actual range for the peak Reynolds number under normal physiological condition is (7250-29100). Therefore, the possibility of turbulence exists in human aorta under (Eq. (2.1)) assumption.

DeGroff et al. (1998) investigated numerically the dependence of the effective orifice area (EOA) on the flow rate and the accuracy of flat velocity profile assumption that is considered in the continuity equation at different flow rate values. They concluded that

the difference between the average and the maximum flow rate was low at high flow rate. In contrast, there was a significant deviation between average and maximum velocities at low flowrate. In fact, by assuming the maximum velocity equal to the average velocity, the velocity is overestimated and consequently the EOA is underestimated. Therefore, indeed, the EOA is flow dependant and the assumption of flat velocity profile is not precise at low Reynolds number.

2.1.2.1 $k-\omega$ turbulence model

Bluestein et al. (2000) numerically and experimentally investigated the occurrence of thromboembolic complications caused by mechanical heart valves. A time dependent numerical study was performed using Wilcox $k-\omega$ turbulence model for internal low Reynolds number flow. Digital Particle Image Velocemetry (DPIV) was conducted also under the same conditions. The comparison between numerical and experimental results shows the ability of Wilcox $k-\omega$ model to simulate the blood flow through a bileaflet valve. In addition to exposing to foreign material and non-physiological blood flow, vortex shedding downstream of the valve's leaflets played an important role in cerebrovascular micro emboli. Moreover, the shed vortices could aggregate the large platelets as well as the small ones. The long residential time with high level of shear stress were noticed during the vortex shedding process.

The effect of the surgical implantation techniques and valve orientation on blood hemodynamics in the valve's wake was studied by Bluestein et al. (2002). Time dependent Computational Fluid Dynamics (CFD) simulations using the Wilcox $k-\omega$

model for low Reynolds number blood flow were conducted on commercial software (FLUENT). The mesh quality near the wall was made fine to maintain $y^+ \leq 1$ (y^+ is the non dimensional viscous sub layer height). The simulation did not consider fluid-structure interaction between the leaflets and the blood, and the valve leaflets were fixed in the fully open position. They concluded that the heart valve misalignment has an important effect on platelet activation and thromobembolism formation.

The study of turbulence detection in a stenosed artery bifurcation was conducted by Ghalichi and Deng 2003. 2-D Low-Reynolds number Wilcox $k-\omega$ model was used to represent the flow. Different severities of stenosis were considered; healthy (0% stenosis), 40%, 55% and 75% stenosis. The validation for this turbulence model was conducted by comparing the low-Reynolds $k-\omega$ model in healthy (non-stenosed) tube with laminar model at relatively low Reynolds number. A good agreement between the two models, in terms of wall shear stress and velocity profiles across the internal carotid, was found. Finally, The 75% stenosis was the cut off for major changes in turbulence characteristics.

Straatman and Steinman 2004 conducted a study on blood flow through a stenosed tube (mimicking an arterial stenosis). A steady case was performed first to check the grid dependence and the inlet condition then followed by unsteady simulations. Two different $k-\omega$ models were used; standard and transitional. Both models in addition to laminar simulation were compared to the experimental results from the literature. In steady and unsteady cases, standard $k-\omega$ model over predicted the turbulence at the stenosis region

and also downstream of the stenosis. In contrast, the transitional $k-\omega$, overall, had a good agreement with the experimental results. The potential of transitional $k-\omega$ model as a promising tool to simulate the pulsatile blood flow at low Re number was noticeable. Moreover, at relatively very low Re number (Re~100), the transitional model predicted the laminar nature of the flow with zero-turbulence magnitude.

2.2 Experimental Studies

Clinically, various in-vivo techniques have been introduced to explain the nature of flow and evaluate the heart valve performance such as: Echocardiography, catheterization and Magnetic Resonance Imaging (MRI). Practically, catheterization is an inadequate method to be used in MHV analysis (Rehfeldt et al., 2002), while echocardiography and MRI represent appropriate techniques for the diagnosis (for more details see chapter one). Moreover, all the techniques mentioned above, as well as more advanced techniques like particle image velocemetry (PIV) and laser Doppler anemometry (LDA) have been used in-vitro to verify the accuracy of in-vivo diagnosis methods and to clarify the nature of the flow downstream of a MHV. (Bruker et al., 2002, Grigioni et al., 2001, and Liu et al., 2000). However, the above mentioned methods appear to be inferior in predicting flow or acquiring quantitative information within the valve housing or near the wall and the need for numerical simulation arises as a promising tool for better understanding of the dynamics of blood flow.

Validations for different measuring techniques through in-vitro studies were discussed by different authors. Browne et al. (2000) tried to demonstrate the difference between laser

Doppler velocimetry and particle image velocimetry. Steady flow measurements near peak systole were carried out through a St. Jude bileaflet MHV in aortic position. In addition, maximum turbulent shear stress (MTSS) and maximum turbulent principal stress (MTPS) were studied and the comparison was made based on them. Large differences in values and trends (up to 200%) between the two methods were shown. Combination between the two techniques was recommended by using PIV to describe the general flow patterns and using LDA in specific areas to get more detailed and accurate results.

Experimentally, Laser Doppler Anemometer (LDA) was used to investigate turbulent flow characteristics downstream of different types of bileaflet valve by Liu et al. (2000). St. Jude Medical, CarboMedics and Edwards Tekna valves were selected to be investigated. The maximum turbulent normal and shear stresses were found 7.8 mm downstream of the valve. For the St. Jude bileaflet valve, the maximum Reynolds normal stress was 1250 dyn/cm^2 and the maximum Reynolds shear stress was 510 dyn/cm^2 (51 Pa). Higher values for the CarboMedics bileaflet valve were measured; Reynolds normal and shear stresses were found, respectively, 1780 dyn/cm^2 (178 Pa) and 680 dyn/cm^2 (68 Pa). The highest values for the Reynolds stresses were measured through Edwards Tekna bileaflet valve, and were around 2630 dyn/cm^2 (263 Pa)for the Reynolds normal stress and 770 dyn/cm^2 (77 Pa) for the Reynolds shear stress. The exposure time valve was very similar in the three types, and the value was in order of 1-10 ms. Moreover, the Kolmogorov length scales of the three valves ranged from 20-70 μm. Finally the authors

concluded that the combination of turbulent stress with exposure time with Kolmogorov scales could initiate blood cells damage.

Lu et al. (2001) re-evaluated and discussed the reference written by Sallam et al. (1984). Sallam et al. (1984) in their paper claimed that the hemolytic thresholds for red blood cells damage in turbulent flow in terms of turbulent shear stress and exposition time was equal to 400 N/m^2 and 1ms, respectively. However, by using the same method and two components laser Doppler anemometer, the new suggested values by Lu and co-workers for hemolytic thresholds were found 800 N/m^2 and 1ms. Moreover, Kolmogorov length scales were estimated to be around 9 μm which is the same order of magnitude of the scale of red blood cells.

Grigioni et al. (2001) paid attention to the leaflet design in bileaflet valves in terms of flow characteristics and turbulent shear stress level. They studied a Sorin Bicarbon (SB) valve (curved leaflet) and a St. Jude valve (straight leaflet). The same diameter and flow conditions were considered and the velocity profiles for four different positions downstream of the valves were measured. Laser Doppler Anemometry (LDA) was used to measure the velocity profiles downstream of the valves. Significant differences for velocity profiles were observed between the two valves. High shear rate was observed for the SB but for shorter time when compared to St. Jude valve, in which, lower shear rate but with longer residency time were found. They suggested that the design of SB valve should be improved to reduce thrombus formation.

A new tri-leaflet MHV in aortic position was studied by Bucker et al. (2002) using Digital particle image velocimetry (DPIV) technique. In addition, a high speed camera was used to capture the leaflet motion during the cycle. The study showed a good consistency between the new MHV and natural one in terms of flow nature and leaflet closing and opening phases.

A comparison between the concept of flow resistance and the concept of Effective Orifice Area (EOA) was made by Blais et al. (2001). The aortic valve resistance (RES) was compared with EOA to evaluate the efficiency of RES to give a trusted indication about the severity of an aortic stenosis. Three different valves were selected to be tested; fixed stenoses, biological and mechanical heart valves with two different diameters for each. Several stoke volumes were conducted for the same ejection time. In addition, RES was found more flow dependent than EOA especially for fixed stenoses and MHV cases. Finally, neither RES nor EOA were sufficient alone to predict accurately the severity of aortic stenosis

In the purpose of getting accurate and confident values for EOA in an in-vitro studies, Kadem et al. (2005) proposed a new experimental method by using the acoustical source term (AST) with PIV results to determine the vena contracta area. Three sharp-edged orifices with different sizes in addition to a bioprosthetic valve were studied. A comparison was made between AST method, Doppler echocardioghraphic measurements and some conventional PIV methods. The potential flow theory for drawing out the EOA was used as a standard reference. Since EOA -which was derived from Doppler

echocardioghraphic measurements- was averaged; the EOA from PIV was taken also as averaged values. A good agreement was found between AST method from one side and potential theory and Echo-Doppler from another side. The new AST method was suggested to be a useful tool to verify the EOA which is calculated by Echo-Doppler especially at low flow rate.

An in-vitro study was conducted by Wei et al. (2004) on two different MHV; bileaflet (CarboMedics) and monoleaflet (Bjork-Shley) valves. In parallel, numerical simulations using Wilcox $k-\omega$ model for transitional/turbulent flow under pulsatile flow were conducted. To measure the shear stress histories of the platelets, numerically, Lagrangian approach for particulate two phase flow was used to calculate approximately the separated trajectories of platelets that close to the valve leaflets. Thromboembolism phenomenon in both MHV was captured. Experimentally, the platelet activation states were two times higher in bileaflet valve than in monoleaflet one. Furthermore, the numerical results showed that the shear stress exposure could be more than four times higher in bileaflet valves.

In bileaflet valves, blood clot formation is regularly observed in the hinge region and also in the valve housing (Fallon et al., 2006 and Simon et al., 2004). It is assumed that the local flow conditions in these regions aggregate the platelets and lead to a thrombus formation. All the studies on bileaflet valves showed that the high velocity leakage flow generates regions of high Reynolds shear stress which are possible regions for platelets activation.

2.3 Wall shear stress (WSS)

Yoganathan et al. (1978) addressed the effect of the WSS on vascular endothelial cells (thin layer on the interior surface of all vessels) and the clinical complications that accompany the change in the endothelial cells state. A wall shear stress about 40 N/m^2 might damage the endothelial cells and higher value around 100 N/m^2 could wash away the endothelial cells. As a result the blood will be in direct contact with subendothelial connective tissue. In this case, the deposition of blood elements and thrombotic material will occur on subendothelial tissue of defective wall. It is important to point out that the level of shear stress that will affect the red blood cells is lower when the red blood cells are adhered to the wall. Only 10 N/m^2 will agitate the adhered red blood cells and in extreme cases some substances will be released from the cell, ensuing thrombus formation.

Methods for wall shear stress measurement and their drawbacks were reviewed by Katritsis et al. (2007). They categorized the methods into in-vitro, in-vivo and numerical methods. Generally, there are two approaches to measure WSS. First approach uses Hagen-Poiseuille formula to estimate the WSS. Therefore, only maximum or average velocity and vessel diameter are required for this purpose. As known the Hagen-Poiseuille formula (see Eq. 2.3) assume a Newtonian nature for the blood.

$$\gamma^{\bullet} = 4\overline{u} / R = 2u_{max} / R \tag{2.3}$$

Where $\gamma^{\bullet}$ is the shear rate (1/s) and $\overline{u}$ is the average velocity (m/s) and u_{max} is the maximum velocity (m/s) and R is the vessel radius (m).

It is obvious that these conditions (parabolic velocity profile and Newtonian fluid) are not satisfied in most of the circulation system. As a result, this should be demand only on an estimation of the WSS. The second approach is more precise and consists in measuring the velocity gradient in the radial direction near the wall. The only approximation in this method is the Newtonian nature for the blood which is reasonable in large vessels. Furthermore, they showed that an accurate determination of WSS is only precise if the measurements of the velocity gradient are very close from the wall (250-300 μ).

Ultrasounds are used, noninvasively, to derive the velocity profile across the vessel by calculating the velocity gradient near the wall and multiply it by the dynamic viscosity to obtain the WSS. However, the limitations of this method are that the method is mainly efficient in relatively straight vessels and an accurate velocity gradient at the wall is difficult to be obtained. ***Pulsed Doppler ultrasound*** represents another noninvasive technique for measuring the WSS. The limitations of pulsed Doppler method are the insufficient spatial resolution and the difficulty in differentiating between the movement of the vessel wall and moving blood near the wall. By pulsed Doppler method, the WSS can be obtained by measuring the velocity gradient near the wall or assuming Hagen-Poiseuille flow (the maximum velocity at the center of the vessel).

Phase-contrast Magnetic Resonance Imaging (MRI) is a promising technique for measuring noninvasively blood flow velocity. As previous methods blood flow velocity cannot be measured close to the wall(less than 1mm), for this reason, the WSS is underestimated by this method. Another limitation is the temporal resolution, as MRI

Chapter 3

Blood Flow through a Defective Mechanical Heart Valve: a Steady Flow Analysis

3.1 Introduction

The aortic valve is located between the left ventricle and the ascending aorta. Its role is to open with minimal obstruction to flow during the ventricular ejection process: the systolic phase and to close with minimal leakage during the ventricular filling phase: the diastolic phase. Aortic stenosis (AS) is defined as the pathological narrowing of the aortic valve. In industrialized countries, AS is the most frequent valvular heart disease and the most frequent cardiovascular disease after systemic hypertension and coronary artery disease. When an AS is severe and the patient is symptomatic, aortic valve replacement is the only treatment that has been demonstrated to be efficient for patients to avoid possible congestive heart failure and to improve heart performance. The native valve can be replaced by a biological valve (porcine valve or pericardial valve) or a mechanical valve. Approximately 250,000 valve replacement operations occur annually around the world and more than two thirds of these operations use mechanical heart valves (MHV) as a preferable choice (Yoganathan et al., 2004). This choice can be explained by the fact that mechanical valves have a longer lifespan when compared to biological valves. However, a patient with a mechanical valve must take anticoagulant medication life long because of risks of thromboembolic complications. Another potential complication associated with mechanical valves is valve malfunction (usually an incomplete opening of one or both leaflets in bileaflet mechanical valves) due to pannus (prevalence 0.14-0.65%

patients/year (Sakamoto et al., 2006)) and/or thrombosis formation. Although the occurrence of such malfunctions is quite low, however, they make the patient under a very high risk that requires an immediate surgery. Once the obstruction becomes severe, cinefluoroscopy or computed tomography can be used to confirm restricted motion of one or two leaflets of the prosthesis. Unfortunately, due to risk associated with X-ray exposure, these methods cannot be used for the routine follow-up of patients with prosthetic valves. It is therefore essential to develop and validate screening non-invasive methods for early detection of prosthetic valve malfunction. However, distinguishing between a normal and a dysfunctional bileaflet mechanical valve, especially when only one leaflet is blocked, using a non-invasive technique such Doppler echocardiography, is a complex problem since 1) as a result of acoustic shadowing from the sewing ring, it can be difficult to image the valve and detect if the leaflets are working properly, 2) transvalvular pressure gradients may be overestimated by Doppler echocardiography due to the recording of localized high gradient. In this situation, it is difficult to determine if the high gradient is due to an intrinsic dysfunction of the prosthesis or to a localized benign phenomenon due to the specific geometry of bileaflet mechanical valves (Baumgartner et al., 1990).

It is, therefore, essential to develop new non-invasive parameters allowing an accurate and an early detection of mechanical valve malfunction. Furthermore, these parameters should be flow independent to be applicable to a large number of patients.

For this purpose, as a first approach, numerical simulations of a continuous flow through a defective mechanical valve under several flow conditions and for different malfunction

severities were performed. This is the first numerical study dealing with mechanical valve malfunction with as a main objective determining a non-invasive parameter able to early detect if one valve leaflet is blocked. It should be noted that the current study focuses only on one blocked leaflet, since this case is more complex to be detected when compared to the case where both leaflets are blocked (Montorsi et al., 2003). In vitro, the flow through a defective CarboMedics mechanical bileaflet valve was only studied by Baumgartner et al. (1993) with as objective showing the discrepancy between catheter and Doppler pressure gradients. They showed that this discrepancy, that usually happen in normal bileaflet valves, decreases with defective leaflets due to energy losses (i.e. friction, flow separation and vortex formation) which lead to noticeable reduction in pressure recovery downstream of the valve. As a result, underestimation for real hemodynamic changes might occur and the clear definition for normal and abnormal flow will be difficult.

The objectives of this study are, therefore, to describe the flow dynamics through a bileaflet mechanical aortic valve with one immobilized leaflet from fully opened (0% malfunction) to fully closed (100% malfunction) position and to find a suitable method of predicting the malfunction by using an invasive parameter, that can be measured by Doppler echocardiography or magnetic resonance imaging. The potential clinical complications in terms of platelets activation and red blood cells damage associated with a defective leaflet in a bileaflet mechanical valve will also be investigated.

measurements will be obtained over 25-30 s. ***Intravascular Doppler Ultrasound*** and ***Intravascular Ultrasound*** can be used invasively to measure the velocity during the cardiac cycle. It is clear that the Hagen-Poiseuille flow assumption is considered for both methods to measure the WSS. The advantage of Intravascular Doppler Ultrasound over Ultrasound method is the ability to measure the velocity in small vessels (i.e. coronary artery).

Finally, Computational Fluid Dynamics (CFD) are widely used to simulate the circulatory system and obtain the data from critical regions where the data are difficult to be obtained with the current instruments or tools.

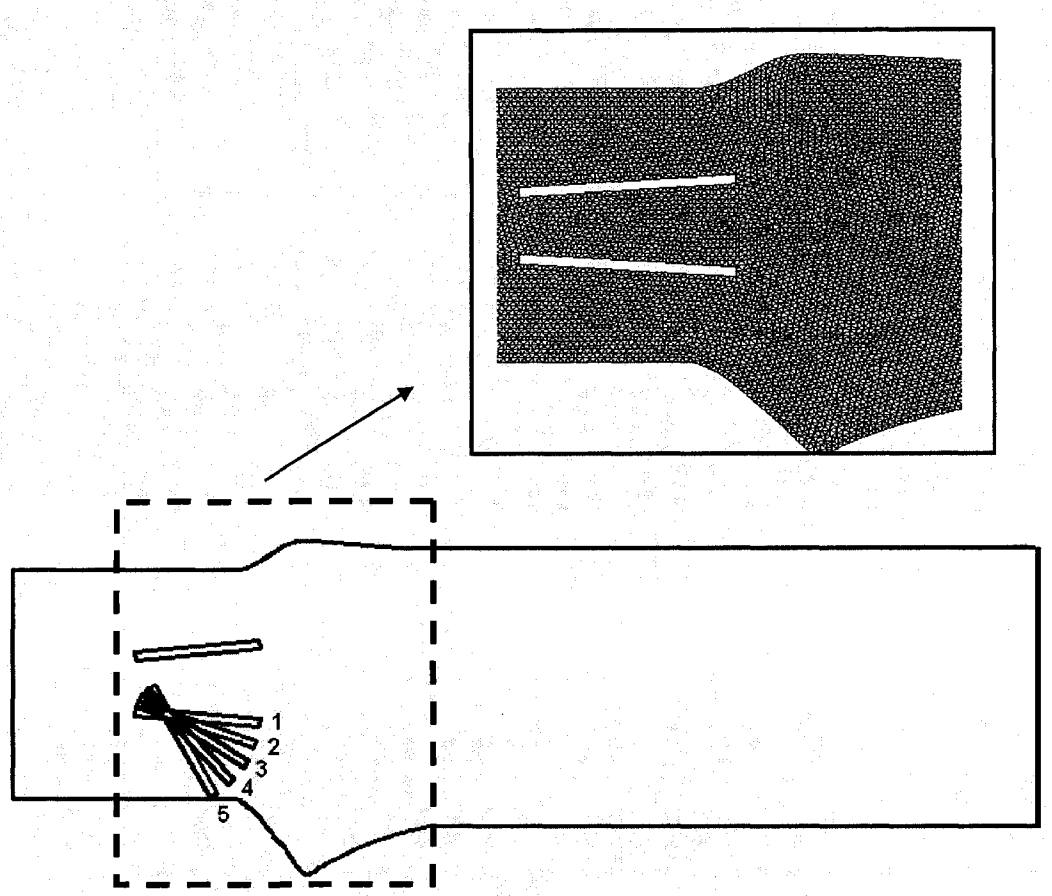

Figure 3.1 Model geometry for five different cases; 1) 0% malfunction, 2) 25% malfunction, 3) 50% malfunction, 4) 75% malfunction, and 5) 100% malfunction. (Mesh quality for the sinuses and leaflets is also shown).

3.2 Models and methods

To investigate the flow through a defective mechanical valve, five 2D models were created in the current study. The lower leaflet was moved from fully opened position (85°; 0% malfunction) to fully closed position (30°; 100% malfunction) with three equally spaced intermediate angles of 71.25° (25% malfunction), 57.5° (50% malfunction) and 43.75° (75% malfunction). As shown in Figure (3.1) non symmetric sinuses were modeled based on the in vivo study performed by Reul et al. (1990) and used in vitro by Grigioni et al. (2001). For the upstream and downstream sections, the inlet section was 15 mm upstream from the valve and the outlet section was 85 mm downstream of the valve. The bileaflet mechanical valve was modeled based on a 25 mm St. Jude Medical Hemodynamic Plus valve. Therefore, the inner diameter was 22.3 mm and the outlet diameter was 32.3 mm. The hinge mechanism of the valve has been neglected and this valve has been chosen since it is the most commonly implanted clinically.

For all the above mentioned severities, several systolic flowrates have been simulated: 7.5, 10.5, 15, 18 and 21 L/min, which represent a cardiac output of: 2.5, 3.5, 5, 6 and 7 L/min respectively. This will simulate normal and strenuous exercise conditions. For blood properties, the common values for density and dynamic viscosity were considered which were equal to 1000 kg/m^3 and 0.0035 kg/m s respectively. Under these conditions, the Reynolds number ranged from 2038 to 5708 based on average inlet velocity; inlet diameter and the viscosity of the fluid. This range of Reynolds number reasonably represents the turbulent nature of the flow downstream of the valve (Ge et al., 2003 and Ge et al., 2005).

Fluent 6.3.26 (Fluent Inc.; Lebanon; NH; USA) commercial software based on finite volume method was used to run the numerical simulations. Due to the absence of a numerical method able to describe the complete physiological flow and the need to simulate flow near and during the peak systolic phase to assess the level of clinical complications, the flow was assumed steady, turbulent, and Newtonian. In this study, standard k-ε model was used with 5% of turbulent intensity and 22.3 mm as hydraulic diameter (Kameneva et al., 2004 and Richards et al., 2004). For the boundary conditions, total pressure was considered as inlet condition and was changed with each case until the desired flow rate was reached. Zero static pressure was used as outlet condition, and no slip condition was used at the solid walls.

3.3 Mesh Independence

In order to get the mesh independence, four models were tested as shown in Figure 3.2 with different elements types and numbers. Although the quadrilateral shape for the element is more suitable than others as it is more aligned with the flow direction, in some cases the triangle element is more efficient, particularly with complex geometries and flow.

Figure 3.3 shows the velocity contours for 50% malfunction for four different meshes as follow: a-quadrilateral element with 26857 elements, b- triangular element with 37310 elements, c- quadrilateral element with 50912 elements and d- quadrilateral element with 91350 elements.

It is important to mention that the purpose of current study was to introduce or propose a technique to evaluate the performance of bileaflet valves based on Echo-Doppler method. The Echo Doppler evaluation uses the maximal velocity to estimate the pressure drop through mechanical heart valves by using the simplified Bernoulli equation (for more details see the introduction). Hence, the maximal velocity is the most important parameter to be checked, the percentage difference of the maximal velocity in the whole domain between the considered mesh (model b) and models (a) and (d) was around 3%. On the other hand, the percentage of difference between model (b) and model (c) was around 8%. However, the relatively high difference between model c and other models can be explained by the presence of highly deformed elements around the leading edge of the leaflets which in some cases results from the complexity of the current geometry.

Figure 3.4 shows the velocity profile across the ascending of the aorta at the vicinity of the valve just before the sinus area. As explained above, in this figure the interest was in the maximum velocity through the bileaflet valve orifices. The percentage of difference along the valve cross section between the four meshes was less than 1%.

Figure 3.5 shows the wall shear stress at the lower wall. The lower wall represents the wall that will be highly affected by the valve malfunction due to the obstruction. The wall shear stress will be expected to be higher at this region comparing to the upper wall. Therefore, the mesh independency checking was conducted only for the lower wall.
The wall shear stress is related to y+ more than the number of elements. The highest wall shear stress value was found with the lowest y+ value. It is important to point out that the

major difference in wall shear stress values between the four meshes was only at the vicinity of the valve. Moreover, the steady part of the current study did not deal with the wall shear stress. Hence, the difference in wall shear stress values will not have a significant effect in the velocity distribution downstream of the valve.

Finally, due to its flexibility with different valve orientations and less element deformability, model-b was adapted in the current simulation.

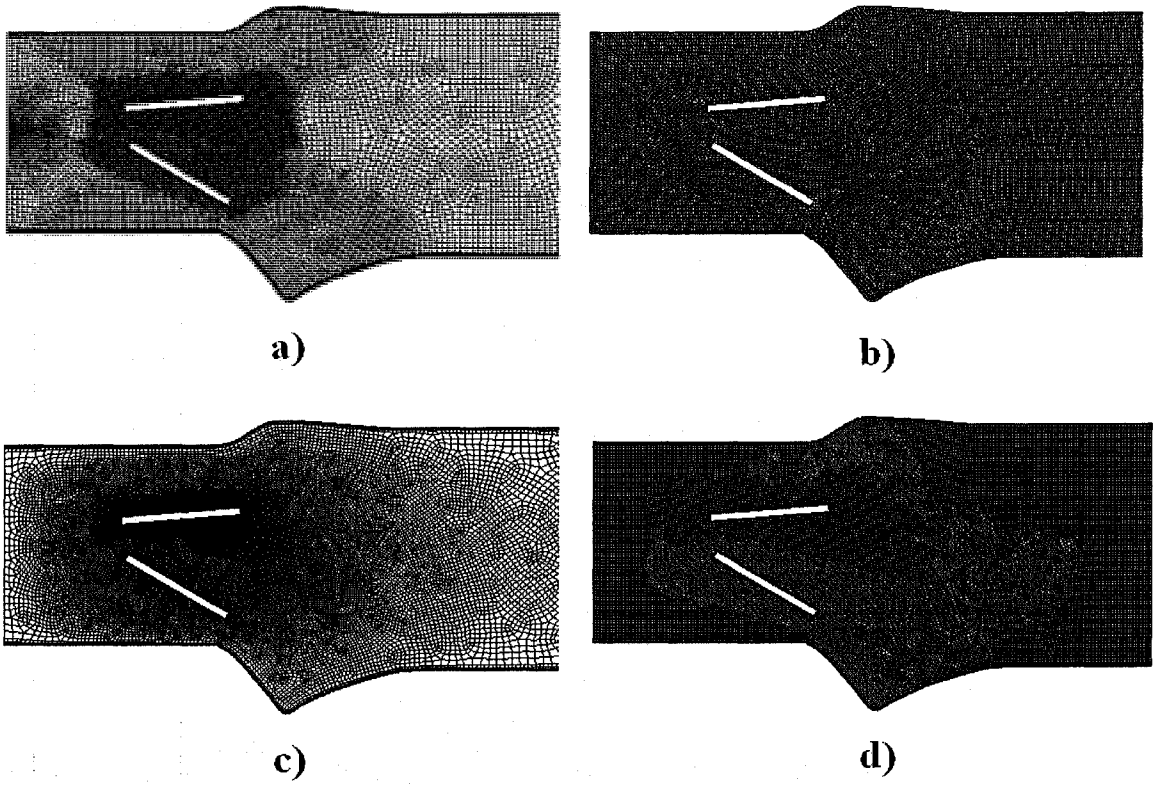

Figure 3.2 Four models with different element type and number: a) Quadrilateral 26857 elements, b) Triangular 37310 elements, c) Quadrilateral 50912 elements and d) Quadrilateral 91350 elements.

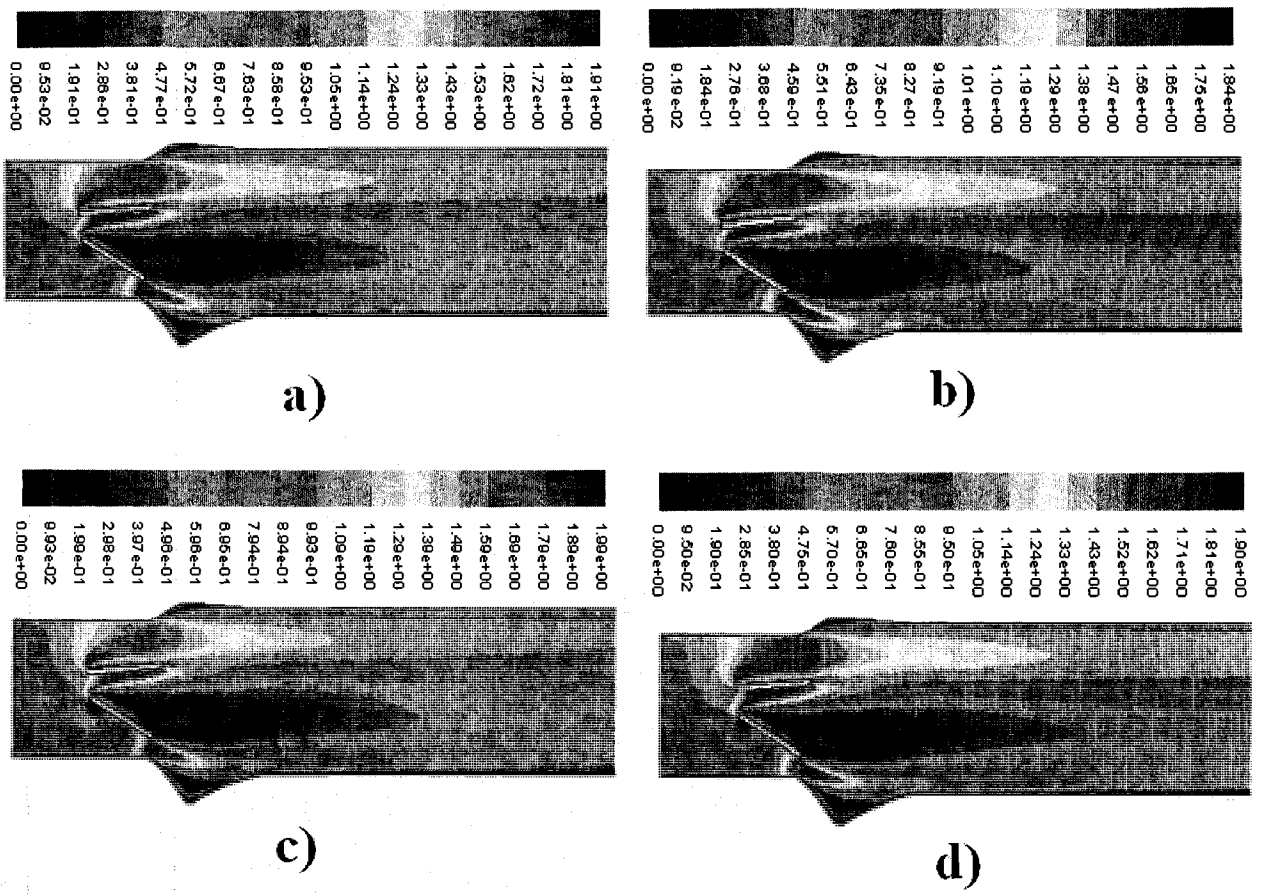

Figure 3.3 Velocity contours for the four types of meshing: a) Quadrilateral 26857 elements, b) Triangular 37310 elements, c) Quadrilateral 50912 elements and d) Quadrilateral 91350 elements.

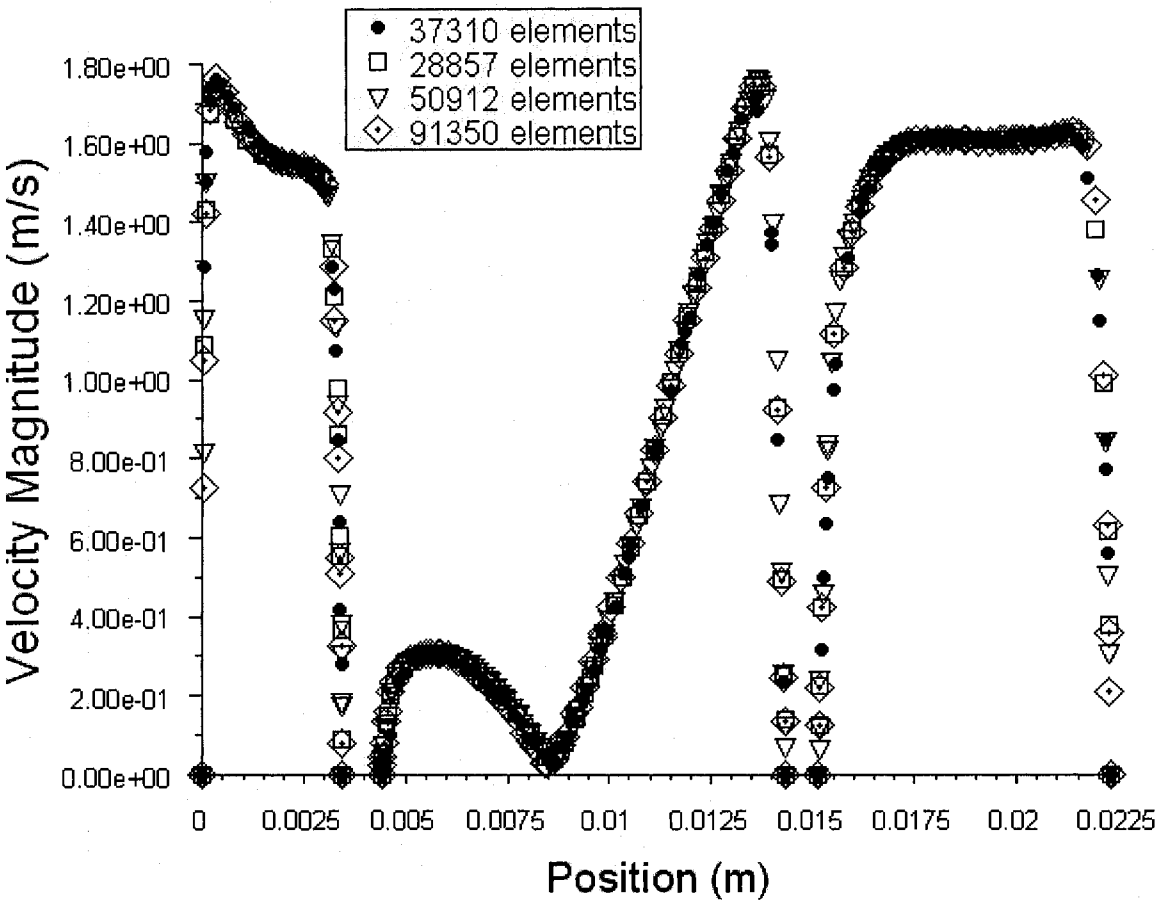

Figure 3.4 Velocity profile in radial direction at the vicinity of the valve for the four types of meshing.

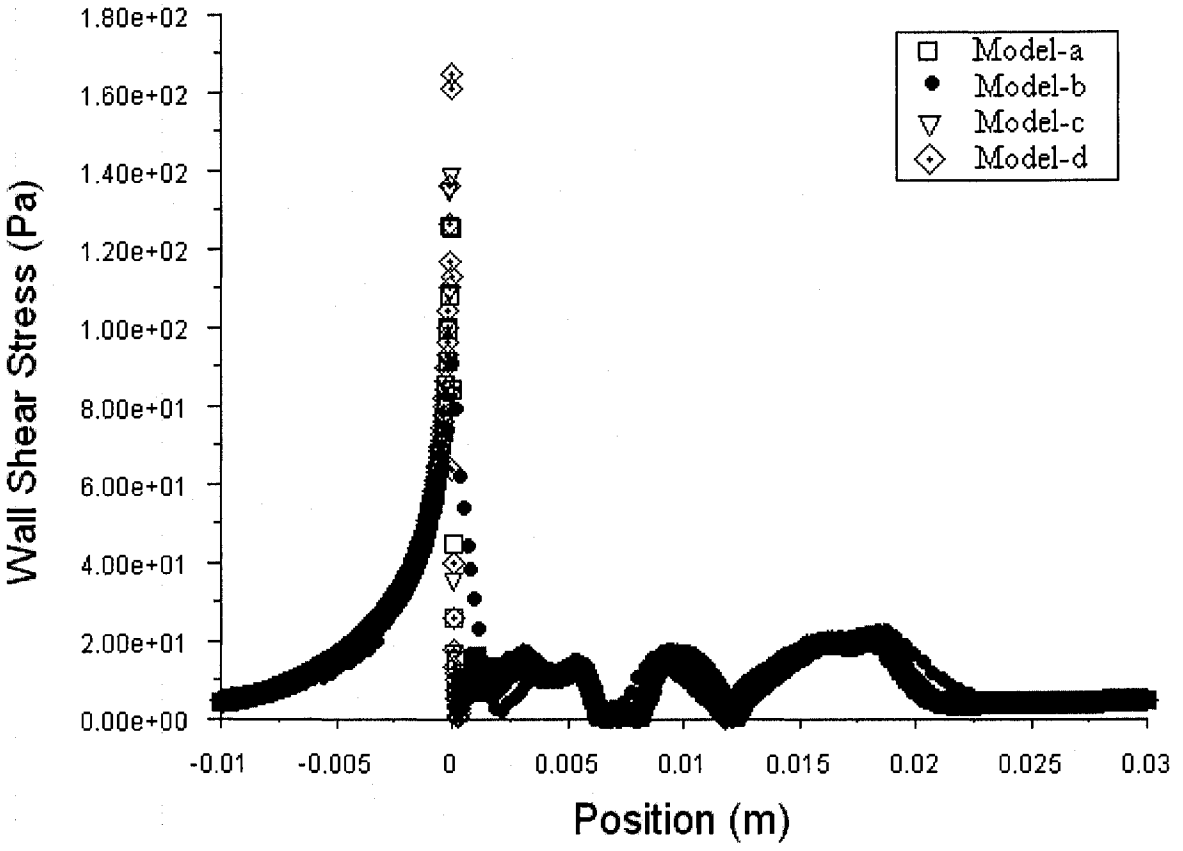

Figure 3.5 Wall Shear Stress (WSS) at the lower wall for 50% malfunction for the four types of meshing.

3.4 Results

3.4.1 Velocity distribution and profiles

Figures 3.6 and 3.7 show the velocity contours for the entire field for different percentages of valve malfunction at flow rates equal to 5 and 7 L/min respectively. Due to the difference in leaflet opening angles, the flow patterns developed upstream and downstream of the defective valves were different from healthy ones. In general, flow separation and vortex formation were noticed in all cases. In Figure 3.6, for Q = 5 L/min, the maximum velocity increased from 1.0 m/s in the healthy case (0% malfunction) to 1.85 m/s for the most severe one (100% malfunction) (+ 85%). Moreover, the flow direction changed from passing through the three orifices (one central and two laterals) in the healthy model to mainly lateral flow through the upper orifice in the completely closed leaflet case. In Figure 3.7, for Q = 7 L/min, the maximum velocity increased from 1.36 m/s in the healthy case (0% malfunction) to 2.63 m/s for the most severe one (100% malfunction) (+ 93%). Furthermore, it can be noticed on Figure 3.8 that the flow is becoming more complex, with increasing malfunction severity, with more small scale vortices and an important recirculation zone behind the defective leaflet. In this figure, the coherent structures where extracted using the λ_2 criterion (Jeong et al., 1995).

Figure 3.9 shows the velocity profiles at inlet section, valve section, 1D downstream of the valve and 2D downstream of the valve for different flow rates and valve malfunctions.

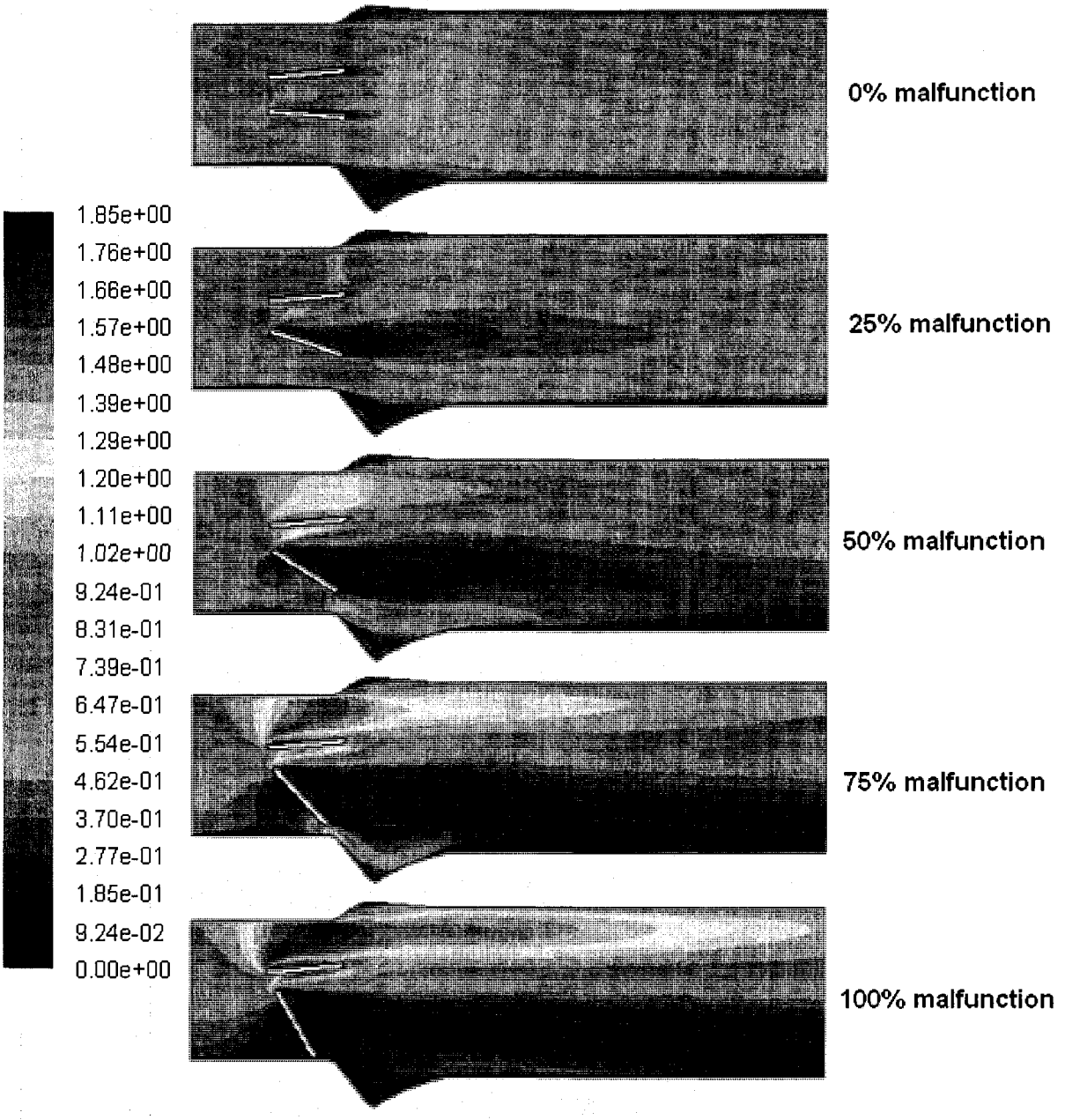

Figure 3.6 Velocity magnitude (m/s) contours for different percentages of valve malfunction at Q = 5L/min.

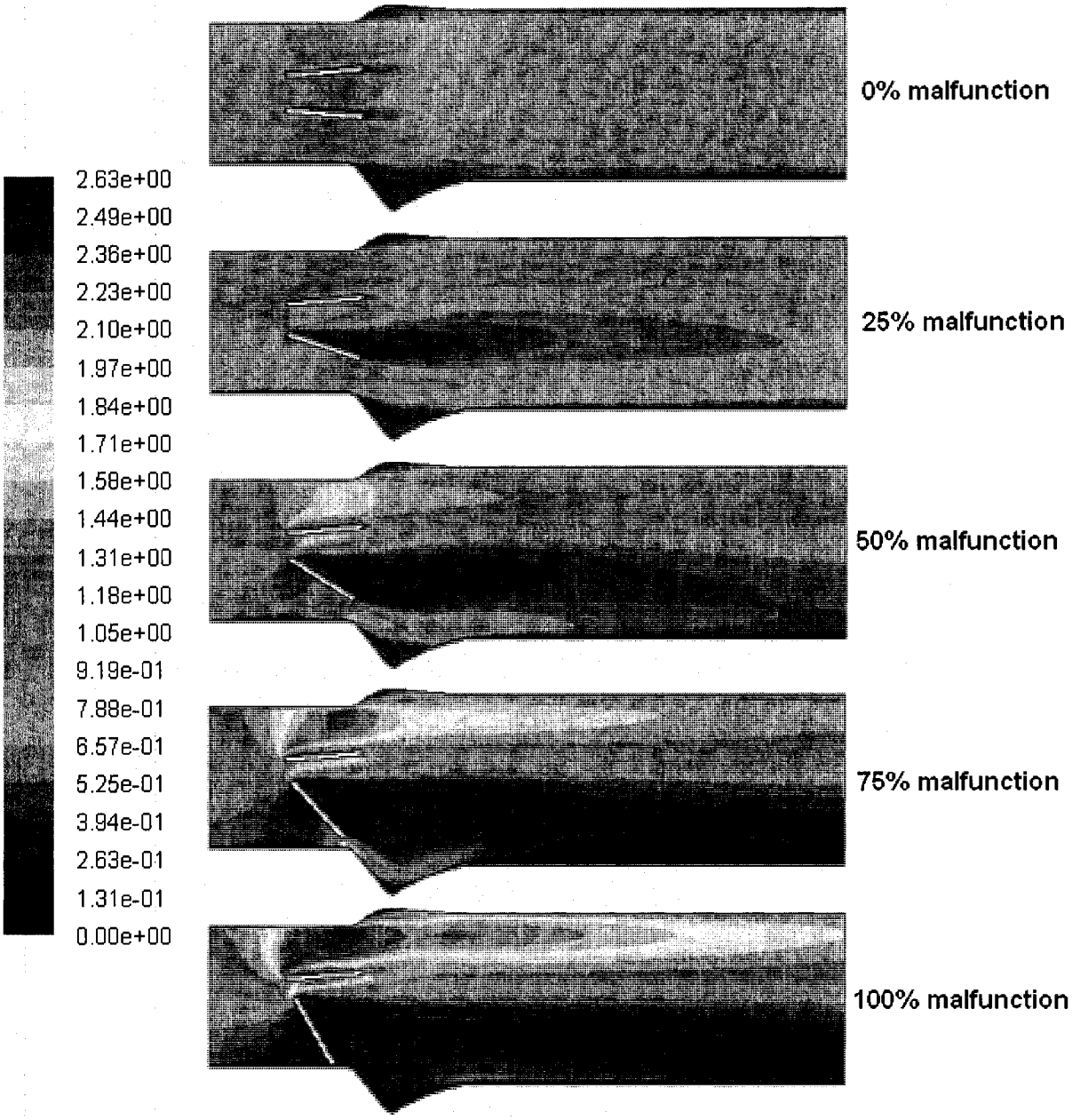

Figure 3.7 Velocity magnitude (m/s) contours for different percentages of valve malfunction at Q = 7L/min.

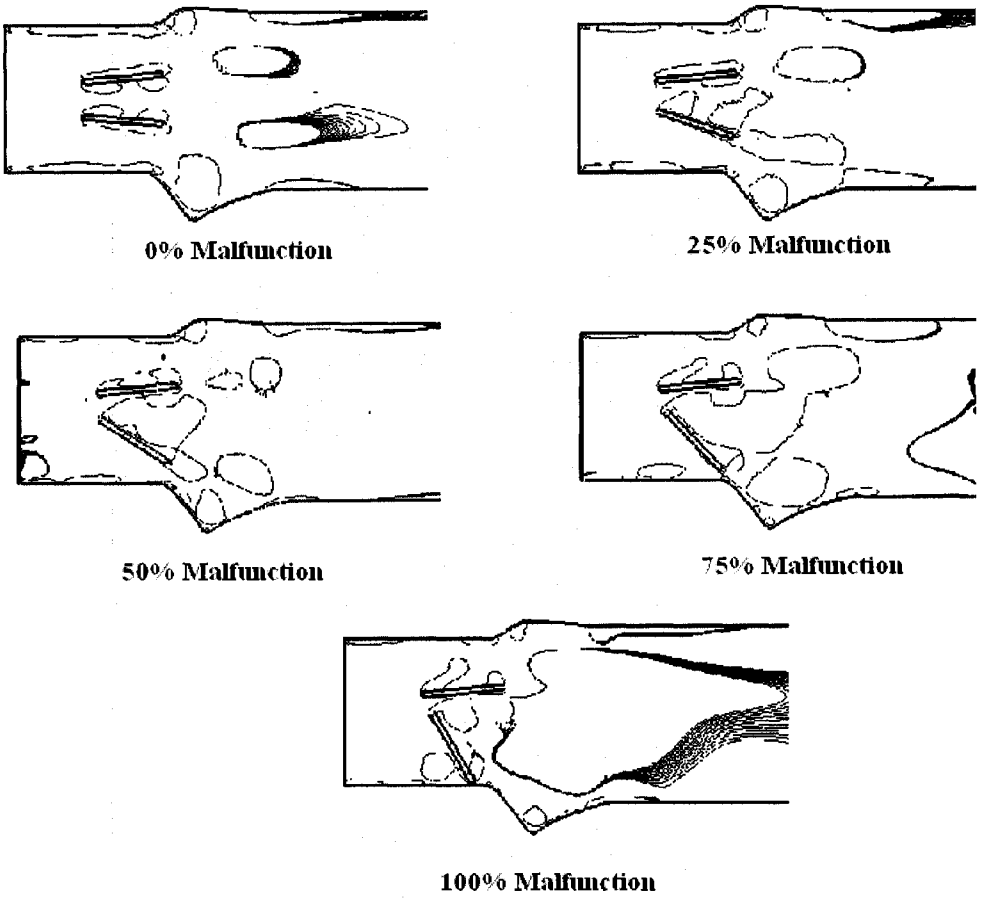

Figure 3.8 Coherent structures downstream of a normal and a defective mechanical valve for 7 L/min (using the λ_2 criterion).

In the healthy model, the velocity profiles are in good agreement with the experimental data obtained by Grigioni et al. (2001) on a St-Jude 19 mm valve, as shown in figure (3.10). For the defective valve, it is important to notice that applying a flat velocity profile few diameters upstream from the valve as an inlet condition for the numerical simulations is not realistic, since the flow is disturbed well before reaching the defective valve; this should also be the case for other obstacles such as a subaortic stenosis (Guivier et al., 2007).

Figure 3.11 shows the position of the maximal velocity for 5 L/min and 7L/min, respectively for different percentages of valve malfunction. During Doppler echocardiography the probe is usually aligned with the valve to let the ultrasound wave beam to pass through the central orifice as the maximum velocity is expected to be at that position. However, from Figure 3.9, this hypothesis seems to be applicable only for healthy or slightly defective valve (25% malfunction). On the contrary, the maximum velocity position started to shift to the lateral side when the severity of valve malfunction increases over 50%. Figure 3.12 shows the difference between average velocity and maximum velocity values for different flow rates and different percentages of valve malfunction. The deviation percentage was independent of flow rates and was only a function of the percentage of malfunction. The maximum deviation was (132.3%). As a consequence, the assumption of a flattened velocity profile downstream of the valve, as used to determine the effective orifice area by Doppler echocardiography, is not applicable for a defective valve.

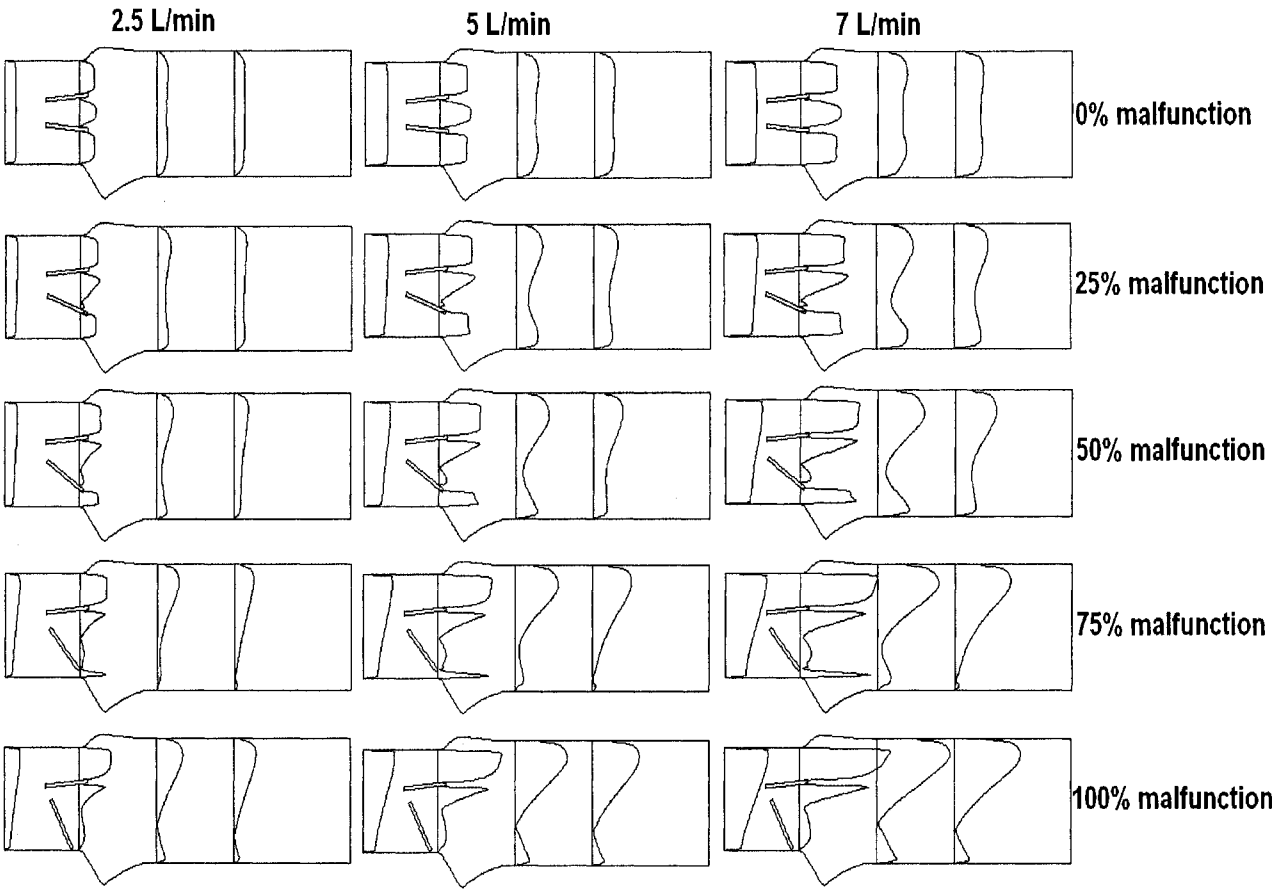

Figure 3.9 Velocity profiles at the inlet, valve section, 1D downstream of the valve and 2D downstream of the valve for different percentages of valve malfunction and different flow rates.

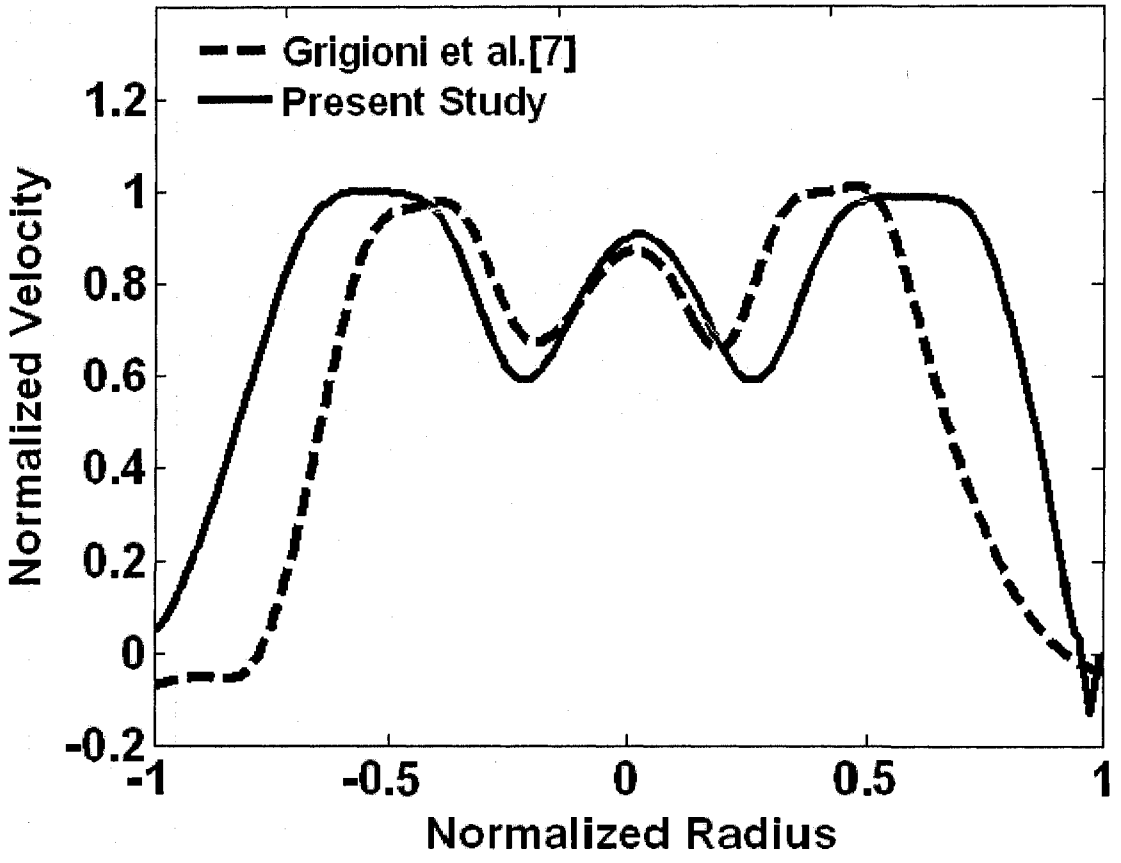

Figure 3.10 Comparison between the normalized velocity profiles at 7 mm downstream of the valve obtained.

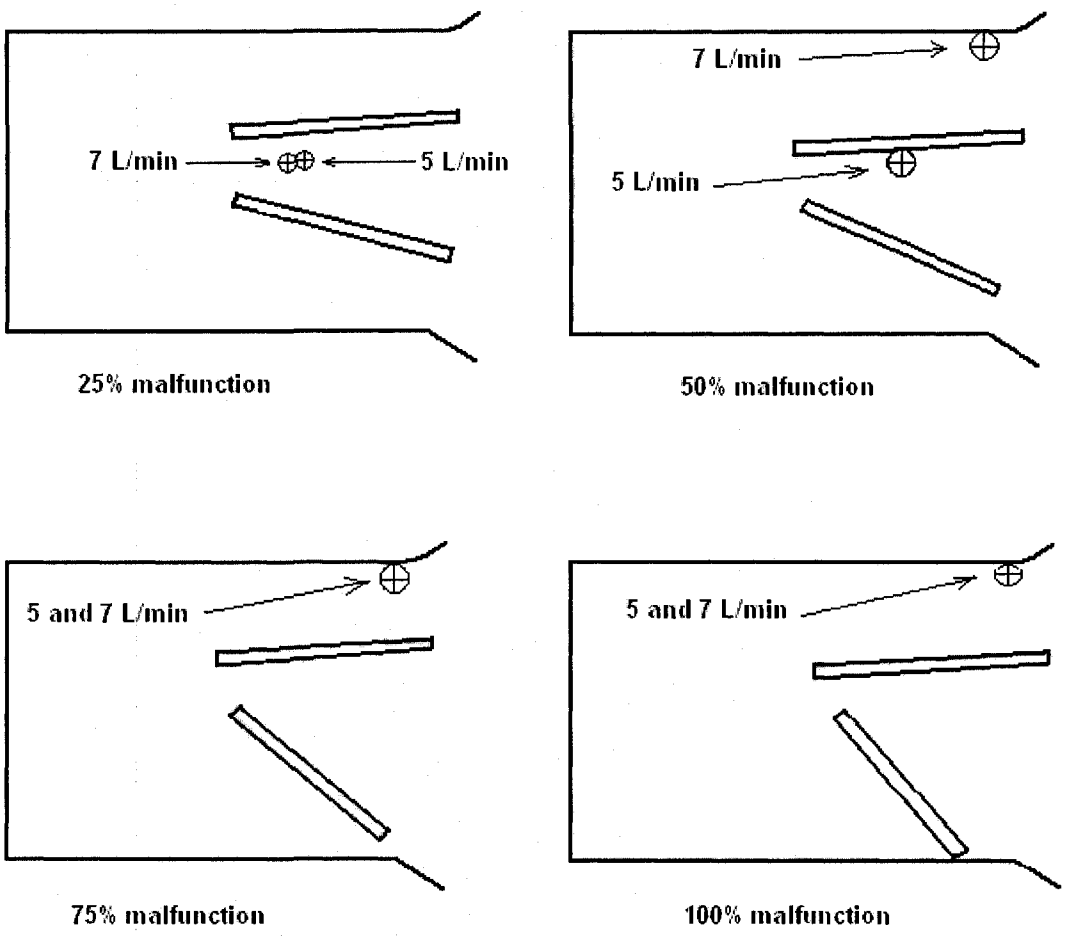

Figure 3.11 Maximal velocity position at Q = 5 and 7 L/min for different percentages of valve malfunction.

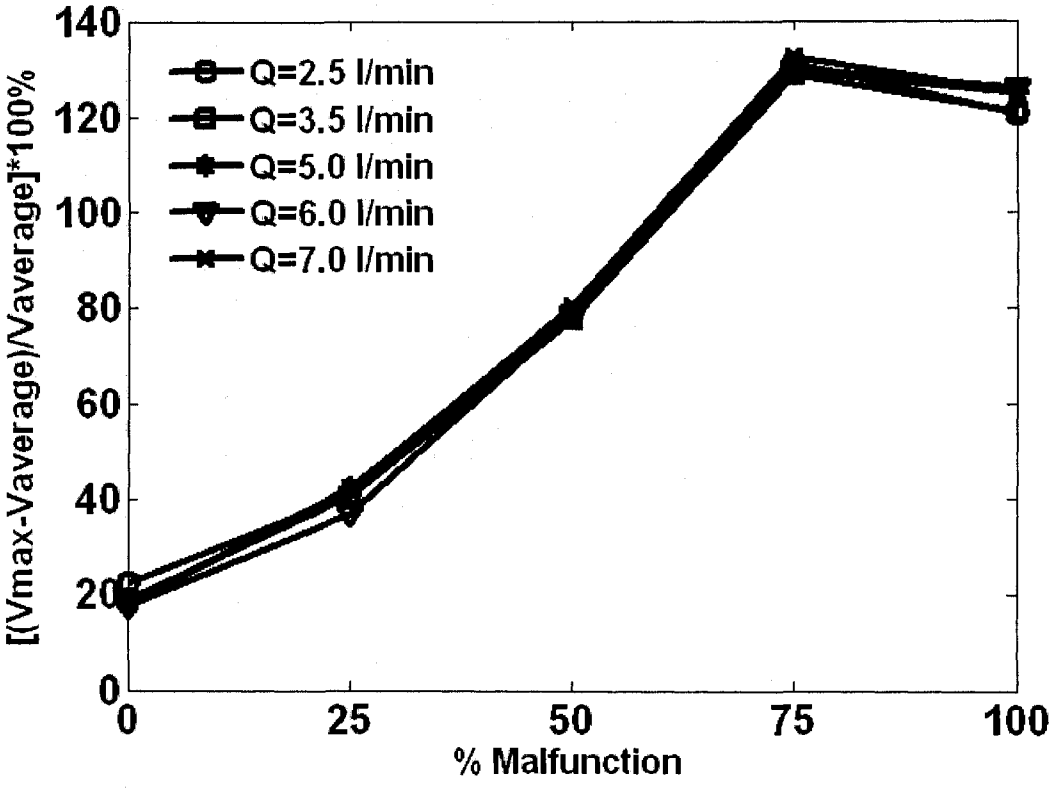

Figure 3.12 The percentage of deviation between the maximal velocity (V_{max}) and the average velocity at 1D downstream of the valve for different percentages of valve malfunction and different flow rates.

3.4.2 Transvalvular Pressure Gradient

Figures 3.13 and 3.14 show the simulated Doppler echocardiographic transvalvular pressure gradient (TPG_{Dop}) obtained using the simplified Bernoulli equation ($TPG_{Dop} = 4V^2$); where: TPG_{Dop} is the transvalvular Doppler pressure gradient (mmHg) and V is the maximal velocity (m/s) (supposed to be at the vena contracta downstream of the valve).

TPG_{Dop} in Figure 3.13 was determined based on the maximal velocity at the center line of the model. The maximum TPG_{Dop} was 11.93 mmHg for Q = 7 L/min and 100% malfunction. In Figure 3.14, TPG_{Dop} was determined, now, using the maximal velocity in the entire field, simulating a conical ultrasound beam. The maximum TPG_{Dop} was, in this case, 27.56 (mmHg) for Q = 7 L/min and 100% malfunction. Figure 3.15 a & b shows the transvalvular pressure gradient, as measured by catheterization (TPG_{Cat}), for different percentages of valve malfunction and different flowrates between the inlet and 1D and 2D downstream of the valve respectively. The TPG_{Cat} 1D downstream of the valve (Figure 3.15.a) was 16.38 mmHg and 14.99 mmHg 2D downstream of the valve (Figure 3.15.b) (Q = 7 L/min and 100% malfunction).

The difference between TPG_{Dop} and TPG_{Cat} is a manifestation of pressure recovery phenomenon. Interestingly, the correlation between TPG_{Dop} and TPG_{Cat} is improved with the increase in valve malfunction (Figure 3.16). This is in agreement with the previous in vitro study performed by Baumgartner et al. (1993) and can be explained by a more important energy loss downstream of the valve induced by a more severe malfunction.

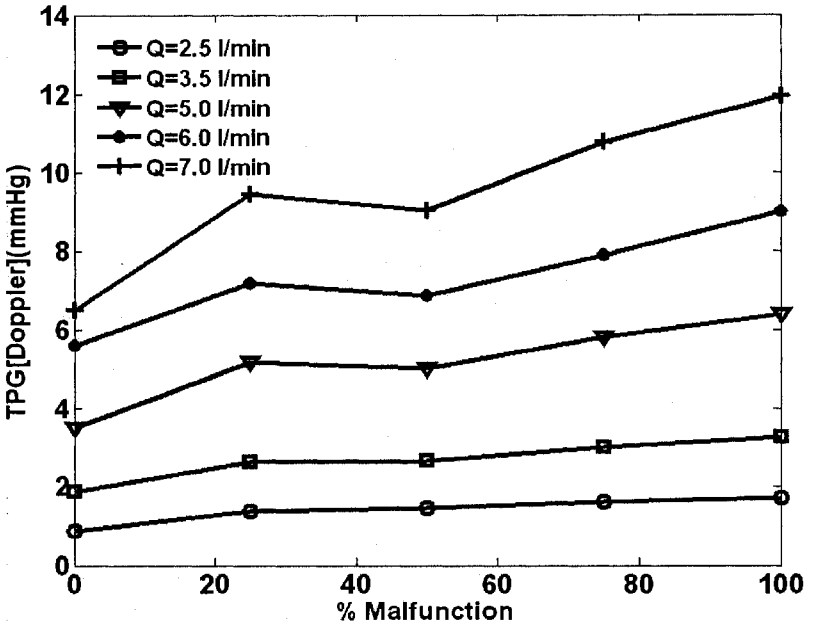

Figure 3.13 Doppler transvalvular pressure gradient using the maximum velocity through the center line.

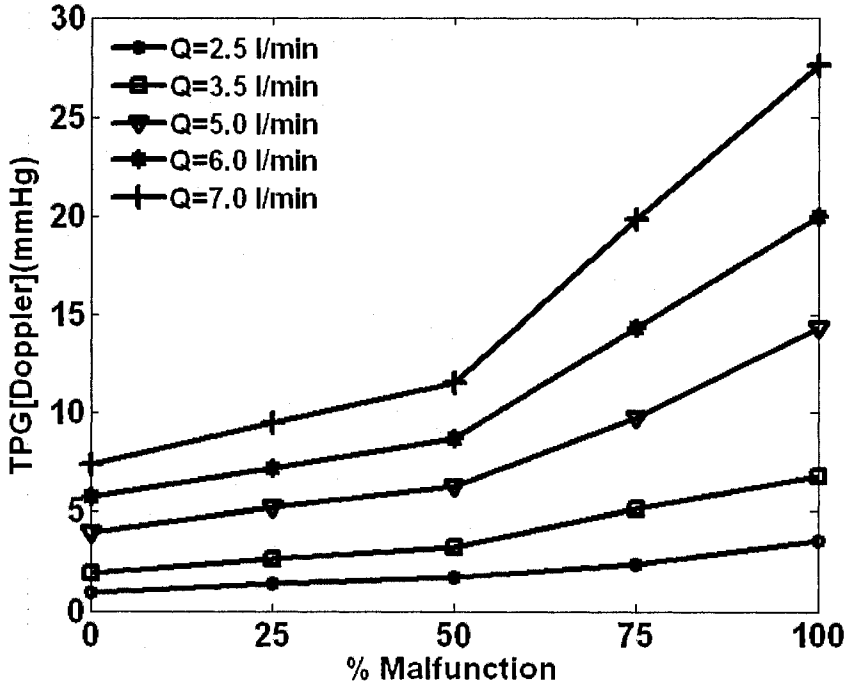

Figure 3.14 Doppler transvalvular pressure gradient using the maximum velocity through the entire field.

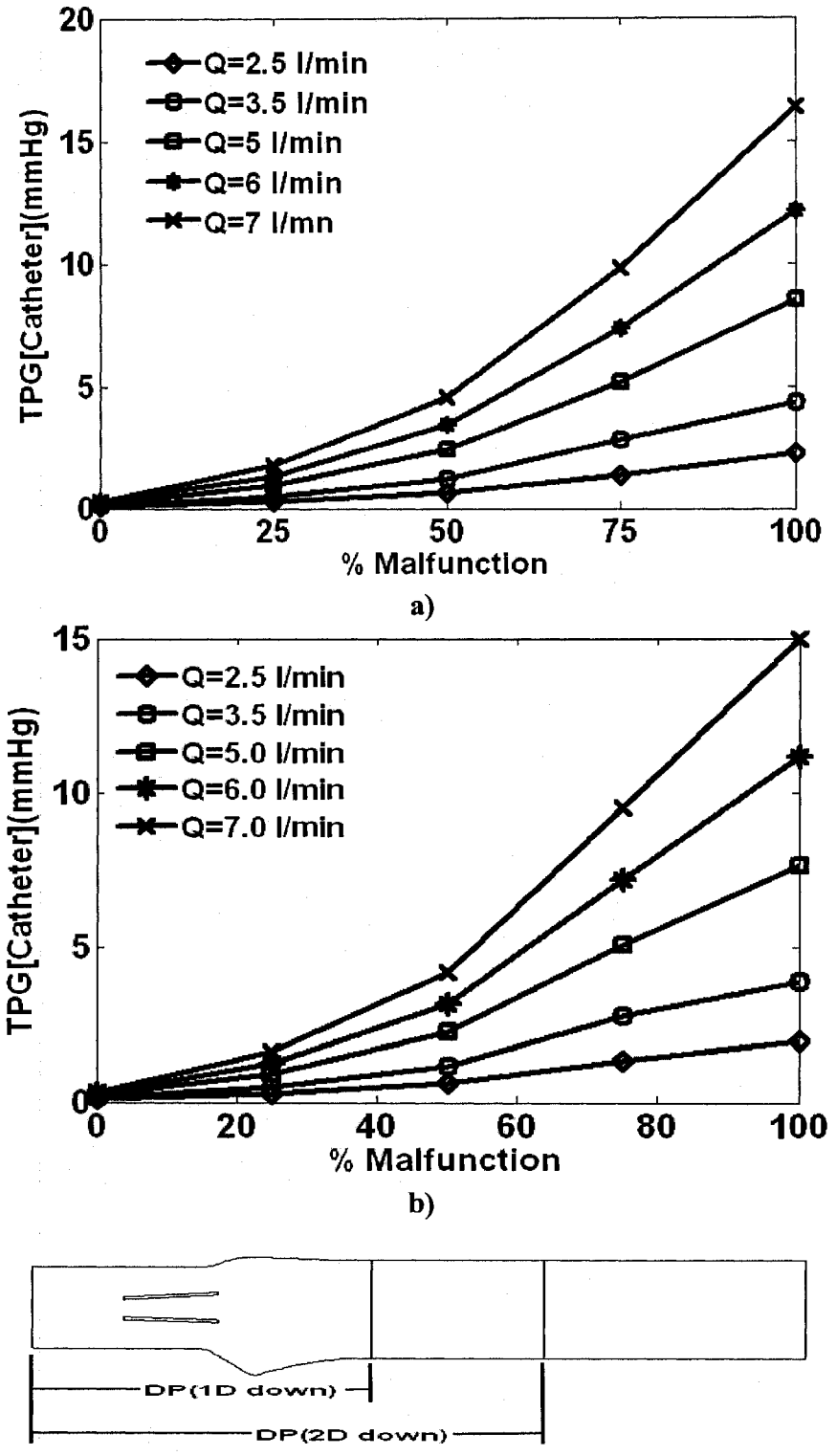

Figure 3.15 (a, b) Catheter transvalvular pressure gradient a) 1D downstream of the valve , and b) 2D downstream of the valve.

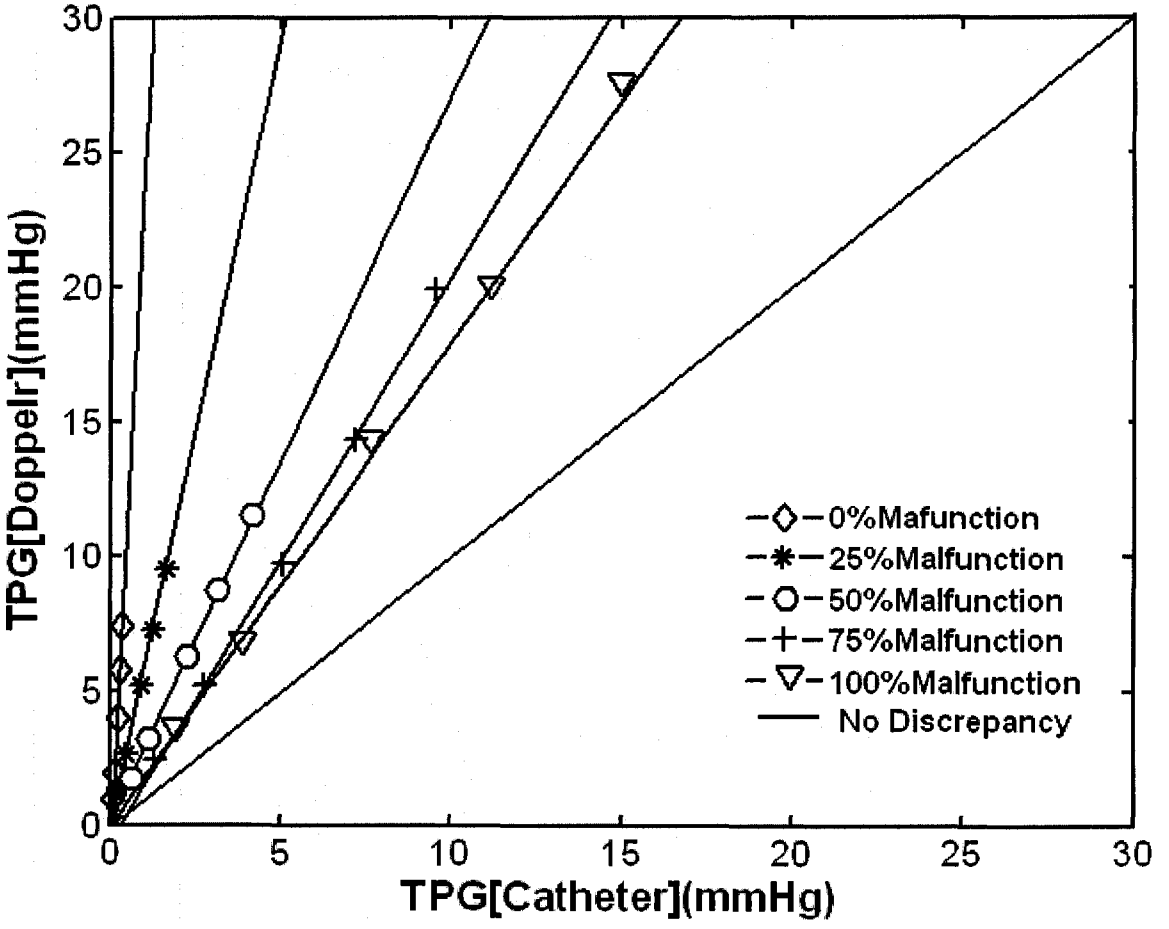

Figure 3.16 Correlation between Doppler transvalvular pressure gradient and catheter transvalvular pressure gradient.

3.4.3 Reynolds Turbulent Shear Stress (TSS)

Figures 3.17 and 3.18 show Reynolds turbulent shear stress in the entire field for 5 L/min and 7 L/min respectively. Five different cases of malfunction have been considered for each flowrate. The TSS was obtained as [9]:

$$TSS = -\rho\overline{u'v'} = \mu_t\left(\frac{\partial u}{\partial y} + \frac{\partial v}{\partial x}\right)$$

where ρ the blood density (kg/m^3), u is the axial velocity (m/s), v is the radial velocity (m/s) and μ_t is turbulent viscosity kg/m s. For both flowrates (Q = 5 and 7 L/min) the maximum TSS was observed when the leaflet was completely closed (100% malfunction).

The maximum TSS were 122 Pa and 205 Pa for Q = 5 L/min and Q = 7 L/min respectively. TSS was dominant in the wake of the leaflet, close to the trailing edge of each leaflet and the lower sinus region. As the percentage of malfunction increased, the dominant regions for the TSS started to be shifted towards the upper side of the valve and through the central orifice until the malfunction reached 100%, then; TSS had its highest value around the upper side of the normal leaflet.

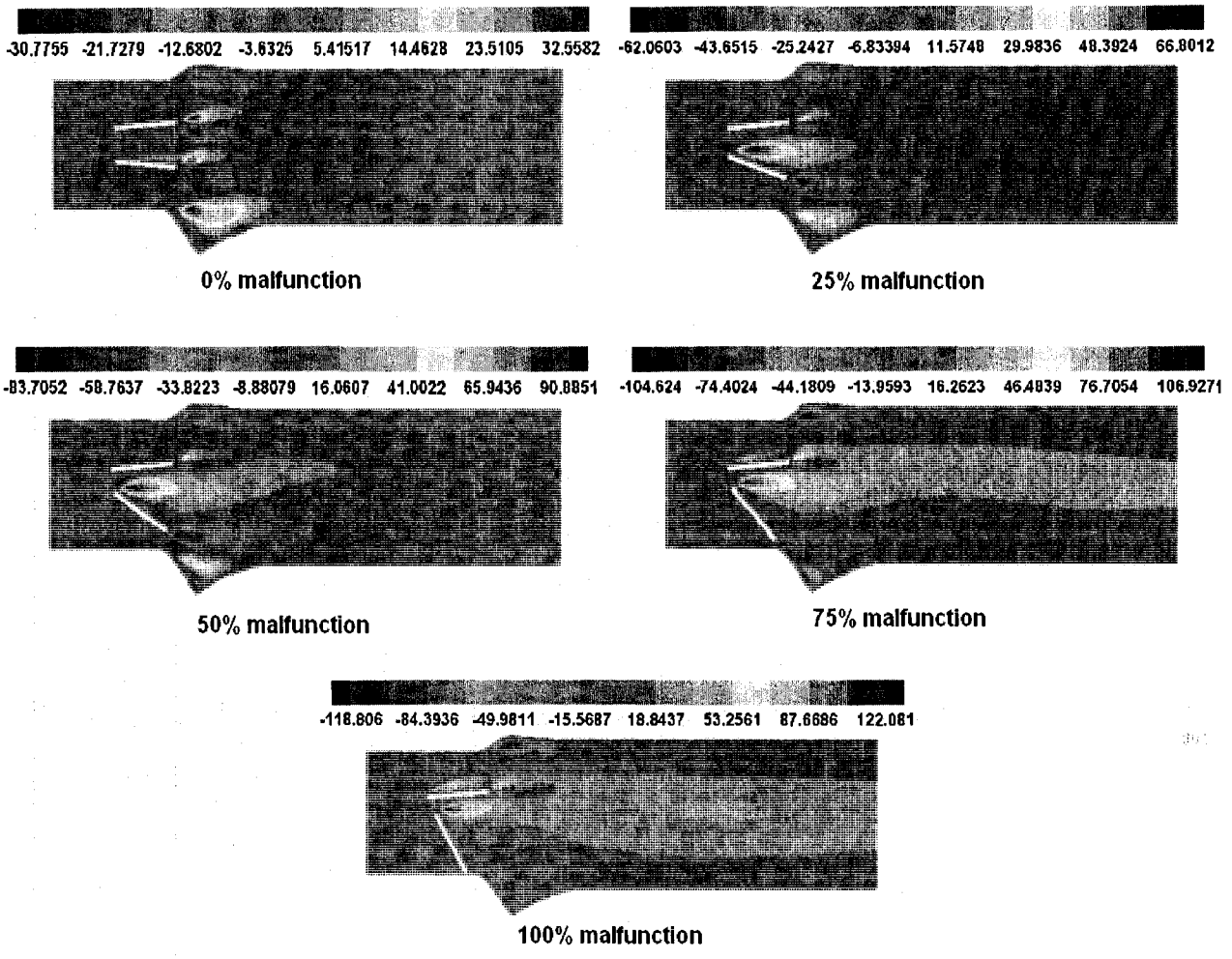

Figure 3.17 Turbulent shear stress (Pa) at Q = 5 L/min for different percentages of valve malfunction.

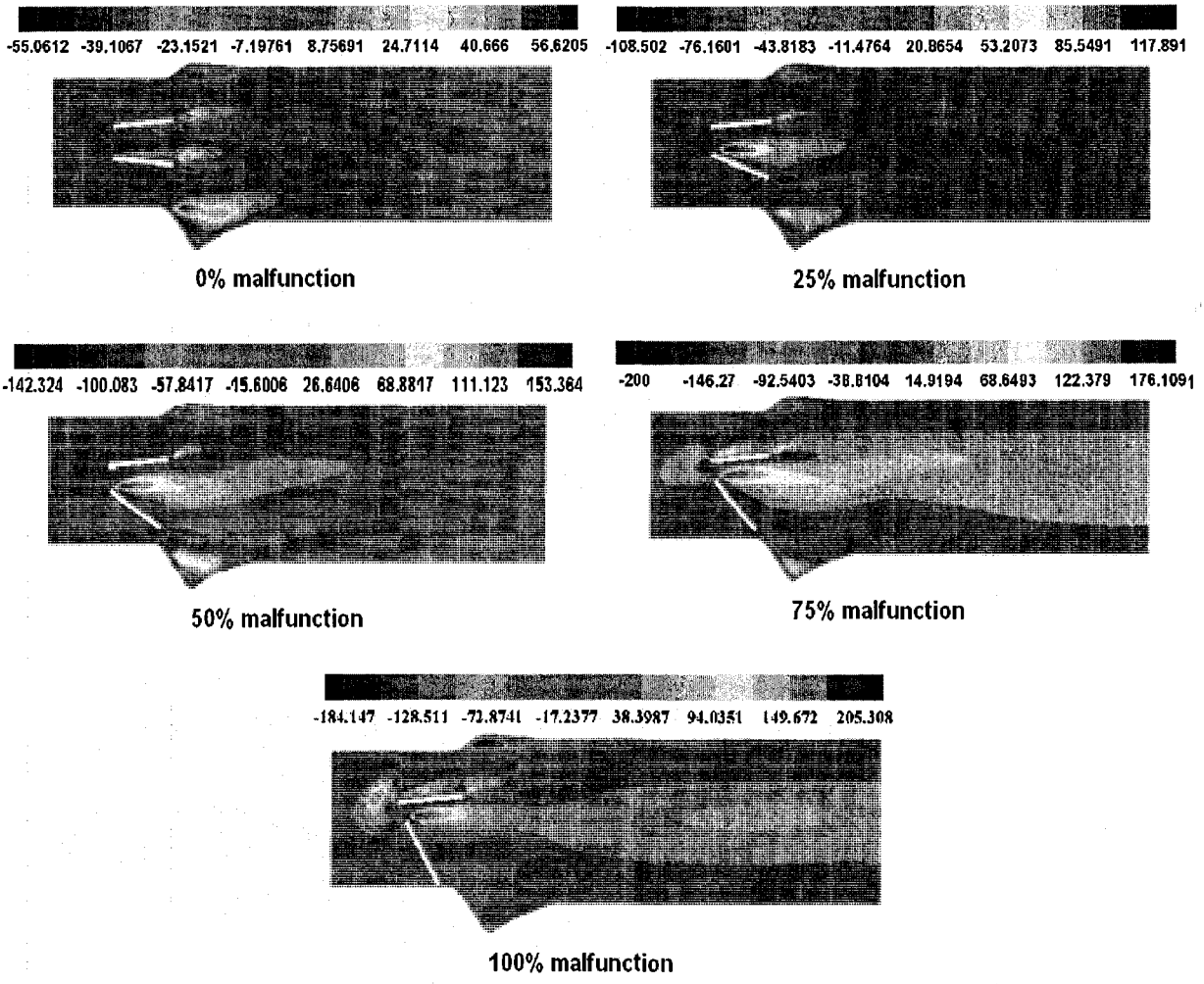

Figure 3.18 Turbulent shear stress (Pa) at Q = 7 L/min for different percentages of valve malfunction.

3.5 Discussion

3.5.1 Boundary Conditions

In general, the assumption of a flat profile (or a constant velocity) is commonly used as an inlet condition in steady and unsteady investigations of the flow through native and prosthetic valves (Ge et al., 2003 and Grigioni et al., 2005). Although this assumption is reasonable in healthy models, it seems to be questionable for defective mechanical valves. Indeed, the velocity profile upstream from the valve is highly dependent upon the percentage of valve malfunction or the presence of any obstruction to the flow such a subaortic stenosis (Guivier et al. 2007). Therefore, it is more realistic to use the pressure difference between the inlet and outlet sections especially when simulating defective valve models. Furthermore, the weakness of the flattened assumption in defective mechanical heart valves raises a question concerning the precision of flow rate determination using pulsed wave Doppler upstream from the valve.

3.5.2 Proposed Diagnosis Techniques

3.5.2.1 Doppler echocardiography

Figure 3.19 shows the ratio between the increase in TPG_{Dop} and the increase in flow rate for different percentages of valve malfunction. The flow rate difference was taken for three cases; 5 L/min, 6 L/min and 7 L/min, simulating a normal case and an increase in flow rate induced by dobutamine injection or exercise. In the healthy valve this ratio was less than 2 for the all cases. Between 25% and 50% malfunction, the ratio increased slightly up to 3. Then, for higher malfunctions, the ratio increased rapidly to reach a maximal value between 5.5 and 7.5 for 100% malfunction. This ratio can be a very

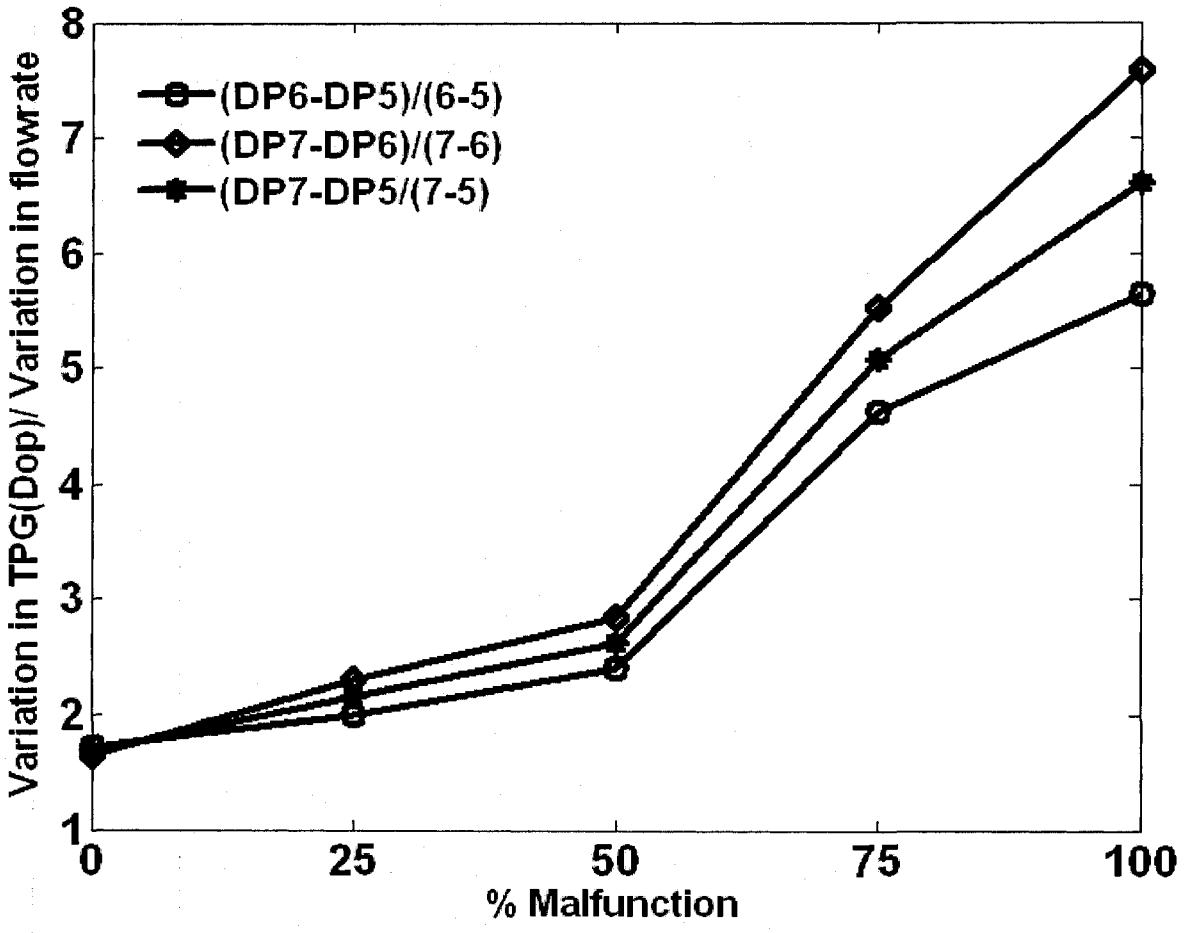

Figure 3.19 Variation in Doppler transvalvular pressure gradient over the variation in flow rate for different percentages of valve malfunction. (TPG_{Dop} is based on the maximal velocity in the entire field).

interesting parameter to early detect a valve malfunction.

3.5.2.2 Magnetic Resonance Imaging

Figure 3.20 shows the ratio between the maximal velocity in the lateral non obstructed orifice and the maximal central orifice velocity, for different flow rates and valve malfunctions. It is very interesting to note that this parameter is flow independent, which allow its potential application in a wide range of patients. As this parameter requires the velocity profile downstream of the valve, it can only be applied in vivo using phase contrast magnetic resonance imaging. A ratio > 1 should be an indication of a potential valve malfunction.

3.5.3 Clinical Complications

The non-physiological flow induced by the presence of the defective mechanical valve is responsible of a significant increase in Reynolds shear stress level, as a consequence, this might lead to platelet activation and red blood cells damage. Platelet activation is the major vector for thrombus formation in healthy mechanical heart valves and this activation occurs at lower shear stress than the ones required for blood hemolysis. A TSS magnitude of 400 N/m^2 and exposure time of 1ms, are commonly used as thresholds for hemolysis (Sallam et al., 1984), however many studies have given different other values (Lu et al., 2001). In this study, the TSS was elevated around fourth times in the case of 100% malfunction compared to healthy case. This will potentially lead to a significant platelet activation and thrombus formation. However, it should be noted that other parameters (other than TSS and exposure time) might play a significant role in platelet

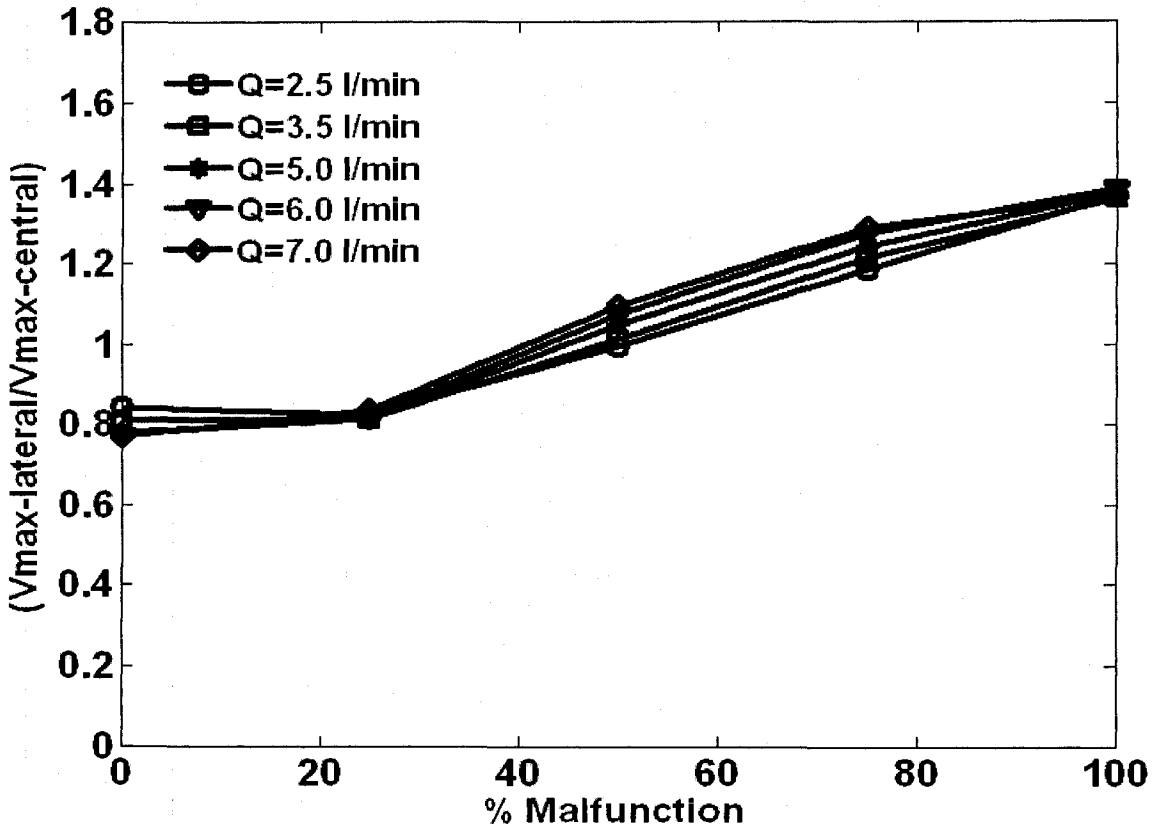

Figure 3.20 Ratio between the maximal lateral jet velocity and the maximal central jet velocity for different flow rates and valve malfunctions.

activation and blood hemolysis, such: shear exposure history, temperature, concentration of red blood cells and plasma components (Kameneva et al., 2004).

3.6 Conclusion

In this chapter, the flow dynamics through a defective mechanical valve under steady state conditions, as a first approach, has been investigated. Discrepancies between Doppler echocardiographic and catheter transvalvular pressure gradients and the failure in the detection of mechanical valve malfunctions were clarified. Furthermore, two potential non-invasive methods, using Doppler echocardiography and magnetic resonance imaging, were proposed for an early detection of mechanical valve malfunction. The effect of such valve malfunction on blood components has also been investigated, and it appeared that it has a significant impact on platelet activation and, as a consequence, on thrombus formation.

Finally, more experimental and numerical studies on defective mechanical heart valves need to be conducted to give a clear idea about the blood hemodynamics and to improve the proposed diagnostic techniques to help clinicians to take the optimal decision.

Chapter 4

Blood Flow through a Defective Mechanical Heart Valve: a Pulsatile Flow Analysis

4.1 Introduction

Valve stenosis or incompetence at severe levels reduce the performance of the heart and place additional stress and strain upon it. In many cases, therefore, surgical replacement of the diseased valve with a bioprosthetic or Mechanical Heart Valves (MHV) is necessary to restore normal heart function. Although the lifelong anticoagulant medication and the possible clinical complications (e.g. blood elements damage and/or thrombus formation), bileaflet MHV are the most commonly implanted valves with over 170,000 implants worldwide each year as a result of high durability and appropriate characteristics for blood hemodynamics (in terms of low pressure gradient and relatively low shear stress level with respect to other MHV types) (Yoganathan et al., 2005).

Unfortunately, in some cases, thromboembolic and/or pannus formation complications are possible after bileaflet valve implantation. Thrombus and/or pannus formation can restrain one or both valve leaflets from moving freely, leading to a valve malfunction. Even though the preponderance of such malfunctions is relatively low (0.2%-6% per patient-year), they are considered as life-threatening events. It is, therefore, extremely important to pay attention to the clinical complications that will accompany valve malfunction and to define non invasive parameters capable of early detecting it (Montorsi et al., 2003).

Recently, Computational Fluid Dynamics (CFD) came into view as a robust tool in arterial blood flow studies. While the majority of numerical simulations of blood flow through aortic MHV have been conducted based on laminar flow assumption (Ge at al., 2003, Grigioni et al., 2005, and Guivier et al., 2007), recently some studies have begun to explore turbulent or transitional blood flow through MHV. In order to find the onset of turbulence in physiological pulsatile flow, Peacock et al. 1997 studied experimentally the pulsatile fluid flow in a straight tube and concluded that the critical Reynolds number is correlated with both Strouhal (St) and Womersley (α) numbers.

Although the laminar-transitional-turbulent nature of blood flow through a MHV, the Wilcox's low-Reynolds model was found able to accurately predict its main flow characteristics (Bluestein et al., 2000). To address the remarkable changes in blood hemodynamics and the clinical complications and to emphasis the importance of early detecting a valve malfunction, the realistic pulsatile physiological blood flow through a defective valve was simulated in normal function and in various states of malfunction by using commercial software (Fluent 6.3.26 - Fluent Inc.; Lebanon; NH; USA) and by adapting transitional turbulence model. Dramatic changes in turbulent shear stress level and vortex formation and shedding and high value of wall shear stress were observed as a result of increasing valve malfunction severity.

4.2 Models and methods

Five 2-D models were created in the current study. Only the lower leaflet of the MHV was moved from fully opened position (85°; 0% malfunction) to fully closed position

(30°; 100% malfunction) with three equally spaced intermediate angles: 71.25° (25% malfunction), 57.5° (50% malfunction) and 43.75° (75% malfunction). As shown in Figure 4.1, non symmetric sinuses were modeled based on the in vivo study performed by Reul et al. (1990) and used in vitro by Grigioni et al. (2001). For the upstream and downstream sections, the lengths were 10D and 4D, respectively. The bileaflet mechanical valve was modeled based on a 25 mm St. Jude Medical Hemodynamic Plus valve. Therefore, the inner diameter was 22.3 mm. The hinge mechanism of the valve has been neglected and this valve has been chosen since it is the most commonly implanted clinically. It should be noted that the current study focuses only on one blocked leaflet, since this case is more complex to be detected when compared to the case where both leaflets are blocked (Montorsi et al., 2003).

4.2.1 Turbulence model

Time-averaging or Reynolds averaging has been used as a means of analyzing turbulence by separating fluctuating properties with their time-mean values. Thus, the true velocity (u_i) is defined by: $u_i = \overline{u}_i + u_i'$, where the overbar refers to time-average and prime refers to fluctuation from this average. When this is substituted in the general Navier-Stokes equations, a new term will be introduced, i.e., the Reynolds stresses ($-\rho\overline{u_i'u_j'}$). To close the governing equations with the new extra variables, in present study, two-equation transitional $k-\omega$ model was used through which these Reynolds stresses are approximated using the Boussinesq relation for incompressible flow [Wilcox 1998]

$$-\rho\overline{u_i'u_j'} = \mu_t\left(\frac{\partial u_i}{\partial x_j}+\frac{\partial u_j}{\partial x_i}\right)-\frac{2}{3}\left(\rho k+\mu_t\frac{\partial u_i}{\partial x_i}\right)\delta_{ij} \tag{4.1}$$

where u_i is the average velocity in i direction and μ_t is the turbulent eddy viscosity and k is the turbulent kinetic energy. Using transitional k-ω model, the eddy viscosity is modeled as

$$\mu_t = \alpha^* \left(\frac{\rho k}{\omega} \right) \tag{4.2}$$

where ω is the specific dissipation rate and α^* is the low-Re correction factor which is computed from

$$\alpha^* = \alpha_\infty^* \left(\frac{\alpha_0^* + \mathrm{Re}_t / R_k}{1 + \mathrm{Re}_t / R_k} \right) \tag{4.3}$$

where $\mathrm{Re}_t = \rho k / \mu\omega$, $R_k = 6$, $\alpha_0^* = \beta_i / 3$, $\beta_i = 0.072$ and $\alpha_\infty^* = 1$.

k and ω are solved by two-equation $k - \omega$ model

$$\rho \frac{\partial(k)}{\partial t} + \rho u_j \frac{\partial}{\partial x_j}(k) = \frac{\partial}{\partial x_j} \left((\mu + \sigma^* \mu_t) \frac{\partial k}{\partial x_j} \right) - \rho \overline{u_i' u_j'} \frac{\partial u_i}{\partial x_j} - \rho \beta^* f_{\beta^*} k\omega \tag{4.4}$$

$$\rho \frac{\partial(\omega)}{\partial t} + \rho u_j \frac{\partial}{\partial x_j}(\omega) = \frac{\partial}{\partial x_j} \left((\mu + \sigma \mu_t) \frac{\partial \omega}{\partial x_j} \right) - \rho \overline{u_i' u_j'} \frac{\partial u_i}{\partial x_j} (\alpha \frac{\omega}{k}) - \rho \beta \, f_\beta \, \omega^2 \tag{4.5}$$

where $\sigma^* = \sigma = 0.5$ and $\beta = 0.09$.

For k-equation, β^* and f_{β^*} are given by

$$\beta^* = \beta_\infty^* \left(\frac{4/15 + (\mathrm{Re}_t / R_\beta)^4}{1 + (\mathrm{Re}_t / R_\beta)^4} \right) \tag{4.6}$$

$$f_{\beta^*} = \begin{cases} 1 & \chi_k \le 0 \\ \dfrac{1+680\chi^2{}_k}{1+400\chi^2{}_k} & \chi_k > 0 \end{cases} \tag{4.7}$$

where $\beta^*_\infty = 0.09$, $R_\beta = 8$ and $\chi_k \equiv \dfrac{1}{\omega^3}\dfrac{\partial k}{\partial x_j}\dfrac{\partial \omega}{\partial x_j}$

For ω-equation, α and f_b are given by

$$\alpha = \frac{\alpha_\infty}{\alpha^*}\left(\frac{\alpha_0 + \mathrm{Re}_t / R_\omega}{1 + \mathrm{Re}_t / R_\omega}\right) \tag{4.8}$$

$$f_\beta = \frac{1+70\chi_\omega}{1+80\chi_\omega} \tag{4.9}$$

where $\alpha_\infty = 0.52$, $R_\omega = 2.95$, $\alpha_0 = 1/9$, $\chi_\omega = \left|\dfrac{\Omega_{ij}\Omega_{jk}S_{ki}}{(\beta^*{}_\infty \omega)^3}\right|$

where $\Omega_{ij} = \frac{1}{2}(\frac{\partial u_i}{\partial x_j} - \frac{\partial u_j}{\partial u_i})$ and $S_{ij} = \frac{1}{2}(\frac{\partial u_j}{\partial x_i} + \frac{\partial u_i}{\partial u_j})$. Ω_{ij} and S_{ij} are the mean rotation and the mean strain rate tensors, respectively.

In the present work, a second-order upwind scheme was selected to be the discretization scheme for the convection terms of all governing equation. For all transient calculations, a second–order temporal discretization scheme was used. The mass-momentum equations were solved using the COUPLED solver and all results were converged to residuals of

less than 10^{-4}, unsteady simulation in general required 15-25 iterations per time step. The cardiac output was considered as 5 L/min and the heart rate as 70 bpm. The common values for blood density and dynamic viscosity were considered which were equal to 1000 kg/m^3 and 0.0035 Pa.s, respectively. Furthermore, typical physiological cardiac cycle was considered as inlet condition as shown in Figure 4.1 and ambient pressure was considered as outlet condition.

Steady flow simulations were conducted first to establish the grid density. Moreover, additional care was made close to the wall and leaflets surfaces to maintain ($y+ << 1$). The time step was set to 0.25 ms to satisfy time step independency. Three cycles were simulated before starting extracting the results in order to reach the periodicity. Finally, as the fluid-structure interaction between the valve leaflets and the fluid was not considered, and even though the simulations were conducted for the whole cardiac cycle, only the period during which the valve can be considered in fully open position (from 65 ms to 250 ms) was investigated.

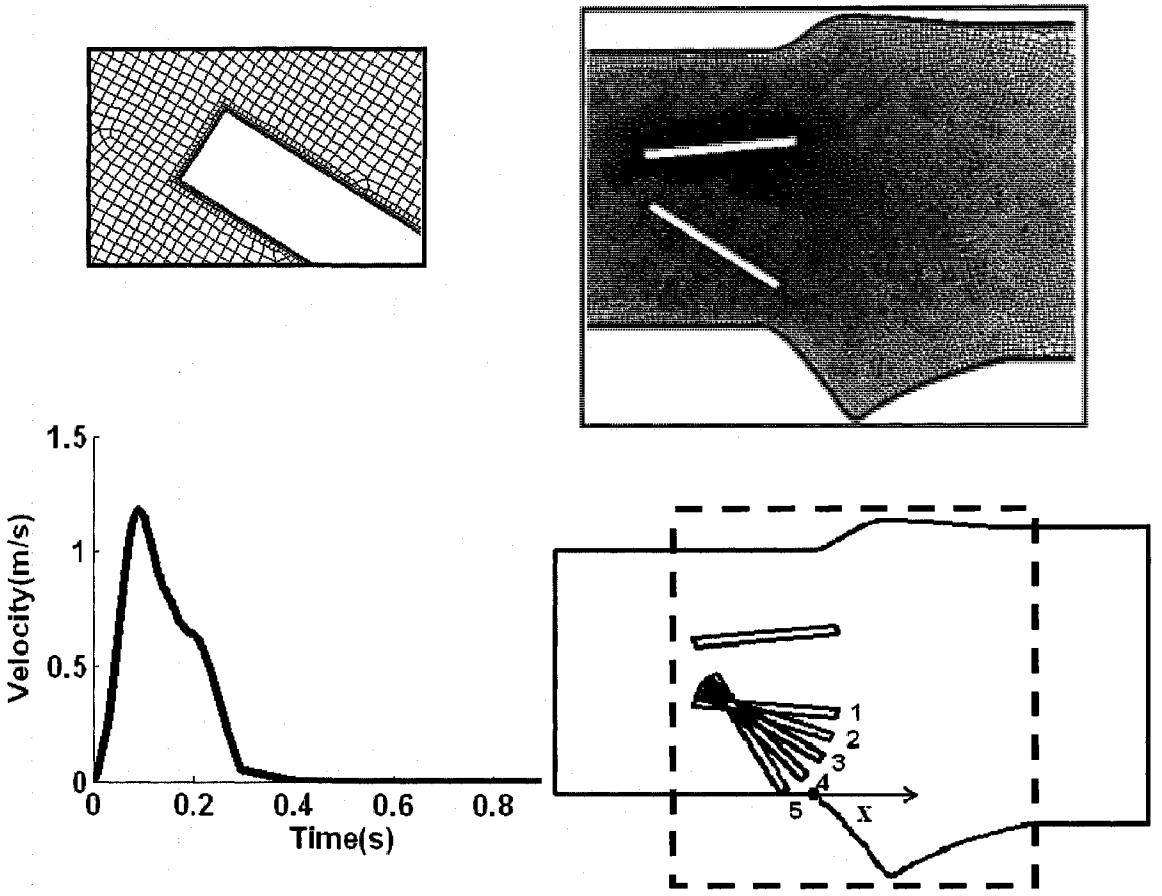

Figure 4.1 Models for the five different cases: 1) 0% malfunction; 2) 25% malfunction; 3) 50% malfunction; 4) 75% malfunction; 5) 100% malfunction. Mesh quality for the sinuses and leaflets is shown and the cardiac cycle which was adapted as the Inlet flow condition is also shown.

4.3 Time independence

In order to get the time independence, two different time steps were tested; 0.25 and 0.125 ms, respectively. The adapted time step in the current study was in consistence with Bluestein et al. (2000). In continuous flow study (chapter 3), the 75% malfunction was shown as the most critical case, therefore, the model with 75% malfunction has been chosen to be tested fro the time independence.

Figure 4.2 shows the velocity contours for 75% malfunction for the two different time steps. The percentage of difference in the maximal velocity in the whole domain between the considered time step (0.25 ms) and (0.125 ms) time step was around 2%.

Figure 4.3 shows the velocity profile across the root of aorta at the vicinity of the valve just before the sinus area. In this figure the interest is in the maximum velocity for each jet through the bileaflet valve orifices (one central and two laterals). The difference between the considered time step (0.25 ms) and (0.125 ms) time step at the peaks of three jets did not exceed 5%. And for the average velocity, the difference was around 0.01%.

Figure 4.4 shows the wall shear stress at the lower wall. The lower wall represents the wall that will be highly affected by the valve malfunction due to the obstruction. The wall shear stress will be expected to be higher at this region comparing to the upper wall. Therefore, time independency checking was conducted only for the lower wall. The maximum difference along the wall was around 3%. While the difference between the average wall shear stresses was 0.01%.

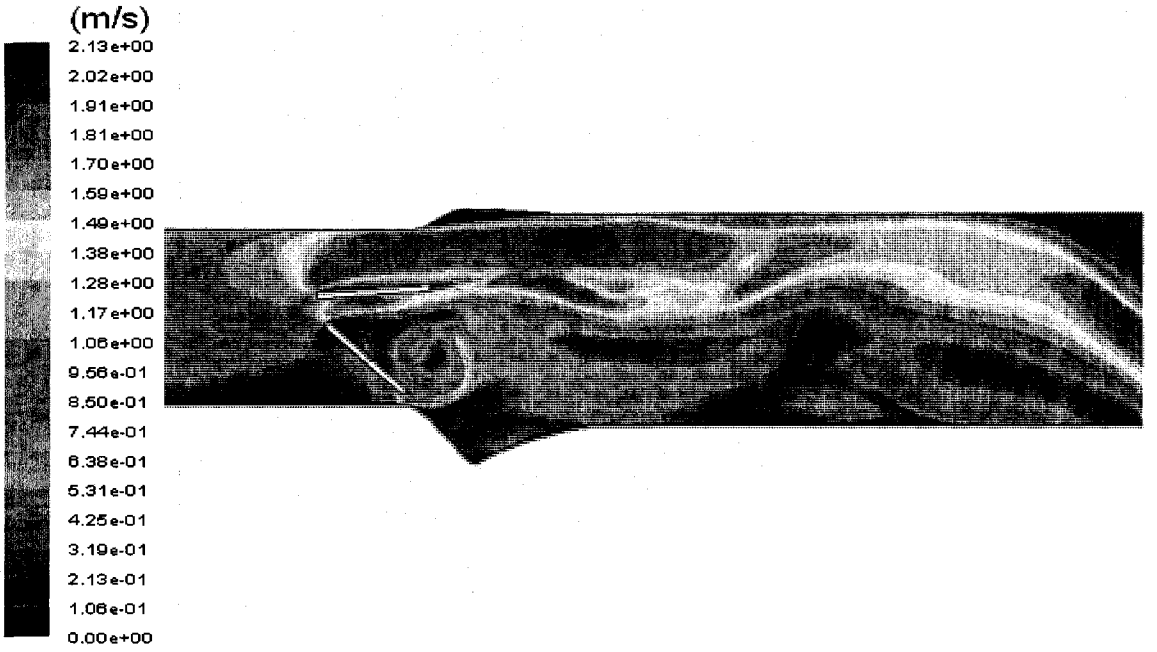

a)

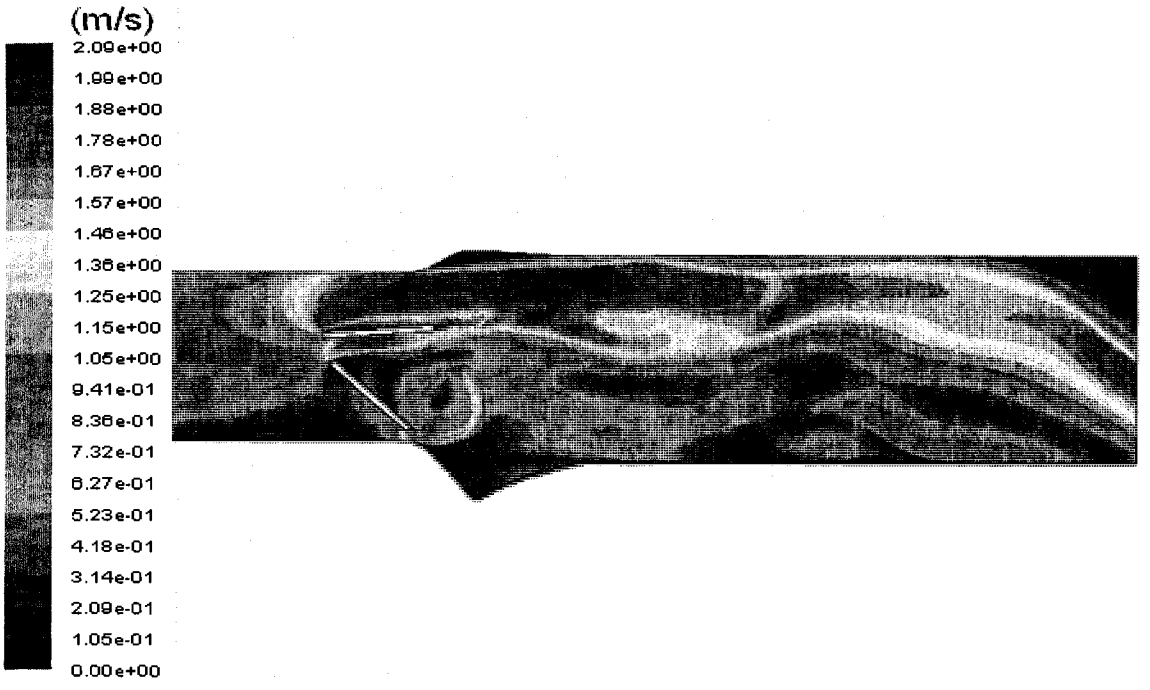

b)

Figure 4.2 Velocity contours (m/s) at 75% malfunction for time steps a) 0.25 ms and b) 0.125 ms.

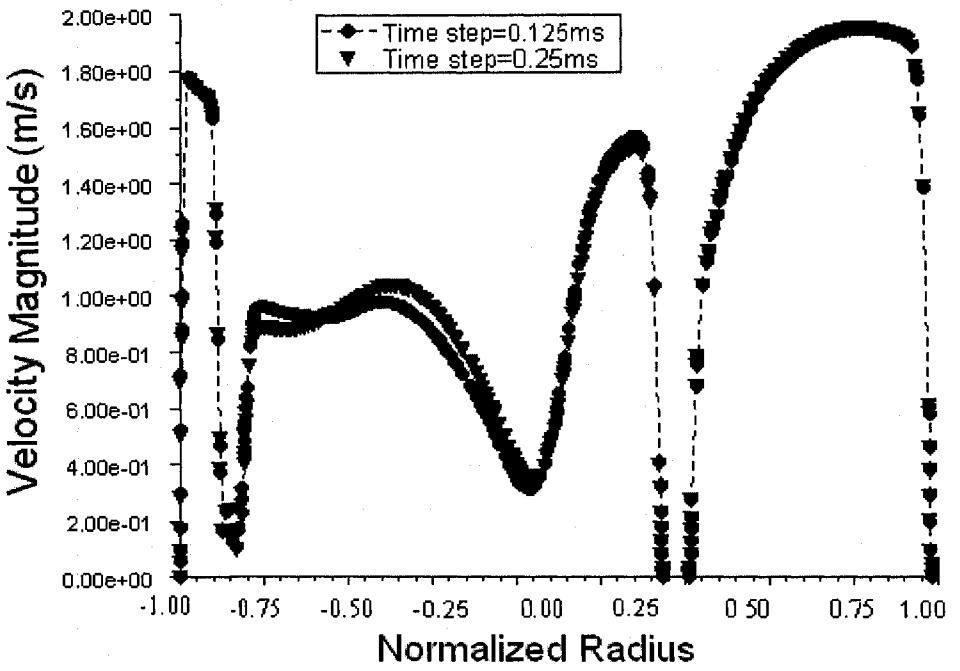

Figure 4.3 Velocity magnitude profiles (m/s) at the vicinity of the valve for 75% malfunction for time steps of 0.125 ms and 0.25 ms.

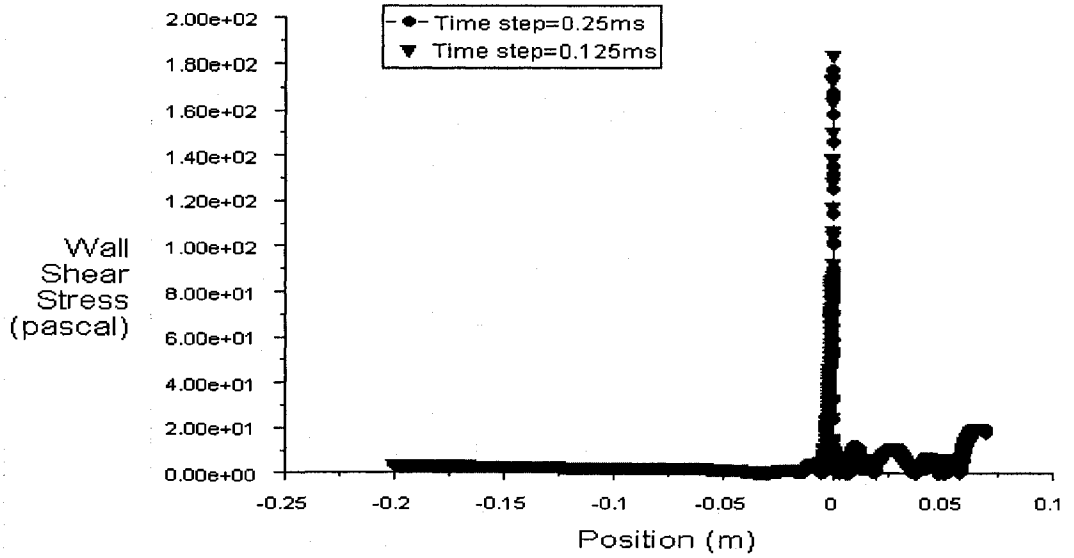

Figure 4.4 Wall Shear Stress (WSS) at lower wall for 75% malfunction for time steps of 0.125 ms and 0.25 ms.

4.4 Results

Figure 4.5 shows the velocity profiles in radial direction at the vicinity of the valve for different time instants and malfunctions. For 0% malfunction, a uniform three-jet configuration can be noticed (through central and lateral orifices) with maximum value at the peak of systolic phase. The three jets have almost the same maximal velocity which is consistent with the experimental work of Grigioni et al. (2001). During the acceleration and deceleration phases, the velocity trend and profile have almost the same shape by keeping three major jets. In the meantime, for 50% malfunction, three jets were still able to develop with a little shifting up in the central one. During the acceleration phase the distribution of the velocity profile was different from the one at the peak and deceleration phases. The velocity profiles for 100% malfunction shows only two major jets, one of them through the central orifice and the second through the upper lateral orifice, while the velocity jet through the lower lateral orifice almost vanished. During acceleration, peak and deceleration phases, the velocity profile for each malfunction showed almost the same trend.

Figure 4.6 presents the velocity profiles at the vicinity of the valve at the peak instant of the systolic phase for the three different malfunctions; 0%, 50% and 100 % malfunction where the maximum velocity magnitude was proportional to the percentage of malfunction (the higher the malfunction is the higher the maximum velocity magnitude). In addition, the flow became more laterally when the malfunction was present.

0% malfunction

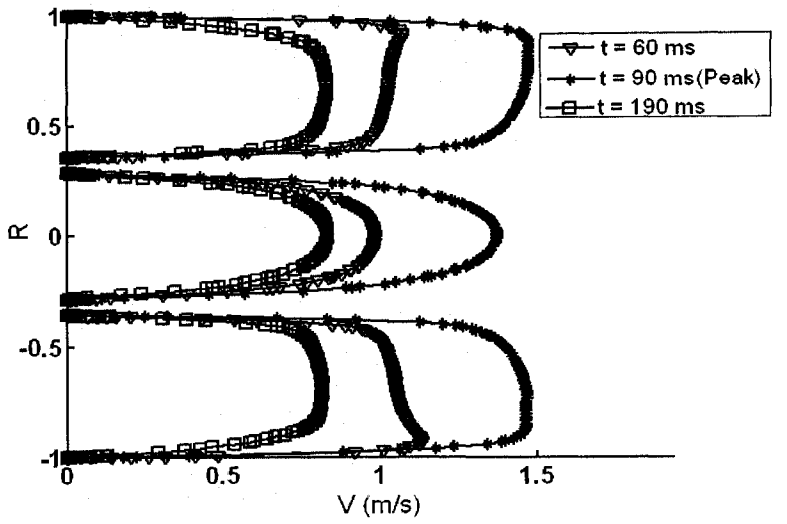

50% malfunction

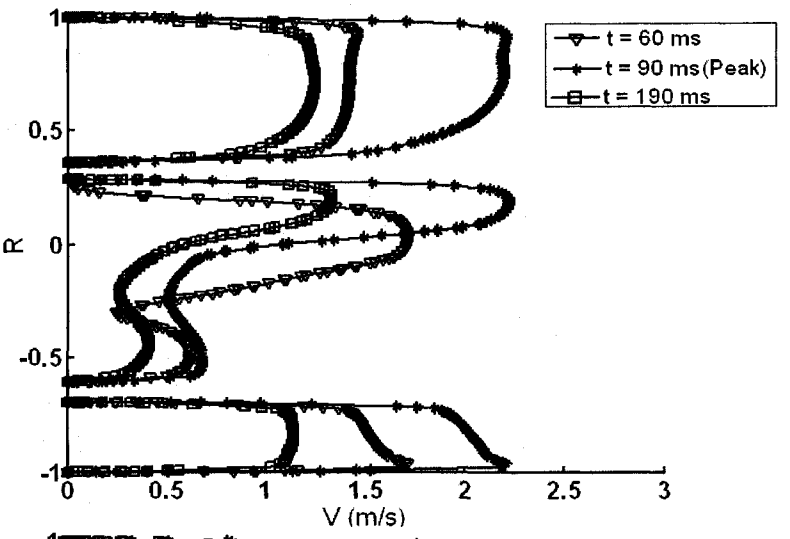

100% malfunction

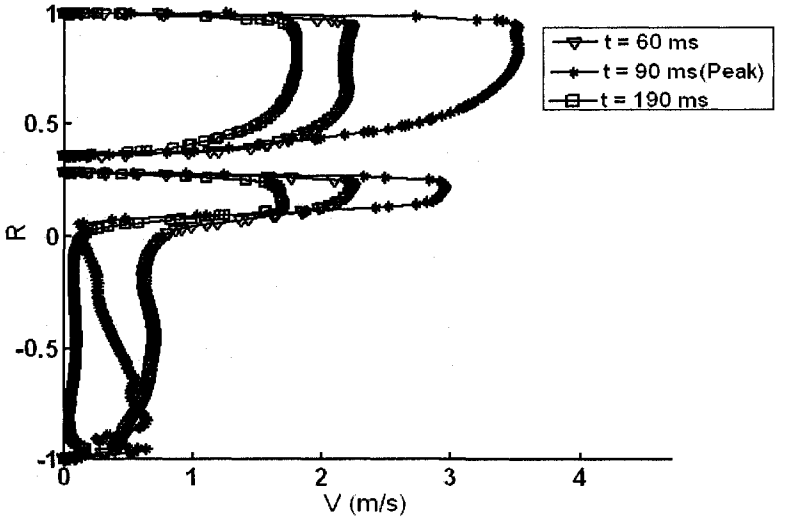

Figure 4.5 Velocity profiles at the vicinity of the valve at different time instants and malfunctions.

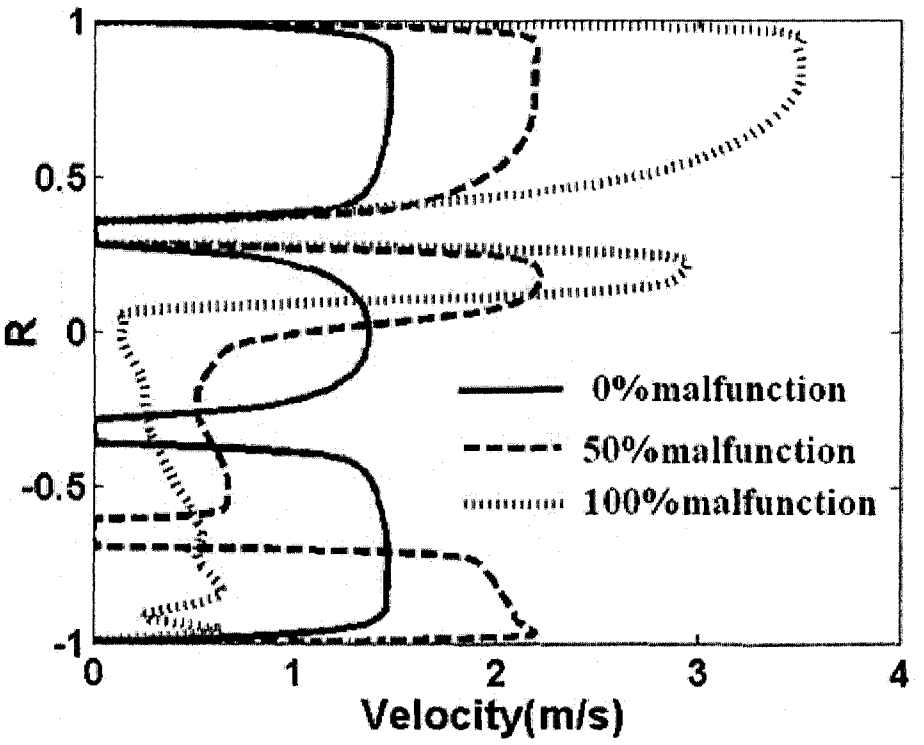

Figure 4.6 Velocity profiles at the vicinity of the valve at the peak of the systolic phase for different malfunctions.

In Figures 4.7 and 4.8 velocity contours and axial velocity profiles at three selected locations and three different instants are reported; 0.3D, 1D and 2D downstream of the valve. In healthy model (0% malfunction), at 0.3D downstream of the valve, the influence of the valve leaflets on the flow field was obvious, with two wakes and three jets (one central and two laterals) in the all three instants. No significant flow has been noticed in the sinus area before the peak of the systolic phase. While during the two other instants (at the peak and 120 ms) represent clearly the circulation in the sinus region by having a negative axial velocity value in the sinus area. For the other two profiles, 1D and 2D downstream of the valve, during the acceleration, the velocity profiles are almost flat. On the other hand, at the peak, at the distance of 1D, there still remain two wakes, but the velocity differences are lower than at 0.3D. The flattening of the velocity profile continues at 2D downstream, where the velocity profile becomes completely flat.

For 50% malfunction, although the three jets still exist, the profile distribution is different from the healthy model, the central and upper lateral jets are getting close from each other by shifting the central jet peak toward the upper lateral side, while the lower lateral jet will go toward the wall. Moreover, the velocity profiles at 1D and 2D downstream of the valve are no more flat. In addition, a recirculation zone appears early in the acceleration phase and remains for the rest of systolic phase (negative velocity sign).

For 100% malfunction, the flow behavior is close from 50% malfunction case except having only two dominant central and upper lateral jets instead of having three jets.

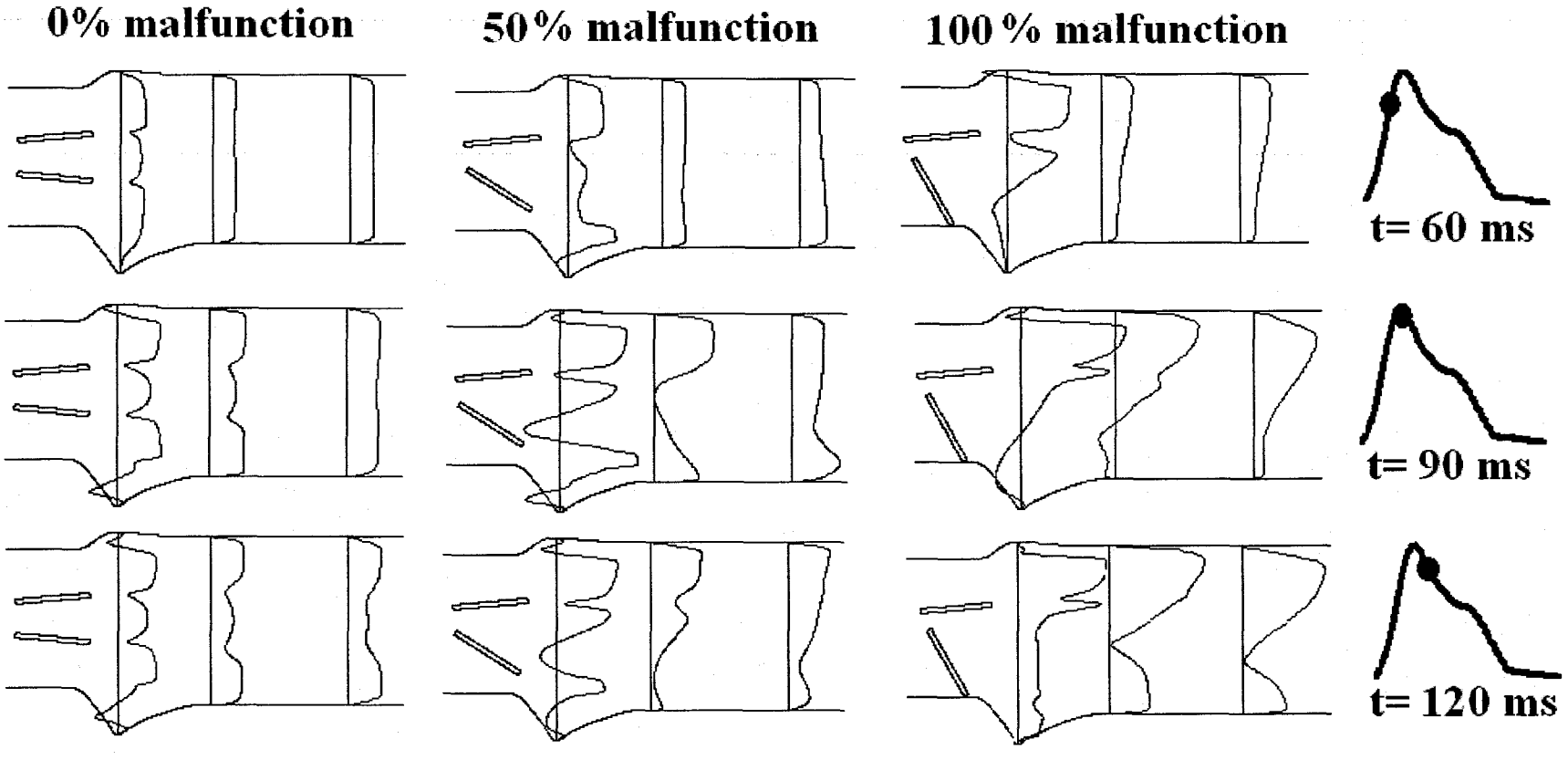

Figure 4.7 Axial velocity profiles at different instants and different levels of malfunction.

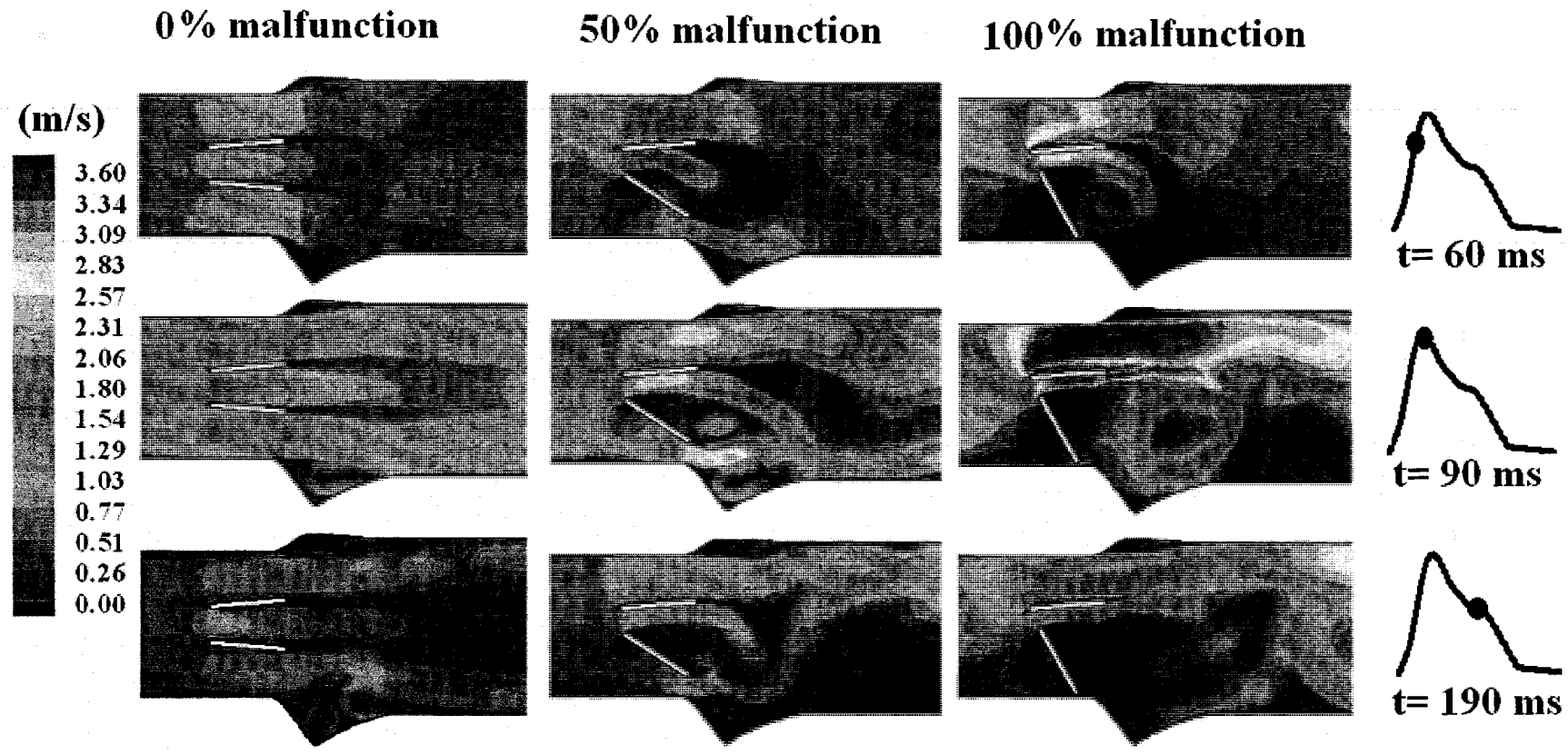

Figure 4.8 Velocity contours at different instants and different levels of valve malfunction.

4.4.1 Vortex formation

The vortex formation was depicted by both vorticity magnitude and λ_2 criterion, respectively, in Figures 4.9 and 4.10. Even though, an explicit definition of what is a vortex is still a matter of debate, the most commonly used criterion is the one proposed by Jeong and Hussain (1995). This criterion defines a vortex structure as a region where the second eigenvalue λ_2 ($\lambda_1 \geq \lambda_2 \geq \lambda_3$) of the symmetric tensor ($\Omega^2 + S^2$) is negative at every point inside the vortex core. For two dimensional incompressible flows, this means that:

$$\lambda_2 = \left(\frac{\partial v_x}{\partial x}\right)^2 + \left(\frac{\partial v_x}{\partial y}\right)\left(\frac{\partial v_y}{\partial x}\right) < 0 \qquad \text{where V } (v_x, v_y, v_z) \qquad (10)$$

The two figures were in excellent agreement in depicting the vortex formation.

In the healthy model, near the aortic walls, the valve housing's shear layers at the upper and lower walls roll up in the sinus region and start forming a vortex. At the peak of systolic phase an obvious single vortex was formed (Dasi et al., 2007). During the early stage of deceleration phase, the single vortex structure still exist, while in the middle stage of deceleration phase the single vortex will break down into two major vortices with other small scale vortices. On the other hand, in the wake of the valve leaflets, periodic vortex shedding (Von Karman vortex streets) was observed (Blustien et al. 2000). However, the vortex shedding phenomenon will only start at the late stage of acceleration phase and persist during the deceleration phase. It is important to point out that the current results are in overall agreement with experimental and numerical results of Dasi et al. (2007).

In partially defective leaflet, the flow behavior is dramatically changed. During the acceleration phase, a single vortex was formed in between the two leaflets and in the sinus area another vortex was build up earlier than in the healthy model. In addition, vortex shedding in the wake of the valve occurred earlier in the defective leaflet than the healthy one. Comparing to the healthy model a more complex vortical flow was noticed downstream of the valve with multiple small and large scale vortices. In completely defective leaflet, as the partially defective leaflet, single vortex was also formed in between the valve but this time shifted toward the sinus area and multiple vortical structures were observed but the number of vortices is less than the partially defective leaflet and the scale is relatively larger. The significant difference between completely closed case and other cases is the existence of vortical flow behind the defective valve (immediately upstream from the valve).

4.4.2 Wall shear stress

Figure 4.11 shows the WSS distribution around the vicinity of the valve at both lower and upper aortic walls at the peak of systolic phase. At the lower wall the WSS magnitude (in 2D) was dramatically elevated with the presence of the malfunction and reached the maximum (~ 750 Pa) with 100% of malfunction. On the other hand, the position of maximum WSS at the lower wall in the case of 100% malfunction was shifted from the vicinity of the valve to slightly upstream from the valve area. At the upper wall the elevation in WSS magnitude was not as high as at the lower wall. Furthermore, the highly exposed area to the WSS did not change its position with the increase in valve malfunction.

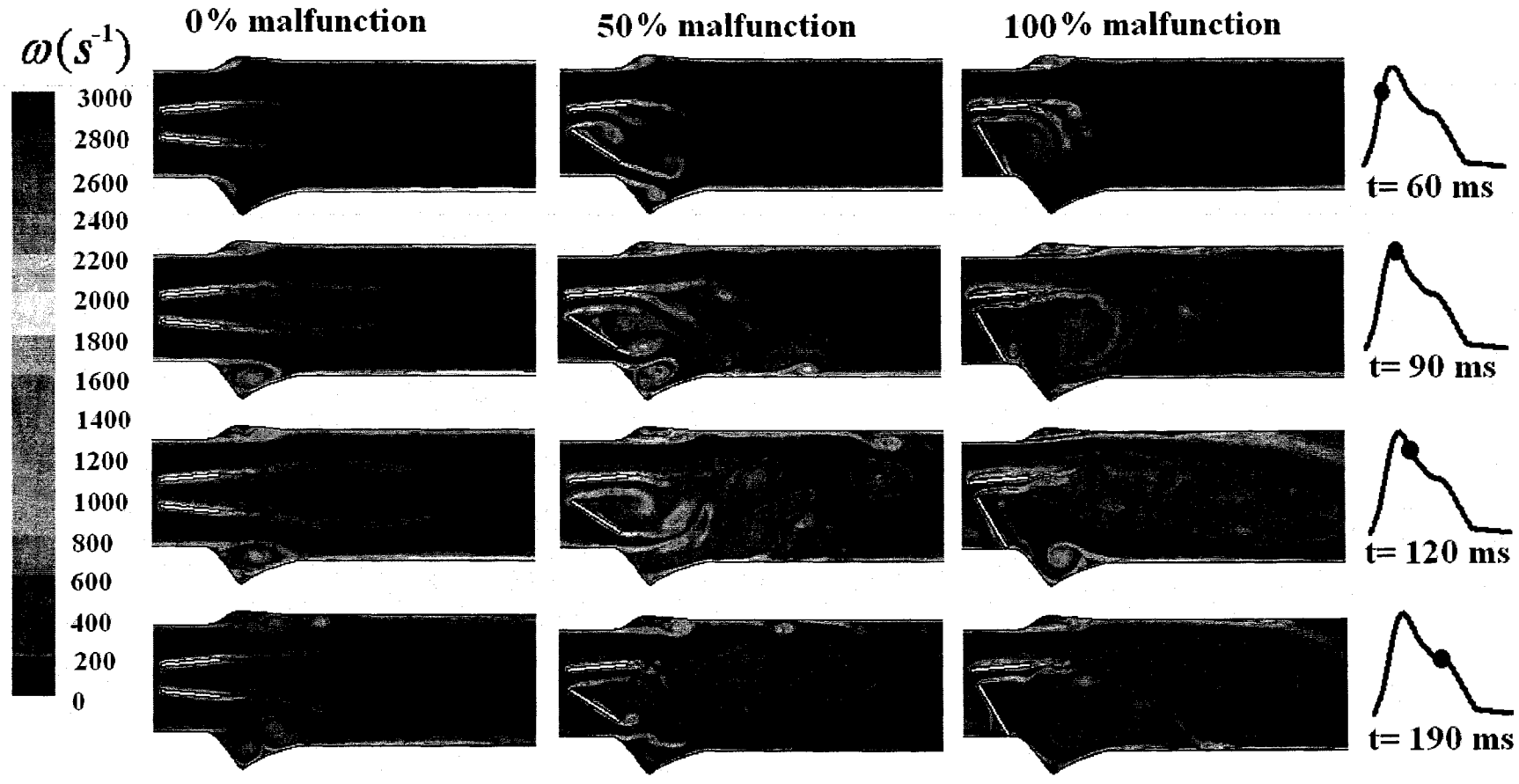

Figure 8

Figure 4.9 Vorticity distributions downstream of a healthy and a defective mechanical valve at different time instants

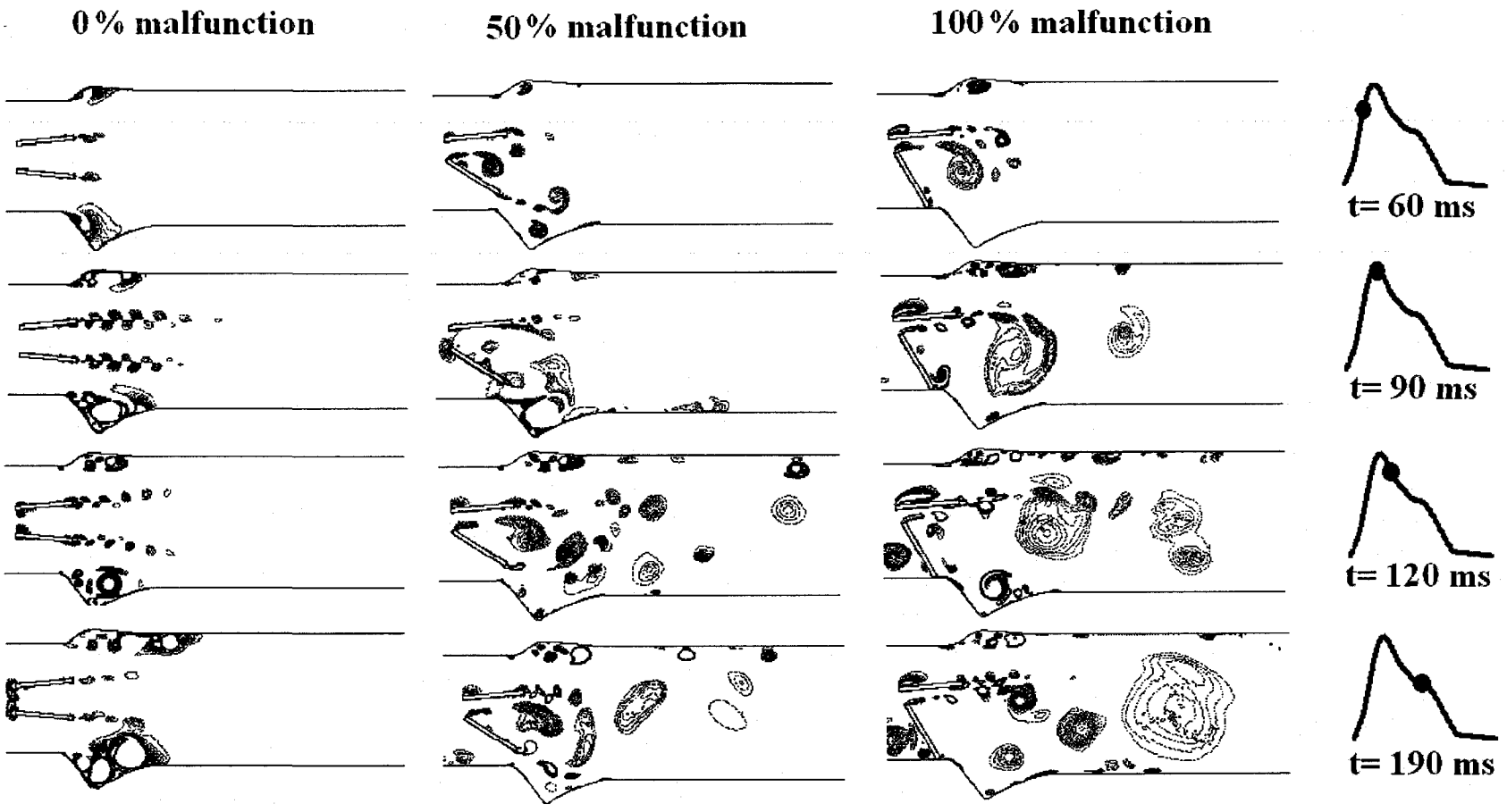

Figure 9

Figure 4.10 Coherent structures downstream of a healthy and a defective mechanical valve at different time instants (using the λ_2 criterion).

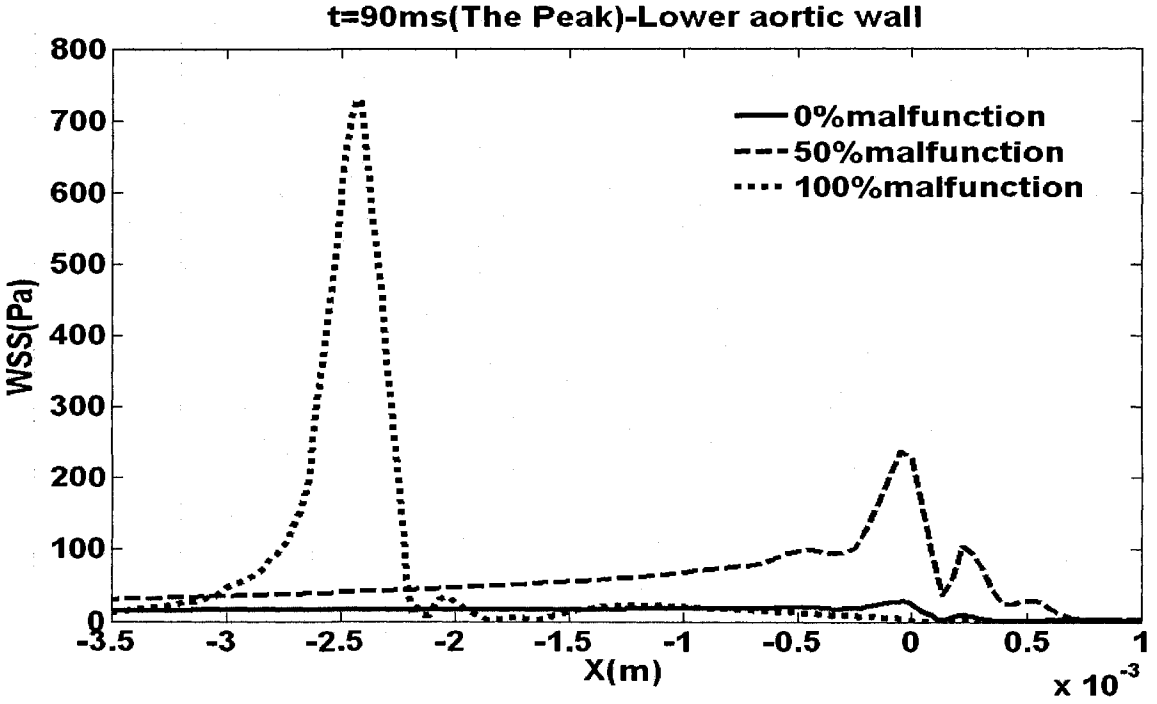

a)

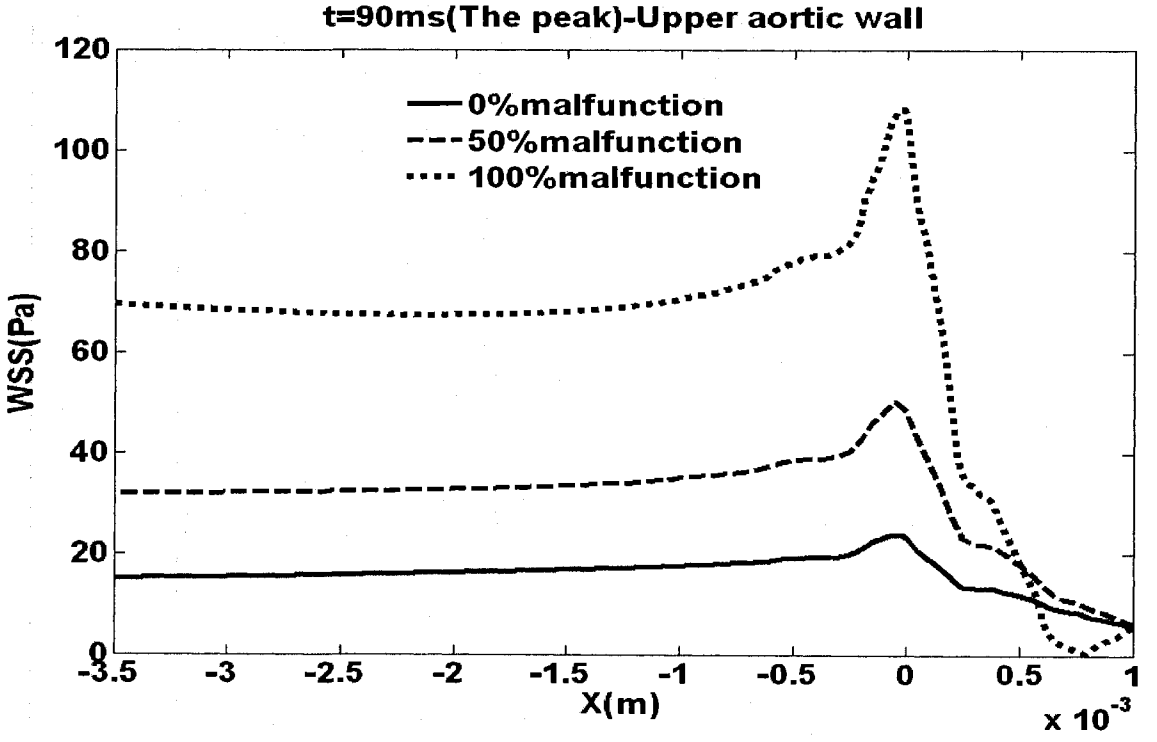

b)

Figure 4.11 WSS for different valve malfunction at the a) lower wall b) upper wall at the peak of the systolic phase.

Figure 4.12 shows the WSS only along the sinus area for both upper and lower aortic walls during the peak of systolic phase. At the lower wall no significant elevation in WSS magnitude was found downstream of the valve in all degrees of malfunction. The only dramatic change occurred around the vicinity of the valve as mentioned above. On the other hand, at the upper wall, a significant increase in WSS magnitude was observed when the valve leaflet was completely defected. Moreover, the elevation in WSS level for the completely defective valve was found in the second half of the wall of sinus cavity far from the valve.

4.4.3 Turbulent shear stress

Figure 4.13 shows Reynolds turbulent shear stress (TSS) in the entire field at the peak of systolic phase, for three different cases of malfunction. The TSS was obtained using the Boussinesq relation for incompressible flow [Wilcox 1998].

The maximum TSS (189 Pa) was observed when the leaflet was completely closed. In the healthy model, TSS was dominant in between and in the wake of the leaflets, close to the trailing edge of each leaflet. In the meantime, in the case of partially defective valve, the dominant regions for TSS started to be shifted toward the lower side of the valve and in the wake of defective leaflet and close from the sinus region of the lower wall. However when the malfunction reached 100%, the TSS had its highest value around the upper side of the normal leaflet and around the sinus region of the upper wall.

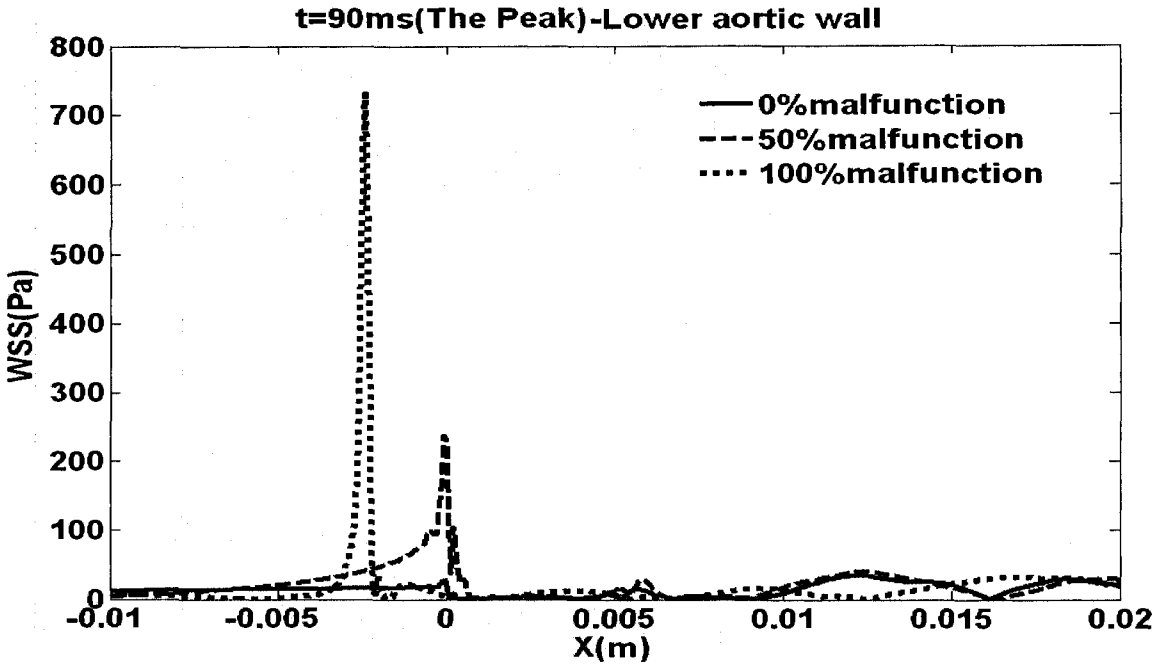

a)

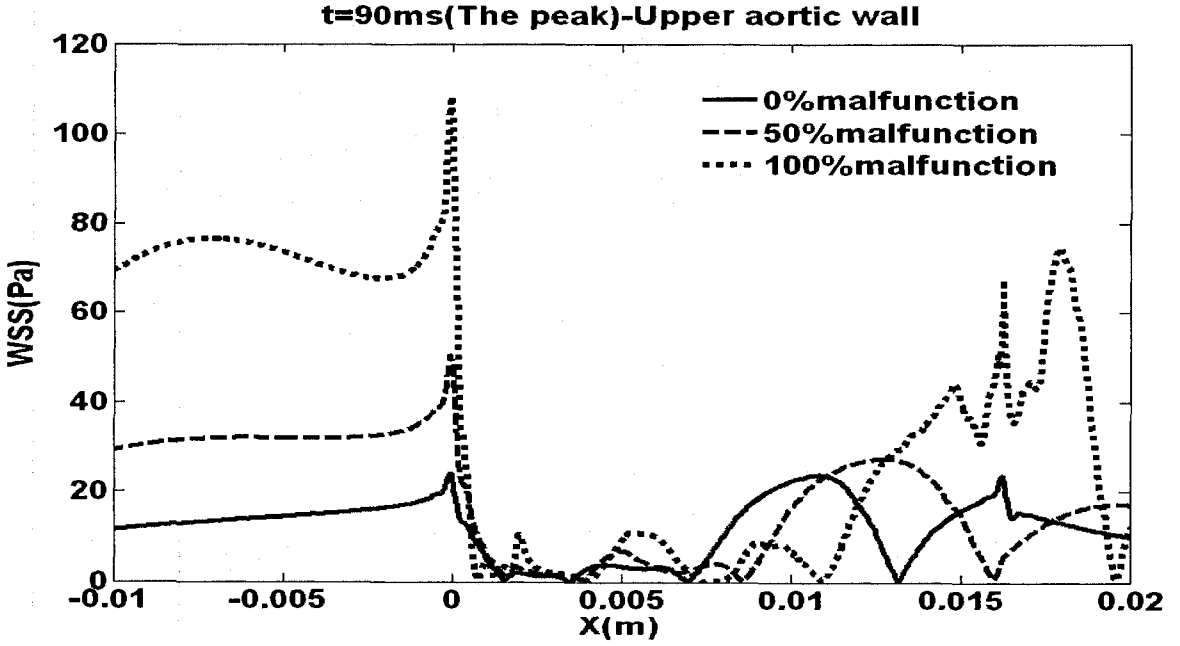

b)

Figure 4.12 WSS for different valve malfunction at the a) lower wall b) upper wall at the peak of the systolic phase.

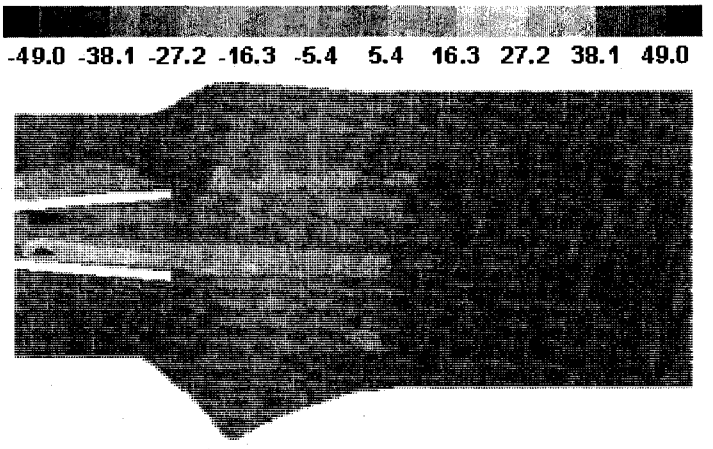

Figure 4.10 Turbulent shear stress at the peak of systolic phase for different valve malfunctions.

4.5 Discussion

4.5.1 Clinical diagnosis

Clinically, the evaluation of valve performance is usually made by Doppler-echocardiography. Maximal velocity during the forward flow will be measured by passing an ultrasound wave beam through the valve. Only the maximal velocity will be used to determine the transvalvular pressure drop and Effective orifice area (EOA). However, in order to get accurate measurements, it is very important to align the ultrasound beam with flow axis (Doppler effect). Furthermore, clinicians usually expect to find the maximal velocity through the central orifice; therefore, the ultrasound wave beam is usually passed through the central jet between the two leaflets. However, as shown in Figure (4.5) this assumption is only reasonable in the case of a healthy valve. In case of completely defective valve, the flow is shifted towards the undefective leaflet and the maximum velocity will be found through the lateral orifice. Consequently, clinicians should be aware of checking the maximal velocity position not only at the central orifice but also through the lateral orifices, when possible. Finding the maximal velocity in the lateral orifice could be an indication of valve malfunction.

4.5.2 Wall Shear Stress (WSS)

WSS is proportional to the percentage of malfunction and reached its maximum (750 Pa) when the leaflet was completely closed as shown in Figures 4.11 and 4.12. However, in this case the maximum WSS was shifted upstream from the valve where the valve housing covers normally the aortic wall. Therefore, the high shear stress level might not affect the aortic wall. In contrast, In the case of partially blocked valve, the WSS is

shifted slightly downstream of the valve which may affect the endothelial cells in the sinus wall.

It is important to point out that a WSS about 40 N/m^2 might damage the endothelial cells and higher value around 100 N/m^2 could wash them away. As a result, the blood will be in direct contact with subendothelial connective tissue. In contrast to endothelial cells, the deposition of blood elements and thrombotic material will occur on subendothelial tissue of the defective wall. In this case, the level of shear stress that will lead to red blood cells damage is lower than the case of healthy aortic wall (Yoganathan et al. 1978).

4.5.3 TSS and residential time

Turbulent shear stress level and position will change in the case of defective valve. In 50% malfunction of the lower leaflet, the relatively high shear stress areas covered most of the domain downstream of the valve with relatively high shear stress values. Therefore, the amount of blood elements that will be exposed to high shear stress level is higher in the case of partially defective valve and as a result the level of platelets activation and thrombus formation will be higher. In the meantime, in the case of completely defective valve the turbulent shear stress reached as high as 189 Pa and the high turbulent shear stress areas were found through the upper orifice and downstream of the valve close from the upper wall. In addition to elevation in shear stress magnitude in the defective valve, the increase in number and scale of formed vortices downstream of the valve will lead to an increase in the residential time of the blood element in these high shear stress regions in the wake of the valve. Although the magnitude of turbulent shear

stress to lead red blood cells damage is higher than the calculated one, the potential of blood hemolysis still exist as there are other factors like exposure time and shear exposure history relevant to blood hemolysis (Kameneva et al., 2004).

Chapter 5

Conclusions and Future Directions

5.1 Conclusions

In the present study, the flow dynamics through a defective mechanical heart valve under steady state and pulsatile flow conditions has been investigated.

For the steady state part, in order to give more accurate description of the problem, five different models were simulated (including five defective models) at five different flowrate conditions (from low flowrate Q= 2.5 L/min to high flow rate Q=7 L/min). In this study the discrepancy between Doppler echocardiographic and catheter transvalvular pressure gradients were explained and an inappropriate diagnosis of mechanical heart valve malfunction by using Doppler was predicted.

To overcome this issue, two potential non-invasive parameters, based on Doppler echocardiography and magnetic resonance imaging velocity measurements, were proposed for an early detection of mechanical valve malfunction. The effect of such valve malfunction on blood components has also been investigated by showing the turbulent shear stress (TSS) and flow behavior downstream of a defective bileaflet valve, can induce platelet activation and thrombus formation.

For the pulsatile flow conditions, only a normal flowrate was studied (Q= 5L/min) but with the same five levels of valve malfunction. In this part, the attention was paid on the blood hemodynamics downstream of the defective valve. Vortex dynamics for different

percentages of malfunctions and time instants were studied. In the healthy model, an overall agreement was observed between the current study and the work performed by Dasi et al. (2007). Two dominant Von Karman vortex streets shed from the trailing edges of the two leaflets and the housing shear layer rolled up into the sinus area and created a vortex coherent structure. Moreover, by changing the orientation of the defective valve, the flow downstream of the valve became more vortical and new vortices appeared with different scales and numbers. As a consequence, the residential time of blood elements might increase leading to platelet activation.

A dramatic elevation in wall shear stress and turbulent shear stress values were found by increasing the severity of valve malfunction. Moreover, the exposed areas to a high shear stress level changed by changing the level of valve malfunction. It is important to point out that not only the aortic wall from the defective valve side (lower wall in the current study) is exposed to high shear stress level but also the aortic wall from the healthy leaflet side (upper wall in the current study), specifically, in the extreme cases of valve malfunction.

5.2 Future Directions

CFD is a major tool for investigating blood flow through mechanical heart valves. Although, up to date, there is no numerical method capable of accurately simulating the blood flow through mechanical heart valve under physiological conditions, CFD is widely used in this field. The turbulent characteristics of the blood flow through mechanical heart valves have motivated us to use 3-D simulations with realistic

geometry, as the turbulence nature is three dimensional and unsteady. Moreover, fluid-structure interaction is another point that should be taken into account in future directions, in order to study the opening and closing phases of defective mechanical heart valves. In the current study, a defective bileaflet valve was studied in aortic position and studying the same problematic mechanical heart valve in mitral position is also important since this will affect the left ventricle diastolic function. Finally, in parallel, an experimental work using Particle Image Velocemetry (PIV) should be done to validate the numerical results and to extract more reliable data that could help in a more accurate diagnosis of valve malfunction using the suggested non-invasive parameters.

References

Aluri, S., and Chandran, K.B., "Numerical Simulation of Mechanical Mitral Heart Valve Closure", Annals of Biomedical Engineering, vol. 29, pp. 665–676, 2001.

Baumgartner, H., Khan, S., DeRobertis, M., Czer, L., and Maurer, M., "Discrepancies Between Doppler and Catheter Gradients in Aortic Prosthetic Valves In Vitro: a Manifestation of Localized Gradients and Pressure Recovery", Circulation, vol. 82, pp. 1467-147, 1990.

Baumgartner, H., Khan, S.S., DeRobertis, M., Czer, L.S., and Maurer, G., "Doppler Assessment of Prosthetic Valve Orifice Area: An In Vitro Study", Circulation, vol. 85, pp. 2275-2283, 1992.

Baumgartner, H., Schima, H., and Kuhn, P., "Effect of Prosthetic Valve Malfunction on the Doppler-Catheter Gradient Relation for Bileaflet Aortic Valve Prostheses", Circulation, vol. 87, pp. 1524-4539, 1993.

Blais, C., Pibarot, P., Dumesnil J.G., Garcia, D., Chen, D., and Durand, L., "Comparison of Valve Resistance with Effective Oriffice Area Regarding Flow Dependence", The American Journal of Cardiology, vol. 88, pp. 45-52, 2001.

Bluestein, D., Rambod, E., and Gharib, M.,"Vortex shedding as a mechanism for free emboli formation in mechanical heart valves", Journal of Biomechanical Engineering, vol. 122, pp.125-134, 2000.

Bluestein, D., Li, Y.M., and Krukenkamp, I.B., "Free Emboli Formation in the Wake of Bi-leaflet Mechanical Heart Valves and the Effect of Implantation Techniques", J. Biomech., vol. 35, pp.1533–1540, 2002.

Browne, P., Ramuzat, A., Saxena, R., and Yoganathan, A.P., "Experimental Investigation of the Steady Flow Downstream of the St.Jude Bileaflet Heart Valve: A Comparison between Laser Doppler Velocimetry and Particle Image Velocimetry Techniques", Annals of Biomedical Engineering, vol. 28, pp. 39–47, 2000.

Brucker, C.H., Steinseifer, U. Schr¨oder, W., Reul. H., "Unsteady flow through a New MechanicalHeart Valve Prosthesis Analysed by Digital Particle Image Velocimetry", Meas. Sci. Technol., vol. 13, pp.1043–1049, 2002.

Cannegieter, S.C., Rosendaal, F.R., and Briet, E., "Thromboembolic and Bleeding Complications in Patients with Mechanical Heart Valve Prostheses", vol. 89, pp. 635-641, 1994.

Cheng, R., Lai, Y.G., and Chandran, K.B., "Two Dimensional Fluid-Structure Interaction Simulation of Bileaflet Mechanical Heart Valve Flow Dynamics", The Journal of Heart Valve Disease, vol. 12, pp. 772-780, 2003.

Cheng, R., Lai, Y.G., and Chandran, K.B.,"Three-Dimensional Fluid-Structure Interaction Simulation of Bileaflet Mechanical Heart Valve Flow Dynamics", Annals of Biomedical Engineering, vol. 32(11), pp. 1471–1483, 2004.

Crawford, M., DiMarco J.P., and Paulus, W.J., *Cardiology*, 2nd edition, Elsevier, 2004.

DeGroff, C.G., Shandas, R., and Valdes-Cruz, L., "Analysis of the Effect of Flow Rate on the Doppler Continuity Equation for Stenotic Orifice Area Calculations: A Numerical Study", Circulation, vol. 97, pp. 1597-1605, 1998.

Dumont, K., Astijen, J.M.,Van De Vosse, F.N., and Verdonck, P.R., "Validation of a Fluid-Structure Interaction Model of a Heart Valve Using the Dynamic Mesh Method in Fluent", Computer Methods in Biomech. And Biomed. Eng., vol. 7(3), pp. 139-146, 2004.

Fallon, A.M, Shah, N., Marzec, U.M., Warnock, J.N., Yoganathan A.P., and Hanson, S.R., "Flow and Thrombosis at Orifices Simulating Mechanical Heart Valve Leakage Regions", Journal of Biomechanical Engineering, vol. 128, pp. 30-39, 2006.

Fukumoto, Y., Tsutsui, H., Tsuchihashi M., Masumoto, A., and Takeshita, A., "The Incidence and Risk Factors of Cholesterol Embolization Syndrome, a Complication of Cardiac Catheterization: A Prospective Study", Journal of the American College of Cardiology, vol. 42(2), pp. 211–217, 2003.

Garcia, D., Dumesnil, J.G, Durand, L., Kadem, L., and Pibarot, P., "Discrepancies Between Catheter and Doppler Estimates of Valve Effective Orifice Area Can Be Predicted From the Pressure Recovery Phenomenon Practical Implications With Regard to Quantification of Aortic Stenosis Severity", Journal of the American College of Cardiology, vol. 41(3), pp. 435–42, 2003.

Ge, L., Jones, S.C., Sotiropoulos, F., Healy, T.M., and Yoganathan, A.P., "Numerical Simulation of Flow in Mechanical Heart Valves: Grid Resolution and the Assumption of Flow Symmetry", Journal of Biomechanical Engineering, vol. 125, pp.709-719, 2003.

Ge, L., Jones, S.C., Sotiropoulos, F., Healy, T.M., and Yoganathan, A.P., "Flow in a Mechanical Bileaflet Heart Valve at Laminar and Near-Peak Systole Flow Rates: CFD Simulations and Experiments", Journal of Biomechanical Engineering, vol. 127, pp. 782-797, 2005.

Ghalichi, F., and Deng, X.,"Turbulence Detection in a Stenosed Artery Bifurcation by Numerical Simulation of Pulsatile Blood Flow Using the Low-Reynolds Number Turbulence Model", Biorheology, vol. 40, pp. 637-654, 2003.

Gott, V.L., Alejo, D.E., and Cameron, D.E., "Mechanical Heart Valves: 50 Years of Evolution", Ann Thorac Surg, vol. 76, pp. 2230 –2239, 203.

Grigioni, M., Daniele, C., D'Avenio, G., and Barbaro, V., "The Influence of the Leaflets' Curvature on the Flow Field in Two Bileaflet Prosthetic Heart Valves", Journal of Biomechanics, vol. 34, pp. 613–621, 2001.

Grigioni, M., Daniele, C., Gaudio, C.D., Morbiducci, U., D'Avenio, G., and Barbaro V., "Three-Dimensional Numerical Simulation of Flow Through an Aortic Bileaflet Valve in a Realistic Model of Aortic Root", American Society for Artificial Internal Organs, vol. 51(3), pp. 176-183, 2005.

Guiviera, C., Deplanoa, V., and Pibarotb, P., "New Insights into the Assessment of the Prosthetic Valve Performance in The Presence of Subaortic Stenosis through a Fluid–Structure Interaction Model", J. of Biomech., vol. 40(10), pp. 2283-2291, 2007.

Hatle L., Anglesen, B., *Doppler Ultrasound in Cardiology*, 2nd Edition, Lea and Febiger, 1985.

Kadem, L., Knapp Y., Pibarot P., Bertrand, E., Garcia, D., Durand, L.G., and Rieu, R., "A New Experimental Method for The Determination of The Effective Orifice Area Based on the Acoustical Source Term", Experiments in Fluids, vol. 39, pp. 1051–1060, 2005.

Katritsis, D., Kaiktsis, L., Chaniotis, A., Pantos, J., Efstathopoulos, E., and Marmarelis, V., "Wall Shear Stress: Theoretical Considerations and Methods of Measurement", vol. 49(5), pp. 307-329, 2007.

King, M.J., David, T., and Fisher, J., "Three Dimensional Study of the Effect of Two Leaflet Opening Angles on the Time Dependant Flow through a Bileaflet Mechanical Heart Valve", vol. 19(3), pp. 235-241, 1997.

Lai, Y.G., Chandran, K.B., Lemmon, J., "A Numerical Simulation of Mechanical Heart Valve Closure Fluid Dynamics", J.of Biomech., vol. 35, pp. 881-892, 2002.

Liu, J.S., Lu, P.C., and Chu. S.H., "Turbulence Characteristics Downstream of Bileaflet Aortic Valve Prostheses", Transactions of ASME, vol. 122, pp.118-124, 2000.

Lu, P.C., Lai, H.C., and Liu, J.S., "A Reevaluation and Discussion on the Threshold Limit for Hemolysis in a Turbulent Shear Flow", Journal of Biomechanics, vol. 34, pp. 1361-1364, 2001.

Montorsi, P., Cavretto, D., Alimento, M., Muratori, M., and Pepi, M., "Prosthetic Mitral Valve Thrombosis: Can Fluoroscopy Predict the Efficacy of Thrombolytic Treatment?", Circulation, vol. 108, pp.79-84, 2003.

Peacock, J., Jones, T., Tock C., and Lutz R., "The onset of turbulence in physiological pulsatile flow in a straight tube", Experiments in Fluids, vol. 24, pp. 1-9, 1998.

Pedrizzetti, G., and Domenichini, F., "Flow-driven Opening of a Valvular Leaflet", J. Fluid Mech., vol. 569, pp. 321–330, 2006.

Redaelli, A., Bothorel, H., Votta, E., Soncini, M., Morbiducci, U., Del Gaudio, C., Balducci, A., and Grigioni, M., "3-D simulation of the St. Jude Medical bileaflet valve opening process: fluid-structure interaction study and experimental validation", The Journal of Heart Valve Disease, vol.13 (5), pp. 804-13, 2004.

Rehfeldt, K.H., and Click R.L., "Prosthetic Valve Malfunction Masked by Intraoperatve Pressure Measurements", International Anesthesia Research Society", vol. 94, pp.857-858, 2002.

Reul, H., Vahlbruck, A., Giersiepen, M., Schmitz-Rode, T.H., Hirtz, V., and Effert, S., "The Geometry of the Aortic Root in Health, at Valve Disease and after Valve Replacement", Journal of Biomechanics, vol. 23 181–191, 1990.

Richards, K.E., Deserranno, D., Donal, E., Greenberg, N.L., Thomas, J.D., and Garcia, M., "Influence of Structural Geometry on the Severity of Bicuspid AorticStenosis", Am J Physiol Heart Circ Physiol, vol. 287, pp.1410–1416, 2004.

Sakamoto, Y., Hashimoto, K., Okuyama, H., Ishii, S., Shingo, T., and Kagawa, H., "Prevalence of Pannus Formation After Aortic Valve Replacement: Clinical Aspects and Surgical Management", Journal of Artificial Organs, vol. 9(3), pp. 199-202, 2006.

Sallam, A.M., and Hwang, H.C., "Human Red Blood Cells Hemolysis in a Turbulent Shear Flow: Contribution of Reynolds Shear Stress", Biorheology, vol. 21, pp. 783-797, 1984.

Shi, Y., Zhao Y., Joon, T., Yeo, H., and Hwang, N., "Numerical Simulation of Opening Process in a Bileaflet Mechanical Heart Valve under Pulsatile Flow Condition", The Journal of Heart Valve Disease, vol. 12, pp. 245-256, 2003.

Simon, H.A., Leo, H., Carberry, J., and Yoganathan, A.P., "Comparison of the Hinge Flow Fields of two Bileaflet Mechanical Heart Valves under Aortic and mitral Conditions", Annals of Biomedical Engineering, vol. 32(12), pp. 1607-1617.

Straatman, J., and Steinman, D., "Two-Equation Turbulence Modeling of Pulsatile Flow in a Stenosed Tube", Journal of Biomechanical Engineering, vol. 126, pp.625-635, 2004.

Thalassoudis, K., Mazumdar, J., Noye, B.J., and Craig, I.H., "Numerical Study of Turbulent Blood Flow through a Caged-Ball Prosthetic Heart Valve Using a Boundary-Fitted co-ordinate System", Medical and Biological Engineering and Computing, vol. 25(2), pp. 173-180, 1987.

Wilcox, D.C., *Turbulence Modeling for CFD*, 2nd Edition, DCW Industries, La Canada, California, 1998.

Yin, W., Alemu, Y., Affeld, K., Jesty, J., and Bluestein, D., "Flow Induced Platlete Activation in Bileaflet and Monoleaflet Mechanical Heart Valves", Annals of Biomedical Engineering, vol. 32(8), pp. 1058–1066, 2004.

Yin, W., Gallocher, S., Pinchuk, L., Schoephoerster, R.T., Jesty, J., and Bluestein, D., "Flow-induced Platelet Activation in a St. Jude Mechanical Heart Valve, a Trileaflet Polymeric Heart Valve, and a St. Jude Tissue Valve", Artificial Organs, vol. 29(10), pp. 826–831, 2005.

Yoganathan, A.P., Corcoran, W.H., and Harrison, E.C., "Wall Shear Stress Measurements in the Near Vicinity of Prosthetic Aortic Heart Valves", Journal of Bioengineering, vol. 2, pp. 369-379, 1978.

Yoganathan, A. P., He Z., and Jones, S.C., "Fluid Mechanics OF Heart Valves", Annu. Rev. Biomed. Eng., vol. 6, pp. 331–62, 2004.

Yoganathan, A.P., Chandran, K.B., and Sotiropoulos, F., "Flow in Prosthetic Heart Valves: State-of-the-Art and Future Directions", Annals of Biomedical Engineering., vol.33 (12), pp 1689–1694, 2005.

Zaret, B.L., Moser, M., Cohen, L.S., Morrow, W., *Heart Book*, 1st Edition, Yale University, School of Medicine, 1992.